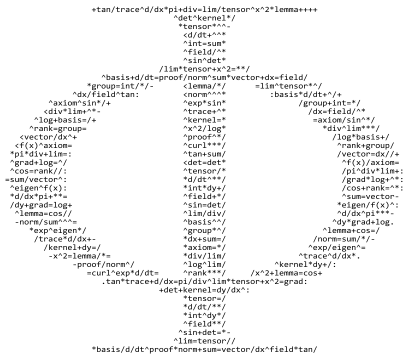
PHI TECHNICAL MONOGRAPHS

Volume V

Uniformization and Geometric Analysis

Riemann surfaces, physical models and certified computation



PHI research collective

Contents

1 Scope, mathematical objects and evidence **1**

1.1 The subject of the monograph 1
1.2 Source order and proof order 1
1.3 Conventions 2
1.4 Comparison contracts 2
1.5 Interpretation of evidence 3
1.6 The intended disciplinary connections 3

2 Topological and analytic foundations **5**

2.1 Covering surfaces and the lifted complex structure 5
2.2 Closed forms and the period obstruction 5
2.3 Dirichlet minimization on a bordered surface 6
2.4 Regularity, boundary values and the maximum principle 7
2.5 Green functions and a normalized logarithmic pole 8
2.6 Topological exhaustion and its exact role 9
2.7 Imported analytic dependencies and noncircularity 9

3 The seven source subsections **10**

3.1 Source §5.1: the three simply connected models 10
3.2 Source §5.2: classification by universal covers 11
3.3 Source §5.3: smooth annuli and the period coordinate 12
3.4 Source §5.4: relatively compact simply connected domains 14
3.5 Source §5.5: the open and compact alternatives 15
3.6 Source §5.6: extension to tame ends 17
3.7 Source §5.7: orbifolds and the necessary qualifications 19

4 Algebraic geometry, periods and topological invariants **22**

4.1 Local coordinates, local rings and multiplicity 22
4.2 Divisors and the global degree ledger 22
4.3 The torus as a lattice quotient 23
4.4 An algebraic equation from a lattice 24
4.5 Hyperelliptic examples and differential bases 25
4.6 Cut surfaces and the bilinear period identity 25
4.7 Degeneration and the logarithmic period scale 26

4.8 Quotient topology and information that coordinates do not erase 26

5 Harmonic, functional and Fourier analysis 28

5.1 Conformal energy and the correct transformed equation 28
5.2 The logarithmic cylinder 28
5.3 A complete error budget for Fourier truncation 29
5.4 Harmonic measure and optimal error allocation 31
5.5 Hyperbolic annular metrics and cusp limits 31
5.6 Conformal pullback on Bergman and Dirichlet spaces 32
5.7 The exact finite-rank model 33
5.8 Spectral heat on a flat quotient 33
5.9 Residual certificates for elliptic solves 33

6 Nuclear, high-energy and M/string-theory applications 35

6.1 The analytical role of a physical model 35
6.2 Nuclear scattering: one square-root threshold 35
6.3 Two thresholds: an explicit rational uniformization 36
6.4 Three and more thresholds: a genus obstruction 37
6.5 Bound states, virtual states and resonant poles 37
6.6 High-energy amplitudes and elliptic cuts 38
6.7 Classical string worldsheets and Weyl scaling 38
6.8 A brane-curve model and exact period differentiation 39
6.9 Cylinders, punctures and conditional conformal-field identities 40
6.10 What can be certified in these applications 40

7 Thermodynamics and computational mathematical physics 42

7.1 Steady conduction through a conformal annulus 42
7.2 Transient diffusion retains a weight 43
7.3 A posteriori energy control for a diffusion step 43
7.4 Gaussian fields and finite determinants 43
7.5 Poisson summation and the heat-trace duality 44
7.6 Liouville's equation and constant curvature 44
7.7 Energy minimization, discretization and best approximation 45
7.8 Inverse problems and conformal nonidentifiability 45
7.9 A computational-physics acceptance specification 46

8 Logical complexity, algorithms, parallelism and cryptography 47

8.1 What a computational uniformization problem contains 47
8.2 Logical complexity as a dependency problem 47
8.3 Typed certificates and soundness 48
8.4 Modal algorithms and exact arithmetic counts 48
8.5 Two-dimensional periodic operators 49
8.6 Parallel work, depth and communication 50
8.7 Distributed averaging and spectral gaps 50

8.8 Branch continuation as a distributed state machine 51
8.9 Temporal logic and finite-model verification 52
8.10 Cryptography: complex tori and finite fields 52
8.11 A finite arithmetic example and a transfer boundary 53
8.12 Algorithm optimization with a certificate cost 53

9 Engineering models and dual certificates 54
9.1 A common mathematical interface 54
9.2 Planar electrostatics and capacitance 54
9.3 An exact network analogue 55
9.4 Corners and field singularities 55
9.5 Circuit response as a half-plane function 56
9.6 Control, stability domains and discrete implementations 57
9.7 Machines, drives and power-network calculations 57
9.8 Signals, transforms and finite observables 58
9.9 Computational geometry and conformal meshes 58
9.10 Software, electronics and the remaining engineering subjects 58

10 Quantitative closure, computability and additional structural proofs 60
10.1 What a finite presentation can establish about uniformization type 60
10.2 Finite observation and the need for an analytic envelope 61
10.3 Uniform conditioning from energy equivalence 61
10.4 A complete contraction estimate for preconditioned descent 62
10.5 Communication-round bounds from a finite spectrum 63
10.6 Branch certificates as invariants of a path subdivision 63
10.7 Why certificate termination needs quantitative input 64
10.8 Formal statement fidelity and nonvacuous comparison 64

11 Solved investigations: geometry and analysis 66
11.1 Conformal type and period structure 66
11.2 Moduli, compactification and quotient geometry 69
11.3 Harmonic observables and spectral calculations 70
11.4 Branch surfaces in mathematical physics 73

12 Solved investigations: physics, algorithms and certificates 75
12.1 Fields, energy and transformed physical equations 75
12.2 Exact algorithms and performance contracts 78
12.3 Objective comparison and limits of inference 81

13 Specialist applications with explicit analytical reductions 83
13.1 Elliptic periods and a complete differential equation 83
13.2 Regular singular equations and projective coordinates 84
13.3 A coupled-channel model with exact unitarity 85
13.4 Cylinder sewing and an exact Schur complement 86

13.5 Homology, vanishing cycles and continuation matrices 87
13.6 Torus isogenies and finite algebraic data 87
13.7 Twisted boundary conditions and observable spectra 88
13.8 Logical complexity and the effect of shared lemmas 89

14 Boundary solvability and a posteriori coordinate control 90
14.1 Harmonic distributions and interior regularity 90
14.2 Boundary barriers and continuity of the Dirichlet solution 91
14.3 The logarithmic singularity and independence of its cut-off 92
14.4 Residuals, admissible fields and a certified capacity interval 92
14.5 Error in the exponential coordinate on a fixed cut surface 93
14.6 A derivative margin and local inverse radius 93
14.7 Boundary approximation and the maximum-principle certificate 94
14.8 Periodic quadrature after uniformization 95

15 Proof status, reproducible certificates and quantitative evidence 96
15.1 A fixed and inspectable obligation universe 96
15.2 What the executed checks establish 97
15.3 Performance measurements with a strong conventional control 98
15.4 Maximality claims replaced by finite completion criteria 98
15.5 Theorem-by-theorem formalization-status register 99
15.6 Reproduction and release criteria 101

References 103

Chapter 1

Scope, mathematical objects and evidence

1.1 The subject of the monograph

Uniformization identifies the simply connected complex curves with three model surfaces. Its applications depend on the maps, metrics, periods and group actions through which that identification is realized. This monograph follows the seven subsections of §5 of Mikhail Lyubich's *Conformal Geometry and Dynamics of Quadratic Polynomials*, and develops the missing intermediate arguments needed to use the stated results quantitatively. The principal result concerns a complex manifold of complex dimension one. No corresponding classification of arbitrary higher-dimensional complex manifolds follows from it.

Three questions organize the applications. Mathematics asks which quantities survive passage to a canonical model and which global obstructions survive in the quotient. Physics asks which field equations and observables transform covariantly, how dimensions and boundary conditions enter, and which approximation errors can be bounded. Computer science asks how a finite representation, an algorithm and a certificate recover the specified mathematical output, with a cost that includes preprocessing, memory, communication and verification.

The previous PHI volumes provide the established expository dependencies on Cantor coding, finite observables, proper holomorphic maps, degree, normal families, conformal distortion and numerical comparisons [2, 3, 4, 5]. Their recorded checks are used with their original interpretation. A written result in those volumes is a written dependency. A tested numerical implementation remains a tested implementation. Neither category is described here as a proof-assistant theorem.

The present edition has been reconstructed from the retained textbook, the preceding public PHI monographs and the associated scientific records. The earlier delivery reports did not contain recoverable §5 manuscripts. Consequently the counts in this edition are obtained from its actual source files and generated registers; unconfirmed counts from the interrupted authoring attempts are not used as completion evidence.

1.2 Source order and proof order

The source sequence is retained in Chapter 3: §5.1, statement; §5.2, quotient classification; §5.3, smooth annuli; §5.4, relatively compact simply connected domains; §5.5, simply connected surfaces; §5.6, ends; §5.7, orbifolds. The proof dependency is not this linear order. In particular, the classification in §5.2 uses the uniformization proved in §5.5. We distinguish an assertion presented for orientation from a proposition already available for use in an argument.

The substantive dependency chain for open surfaces is

$$\begin{array}{c}\text{Dirichlet and local potential theory} \Downarrow \\ \text{annular coordinates and bounded disk uniformization} \Downarrow \\ \text{normalized disk exhaustion and compact convergence} \Downarrow \\ \text{global injectivity and surjectivity} \Downarrow \\ \text{disk–plane classification and quotient geometry.}\end{array}$$

The compact case then follows by removing one point and controlling the resulting end. Orbifold uniformization additionally requires an effective, orientable, good orbifold structure; the topological developability input is separated from the analytic uniformization.

1.3 Conventions

A Riemann surface is connected, Hausdorff and second countable, with holomorphic coordinate changes and no boundary unless a bordered surface is explicitly specified. A relatively compact domain has compact closure in the ambient surface. Smooth boundaries mean embedded smooth circles. Piecewise smooth boundaries are taken to be Jordan boundaries with finitely many nondegenerate corners and the usual local barrier property. Pathological non-Jordan boundary sets require a separate prime-end formulation and are not silently included.

The positive Laplacian in local Euclidean coordinates is

$$\Delta = \partial_x^2 + \partial_y^2 = 4\partial_z\partial_{\bar{z}}.$$

Thus $-\Delta$ is nonnegative in a Dirichlet energy problem. For a real function u, put

$$*du = -u_y\,dx + u_x\,dy.$$

Then $d(*du) = (\Delta u)\,dx \wedge dy$. A local conjugate v satisfies $dv = *du$, so $u + \mathrm{i}v$ is holomorphic. Circles about the origin are positively oriented counterclockwise. The inner boundary of a positively oriented annulus has clockwise orientation.

For $0 < r < R < \infty$, write

$$A(r,R) = \{z \in \mathbb{C} : r < |z| < R\}, \qquad L = \log(R/r), \qquad \operatorname{mod} A(r,R) = \frac{L}{2\pi}.$$

The condenser capacity for boundary values zero and one is the unhalved Dirichlet energy. In this convention $\operatorname{cap} A = 2\pi/L$ and $\operatorname{cap} A \cdot \operatorname{mod} A = 1$. The convention fixes every factor of 2π in the annular exponential map.

For a conformal metric $g = \rho^2|dz|^2$, $dA_g = \rho^2 dx\,dy$ and $\Delta_g = \rho^{-2}\Delta$. The canonical hyperbolic metric has curvature -1 and is $2|dz|/(1-|z|^2)$ on $\mathbb{D}$. A complex torus is $\mathbb{C}/(\mathbb{Z}\omega_1 + \mathbb{Z}\omega_2)$, where $\operatorname{Im}(\omega_2/\omega_1) > 0$ after orienting the basis.

1.4 Comparison contracts

A valid comparison begins with a common input class $\mathcal{X}$, a required output relation $\mathcal{R}(x,y)$ and an admissible error. Algorithms returning a scalar capacity and algorithms returning a full sampled field have different output obligations. Their costs are compared only after that distinction has been fixed.

For an implementation M and input x, the cost record is

$$\mathsf{C}(M,x) = (C_{\text{setup}}, C_{\text{arithmetic}}, C_{\text{bit}}, C_{\text{memory}}, C_{\text{depth}}, C_{\text{communication}}, C_{\text{checking}}).$$

It is accompanied by a normed error bound, a conditioning statement and the domain of validity. For q repeated evaluations, the total includes the single setup cost and all q queries. A fixed precision scalar operation count does not measure arbitrary-precision bit complexity. An expression involving log, exp or an elliptic integral has evaluation and rounding obligations of its own.

Logical complexity has two separate uses. The first is the structure of a derivation: premises, dependencies, branch cases and uniform versus instance-wise reasoning. The second is complexity in computational logic: decision problems, proof verification and finite-state temporal properties. A shorter proof may improve exposition without implying lower computational complexity. A finite-state model check can be complete for its model while saying nothing about an unmodeled network delay.

1.5 Interpretation of evidence

Written theorem.
A precise assertion with an argument in the document, relative to its identified prerequisites.

Imported prerequisite.
A stated result cited from an earlier PHI development or a standard primary mathematical source. The extent of the import is explicit.

Exact finite certificate.
A finite witness accepted by the delivered exact-arithmetic checker, together with a written soundness argument for the checker.

Numerical diagnostic.
A floating-point calculation with defined inputs, tolerances and output. Agreement is not a universal theorem.

Formalization specification.
A target for Lean, Rocq or another verifier. A specification is counted as kernel accepted only after the corresponding proof object has actually been checked.

Physical model.
An assumed constitutive or probabilistic model with an analytically derived consequence. The calculation does not validate the model experimentally.

No new proof-assistant kernel acceptance is asserted in this edition. The theorem register records the proof location, the dependency class and the available certificate for each registered assertion. The compiler, reference, privacy and checksum checks are publication checks and retain that designation.

1.6 The intended disciplinary connections

The mathematical analysis includes quotient classification, periods, divisors, algebraic curves, homology, harmonic conjugacy, Sobolev energy, Fourier operators and extremal approximation. Applied and theoretical physics enter through threshold scattering, periodic spectral problems, Euclidean field equations, thermal diffusion, classical worldsheet actions, elliptic moduli and brane-curve models. The high-energy and M/string-theory sections distinguish the derived mathematical identities from physical assumptions imported from the cited models [6, 7, 8].

Computational applications include graph and surface discretization, spectral solvers, condition-aware approximation, parallel work and depth, consensus, certified branch continuation and

finite-field cryptographic interfaces. Encryption does not follow from the existence of a complicated conformal map. Several negative examples identify precisely which information remains publicly invertible.

The engineering applications retain conservation laws, dimensional analysis, source and boundary data, discrete stability and implementation limits. Every subject is assigned either a concrete mathematical subproblem or an explicit boundary of applicability. An application inventory cannot establish that a particular mathematical transformation optimizes every problem in a discipline.

Chapter 2

Topological and analytic foundations

2.1 Covering surfaces and the lifted complex structure

Source relation: The construction supplies the transition from the statement in source §5.1 to the classification in §5.2. Covering and local-degree prerequisites are treated in the preceding PHI volume [2, Chapter 2].

Proposition 2.1 (U01: holomorphic structure on an unbranched cover)**.** *Let $p : \widetilde{S} \to S$ be a topological covering of a Riemann surface. There is a unique complex structure on $\widetilde{S}$ for which p is locally biholomorphic. Every deck transformation is holomorphic.*

Proof. Take an evenly covered coordinate neighborhood $U \subset S$ with coordinate $z : U \to z(U) \subset \mathbb{C}$. For each component $\widetilde{U}$ of $p^{-1}(U)$, use $z \circ p$ as a coordinate. A transition from $z \circ p$ to $w \circ p$ is exactly $w \circ z^{-1}$, restricted to the relevant overlap, and is holomorphic. These coordinates cover $\widetilde{S}$ and define a complex atlas. A second structure making p locally biholomorphic has the same local coordinates, so it is identical. If γ is a deck transformation, then $p \circ \gamma = p$; in the displayed coordinates γ is the identity between two sheets. Hence it is locally holomorphic, and its inverse has the same property. □

A connected Riemann surface is locally path connected and semilocally simply connected. Its universal cover may be constructed from homotopy classes of paths beginning at a fixed point. An evenly covered disk acts by appending a short path inside that disk. The lifting rule is well-defined because any two such short paths are homotopic relative to their endpoints. A loop acts by concatenation and determines a deck transformation. The construction identifies the deck group with the fundamental group after a convention for left or right concatenation has been fixed.

The covering acts freely: a deck transformation that fixes a point agrees with the identity on an evenly covered neighborhood. Path lifting then propagates that equality along every path, so it is the identity on the connected cover. Proper discontinuity is the local sheet-separation property. For quotient constructions, both properties are necessary. A discrete group with a stabilizer gives an orbifold quotient at the stabilized point, not an unbranched surface cover.

2.2 Closed forms and the period obstruction

Lemma 2.2 (U02: periods characterize exactness)**.** *Let α be a smooth closed real one-form on a connected smooth surface. It has a global primitive if and only if its integral around every closed piecewise smooth path is zero. If the surface is an annulus, it is enough to check one positively oriented generator of its first homology.*

Proof. If $\alpha = dv$, the integral along a path is the difference of endpoint values and vanishes on a loop. Conversely, choose a base point p and define $v(q) = \int_p^q \alpha$. Two paths from p to q differ by a closed path, so the hypothesis makes v well-defined. On a coordinate disk, the local Poincare lemma supplies a smooth primitive; v differs from it by a constant. Thus $dv = \alpha$. For an annulus, deformation retraction to a core circle identifies its first homology with $\mathbb{Z}$. Stokes' theorem makes integrals of a closed form invariant under homology. Every period is therefore an integer multiple of the period on the chosen core. □

For a harmonic function u, the form $*du$ is closed. The obstruction to a global harmonic conjugate is consequently finite-dimensional on a finite-type surface: one must retain its periods on a homology basis. This is the exact global information that disappears in a calculation performed solely in local coordinate disks.

Proposition 2.3 (U03: exponentiation kills an integral period lattice)**.** *Suppose a locally defined holomorphic function $F = u + \mathrm{i}v$ changes by $\mathrm{i}pk$, $k \in \mathbb{Z}$, on analytic continuation around a loop, where $p \neq 0$. Then*

$$z \longmapsto \exp\left(\frac{2\pi}{p} F(z)\right)$$

is single valued and holomorphic. Its winding on a generator with period p is one.

Proof. Continuation changes the exponent by $2\pi\mathrm{i}k$, which leaves the exponential unchanged. Local definitions therefore agree on overlaps and patch to a holomorphic function. Along the generator, the change in its continuous argument is $(2\pi/p)p = 2\pi$, so its winding is one. This calculation does not assert injectivity; properness and degree will supply that conclusion in the annular application. □

The same argument works for a period group contained in $2\pi\mathrm{i}\mathbb{Z}$ without choosing a preferred generator. For a rank-two period lattice, one exponential does not remove both periods. Quotienting by the full lattice produces a complex torus. This distinction becomes decisive in the three-channel scattering model of Chapter 6.

2.3 Dirichlet minimization on a bordered surface

Let Ω be a compact connected smooth bordered Riemann surface with nonempty boundary. Choose any smooth conformal metric. The Dirichlet integral

$$E(v) = \int_\Omega |dv|_g^2 \, \mathrm{d}A_g$$

is independent of the conformal factor. Locally, the inverse metric contributes ρ^{-2} and area contributes ρ^2, leaving $v_x^2 + v_y^2$.

The construction below uses the Sobolev completion of smooth functions and the trace-zero space $H_0^1(\Omega)$. The standard Hilbert-space completeness of these spaces and the local trace theorem are foundational analytic inputs. They are distinguished from uniformization: neither requires a global conformal coordinate on Ω.

Lemma 2.4 (U04: coercivity of the trace-zero energy)**.** *There is a constant C_Ω such that*

$$\|v\|_{L^2(\Omega)} \leq C_\Omega \, \|dv\|_{L^2(\Omega)}, \qquad v \in H_0^1(\Omega).$$

Thus $\langle v, w\rangle_E = \int_\Omega \langle dv, dw\rangle_g \, \mathrm{d}A_g$ is a complete inner product on $H_0^1(\Omega)$ equivalent to its H^1 inner product.

Proof. First work in a coordinate rectangle with one boundary side on which $v = 0$. The fundamental theorem of calculus and Cauchy–Schwarz give

$$|v(x,y)|^2 = \left| \int_0^y v_y(x,s)\,\mathrm{d}s \right|^2 \le h \int_0^h |v_y(x,s)|^2\,\mathrm{d}s,$$

so integration bounds the L^2 norm by the gradient on that rectangle. For an interior rectangle, its mean can be compared to the mean on an overlapping rectangle by applying the same one-dimensional estimate to differences along horizontal and vertical segments. A finite connected chain of overlapping coordinate rectangles connects every member of a finite cover to a boundary rectangle. Summing the resulting estimates gives a finite constant depending on the cover and the metric comparison bounds. Smooth trace-zero functions are dense in H_0^1 by definition, so the inequality extends by completion. Equivalence with the complete H^1 norm proves completeness for the energy norm. □

Theorem 2.5 (U05: existence, uniqueness and energy orthogonality)**.** *For smooth prescribed boundary data and any H^1 extension g, there is a unique $u \in g + H_0^1(\Omega)$ minimizing E. It satisfies*

$$\int_\Omega \langle du, dw\rangle_g \,\mathrm{d}A_g = 0 \quad (w \in H_0^1(\Omega)),$$

and for every competitor v with the same trace,

$$E(v) = E(u) + E(v-u).$$

Proof. On the energy Hilbert space, $\ell(w) = -\int \langle dg, dw\rangle$ is a bounded linear functional. The Riesz representation theorem gives a unique $h \in H_0^1$ with $\langle h, w\rangle_E = \ell(w)$. Set $u = g + h$. The displayed weak equation follows. Write $v = u + w$ with $w \in H_0^1$ and expand the square. Its cross term vanishes by the weak equation. The identity proves minimality; equality implies $E(w) = 0$, and coercivity implies $w = 0$. Thus the minimizer is unique. The representation argument may equivalently be written as orthogonal projection onto the closed affine space of admissible traces. □

For completeness, the Riesz representation used here has a direct Hilbert proof. If $\ell \neq 0$, its kernel is closed and has codimension one. Choose a unit vector e perpendicular to that kernel. Decomposing $w = w_0 + te$ gives $\ell(w) = t\ell(e)$, so ℓ is represented by $\ell(e)e$ in the real Hilbert convention. The needed perpendicular projection follows from a minimizing sequence for distance to a closed convex subspace: the parallelogram identity makes that sequence Cauchy, and its limit is orthogonal by differentiation in each subspace direction.

2.4 Regularity, boundary values and the maximum principle

The weak solution is classically harmonic in every interior coordinate disk. One route to this fact is to mollify on smaller disks. The weak equation commutes with convolution, giving smooth harmonic mollifications. Their local mean-value property passes to the L^1 limit. A function with the mean-value property has a smooth Poisson representation on each smaller disk and is harmonic there. This is the local Weyl lemma in the form required by the construction.

The smooth boundary case has a barrier in a coordinate neighborhood. An exterior tangent circle supplies a logarithmic harmonic barrier, positive on the local interior and zero at the tangency point. At a nondegenerate corner, an exterior cone and the harmonic functions $r^a \sin(a\theta)$ in an appropriate wedge supply a positive barrier after rotation. Comparison with the barrier controls the solution by the oscillation of its boundary data. Smooth data are first extended smoothly, and the local estimates pass from smooth approximations to the variational solution.

The solution therefore extends continuously with the prescribed values. Corners require the stated barrier assumption; a bare use of the phrase "piecewise smooth" does not justify arbitrary accumulating cusps.

Lemma 2.6 (U06: maximum and strict positivity)**.** *A continuous function on $\overline{\Omega}$, harmonic on connected Ω, takes its maximum and minimum on the boundary unless it is constant. In particular, a nonconstant harmonic function with boundary values zero and one satisfies $0 < u < 1$ in Ω.*

Proof. At an interior maximum, the mean-value property says that the average on each sufficiently small circle equals the maximum. Continuity and the upper bound force equality on the entire circle, and the Poisson formula forces constancy in the disk. The set on which the function equals its maximum is consequently both open and closed in the connected domain. It is the whole domain. Applying the same argument to $-u$ handles a minimum. Compactness of the closure and continuity supply existence of the extrema. □

This argument also proves a sup-norm error certificate. If u and $\widetilde{u}$ are harmonic with boundary discrepancy at most ε, then $\|u - \widetilde{u}\|_{\infty} \le \varepsilon$ on the full domain. Its cost is the cost of certifying the boundary discrepancy, not the number of interior visualization pixels.

2.5 Green functions and a normalized logarithmic pole

The sign convention is fixed by $\Delta \log|z| = 2\pi\delta_0$ in distributions. To verify it, integrate by parts outside a circle of radius ε, retain the inward normal of the punctured domain, and let $\varepsilon \to 0$. The boundary integral of the radial derivative supplies 2π; the remaining term vanishes because the test function differs from its value at zero by $O(\varepsilon)$.

Proposition 2.7 (U07: Green function with a single pole)**.** *On a smooth relatively compact bordered domain D, for each $p \in D$ there exists a function $G_D(\cdot, p)$, zero continuously on ∂D, positive on $D \setminus \{p\}$, harmonic away from p, and satisfying*

$$G_D(z, p) = -\log|z| + h(z)$$

in a local coordinate $z(p) = 0$, with h harmonic near zero. It is unique.

Proof. Choose a smooth cutoff χ supported in a coordinate disk and equal to one near p. The function $s = -\chi \log|z|$ has zero boundary trace and $-\Delta s = 2\pi\delta_p + q$, where q is a smooth compactly supported function away from p in the distribution-density convention. Solve $-\Delta h = -q$ with zero trace by the same coercive Hilbert-space argument as in Theorem 2.5. Local regularity makes h smooth, and $G = s + h$ has the stated pole and boundary data. On the complement of a small disk, its inner boundary values are positive for sufficiently small radius; the maximum principle gives $G \ge 0$. Strict positivity follows from connectedness and the pole. The difference of two candidates is bounded near p, hence removable there, harmonic throughout D and zero on its boundary. The maximum principle gives uniqueness. □

The inhomogeneous weak equation uses $\int qv$, bounded by the Poincare inequality. The local regularity of a smooth right-hand side follows by subtracting a local fundamental-solution convolution, leaving a distributionally harmonic remainder. Thus the construction does not invoke disk uniformization of D.

2.6 Topological exhaustion and its exact role

The global proof uses a surface-theoretic fact: a noncompact simply connected second-countable surface admits a nested exhaustion by relatively compact Jordan disks with smooth boundary. Here the topology is independent of the subsequently constructed complex coordinate.

A constructive route begins with a locally finite triangulation and a countable compact exhaustion. Connect each finite compact stage to a fixed base disk by finitely many arcs, and take a compact regular neighborhood. Boundary circles can be filled on the side not containing the chosen unbounded end. The Jordan–Schoenflies theorem for simply connected surfaces guarantees those filling disks and prevents a handle. Only finitely many boundary components occur at each stage. Enlarging the finite stage and smoothing its boundary produces the desired nest. The absence of handles follows alternatively by abelianizing the standard polygon presentation: a handle contributes two independent first-homology classes, impossible on a simply connected surface.

Evidence classification. Locally finite triangulation, regular neighborhoods and the Jordan–Schoenflies theorem are explicitly declared topological prerequisites, as in the source's Lemma 1.80. Their full foundational formalization is not supplied by a polygon drawing or by the finite checks in this release.

A similar finite polygon classification gives that a compact simply connected orientable surface is a sphere. Cutting along a spanning tree in the triangulation and a dual spanning tree produces a paired-edge polygon. Each surviving oriented handle pair contributes two generators to the abelianization of its fundamental group. Simple connectedness eliminates all handle pairs, leaving the sphere. This identifies the topological input used in source Theorem 5.6; the complex structure is still to be determined analytically.

2.7 Imported analytic dependencies and noncircularity

The preceding PHI monograph establishes the local power model for holomorphic maps, proper-map degree, the argument principle, Little Montel, injective normal limits and the Koebe growth and quarter estimates [2, Chapters 2 and 4]. Their uses in this volume are local or planar. In particular, Koebe's theorem is applied to a holomorphic injection whose domain is an already uniformized finite disk. It is not applied to the unknown global surface before the exhaustion limit has been constructed.

For reference, the specific planar inequalities used below are, for a univalent $g : \mathbb{D} \to \mathbb{C}$ with $g(0) = 0$ and $g'(0) = 1$,

$$\frac{|z|}{(1+|z|)^2} \le |g(z)| \le \frac{|z|}{(1-|z|)^2}, \qquad \mathbb{D}_{1/4} \subset g(\mathbb{D}).$$

The local uniform limit of injective holomorphic functions is injective or constant. At a normalized base point its derivative is one, excluding the constant case. Cauchy's formula proves derivative convergence on every smaller coordinate disk, so this normalization survives the limit.

These are precise dependency imports. The results of §5 do not depend on any numerical graph or application later in this monograph. The dependency register keeps the theoretical proof graph separate from the computational and publication graphs.

Chapter 3

The seven source subsections

3.1 Source §5.1: the three simply connected models

Source relation: Source Theorem 5.1, physical page 115. The statement is a classification up to biholomorphism, with the surface conventions fixed in Chapter 1.

Theorem 3.1 (U08: uniformization, with the proof dependencies exposed)**.** *Every simply connected Riemann surface is biholomorphic to exactly one of* $\mathbb{P}^1(\mathbb{C})$*,* $\mathbb{C}$ *and* $\mathbb{D}$*.*

Proof. For a noncompact surface, Theorem 3.11 below constructs a normalized conformal map onto a disk of finite radius or onto $\mathbb{C}$. A finite-radius disk is biholomorphic to $\mathbb{D}$ by scaling. For a compact surface, Theorem 3.12 below gives the sphere. Compactness distinguishes the sphere from the two noncompact models. If $\mathbb{C}$ and $\mathbb{D}$ were biholomorphic, the resulting bounded nonconstant entire function would contradict Liouville's theorem. That theorem follows from Cauchy's estimate: for an entire function bounded by M, $|f'(z)| \leq M/R$ for every $R > 0$, so $f' = 0$. □

The order of this proof is deliberately explicit. U08 names the final theorem; its construction is in U18 and U19, whose arguments do not appeal back to U08. The finite source statement does not yield a finite running-time algorithm on an arbitrary encoded surface. A computational uniformization algorithm must specify its domain representation, target normalization and error criterion.

3.1.1 Normalization and its remaining freedom

A sphere has a three-complex-parameter Mobius group. Three distinct marked points determine a unique Mobius normalization. For a disk, a point and a tangent direction determine a normalization. For the plane, an affine normalization fixes a point and a nonzero derivative. These freedoms are mathematical symmetries of the output; failure to fix them makes a numerical comparison of two otherwise correct maps meaningless.

Proposition 3.2 (U09: uniqueness of a normalized disk coordinate)**.** *Let* $f, g : S \to \mathbb{D}$ *be biholomorphisms with* $f(p) = g(p) = 0$ *and positive real derivatives in the same local coordinate. Then* $f = g$*.*

Proof. The automorphism $h = g \circ f^{-1}$ fixes zero. Schwarz's lemma gives $|h(z)| \leq |z|$, and its application to h^{-1} gives the reverse inequality. Equality in Schwarz's lemma makes $h(z) = \mathrm{e}^{\mathrm{i}\theta} z$. The ratio of the two positive derivatives is positive real and has modulus one, hence is one. Thus h is the identity. □

For algorithmic use, normalization is an input contract. A discretization that pins a boundary vertex, an analytic proof that fixes an interior point, and a physical model that fixes a flux are not using the same gauge. The transformation between their normalizations must be carried through any error or sensitivity calculation.

3.2 Source §5.2: classification by universal covers

Source relation: Source Theorem 5.2, physical page 116. The word "isometries" in the hyperbolic case requires orientation preservation, freeness and proper discontinuity for an ordinary Riemann-surface quotient.

Theorem 3.3 (U10: quotient classification)**.** *A Riemann surface is either the sphere; a quotient* $\mathbb{C}/\Lambda$ *by a discrete translation group of rank zero, one or two; or* $\mathbb{D}/\Gamma$*, where* $\Gamma < \mathrm{Aut}(\mathbb{D})$ *is discrete, acts freely and properly discontinuously. The rank-zero and rank-one flat cases are* $\mathbb{C}$ *and* $\mathbb{C}^*$*.*

Proof. Lift the complex structure to the universal covering by U01 and apply U08. In the spherical case, every nonidentity Mobius map has a fixed point: its fixed-point equation is quadratic, with the point at infinity included. Since deck transformations act freely, the deck group is trivial.

An automorphism of $\mathbb{C}$ is affine. To see this without assuming polynomiality, regard infinity as an isolated singularity. An essential singularity there is incompatible with injectivity: choose a regular attained value in a fixed compact region and use the Casorati theorem followed by the local inverse near that value; a sufficiently close value obtained far away also has a preimage near the chosen point. A removable singularity would make the entire map bounded. Thus infinity is a pole, so the map is polynomial. An injective polynomial has degree one, by its local critical-point structure or generic fibre count. An affine map $az + b$ with $a \neq 1$ has a fixed point. Hence every nonidentity deck transformation is a translation.

A discrete subgroup $\Lambda \subset \mathbb{R}^2$ is free abelian of rank at most two. For rank one, choose its shortest nonzero vector ω; division along its line shows every collinear vector is an integral multiple. If noncollinear vectors exist, choose a vector with least positive perpendicular distance after reducing the parallel coordinate modulo ω. Discreteness guarantees the minimum in a compact strip. Subtracting integer multiples of these two vectors reduces any lattice vector to a bounded fundamental parallelogram; minimality of the perpendicular coordinate and then of $|\omega|$ forces the remainder to zero. This gives a rank-two lattice. In the rank-one case $\exp(2\pi \mathrm{i} z/\omega)$ identifies the quotient with $\mathbb{C}^*$.

In the disk case the lifted atlas identifies deck transformations with holomorphic disk automorphisms. Their action inherits freeness and proper discontinuity from covering theory. Conversely, the listed actions produce Riemann-surface quotients using evenly covered coordinate disks. Thus every listed quotient is admissible. □

3.2.1 Metric content of the classification

For $a \in \mathbb{D}$, the disk automorphism $b_a(z) = (z - a)/(1 - \bar{a}z)$ satisfies

$$1 - |b_a(z)|^2 = \frac{(1 - |a|^2)(1 - |z|^2)}{|1 - \bar{a}z|^2}, \qquad |b_a'(z)| = \frac{1 - |a|^2}{|1 - \bar{a}z|^2}.$$

Consequently $2|db_a|/(1 - |b_a|^2) = 2|dz|/(1 - |z|^2)$. The metric descends to every hyperbolic quotient. It is complete because a finite-length path lifts locally and cannot escape to the disk boundary: the radial distance to $|z| = 1$ diverges. The quotient construction therefore supplies a complete curvature--1 metric.

The projective structure on the sphere is canonical. A particular round metric requires a normalization of the spherical coordinate. A flat torus has a translation-invariant metric unique up to scale inside its fixed conformal class. These statements concern different levels of geometric structure; a conformal equivalence does not generally preserve physical Euclidean length or area.

3.2.2 Example: a rectangular torus

Let $\Lambda = \mathbb{Z} + \mathrm{i}b\mathbb{Z}$, $b > 0$. The function $\mathrm{e}^{2\pi\mathrm{i}(mx+ny)}$, with $z = x + \mathrm{i}by$ and $(x, y) \in [0, 1]^2$, is single valued on the quotient. For the induced flat metric,

$$-\Delta \mathrm{e}^{2\pi\mathrm{i}(mx+ny)} = 4\pi^2 \left(m^2 + \frac{n^2}{b^2} \right) \mathrm{e}^{2\pi\mathrm{i}(mx+ny)}.$$

This spectral output retains the modulus b. Replacing every flat torus by a unit square would change its spectrum even though all tori have the same topological genus.

3.3 Source §5.3: smooth annuli and the period coordinate

Source relation: Source Proposition 5.3, physical page 116. The proof below establishes degree independently of an assumed equipotential foliation.

Theorem 3.4 (U11: capacity, period and annular uniformization)**.** *Let A be a relatively compact smooth annulus. Let u be harmonic, with value zero on the inner boundary and one on the outer boundary. With a positively oriented core γ, set*

$$p = \int_\gamma *du.$$

Then $p = E(u) > 0$, and a local conjugate v defines a biholomorphism

$$F = \exp\left(\frac{2\pi}{p}(u + \mathrm{i}v) \right) : A \longrightarrow A(1, \mathrm{e}^{2\pi/p}).$$

In particular, $\operatorname{mod} A = 1/p$.

Proof. Existence, uniqueness and boundary continuity of u follow from U05 and the boundary argument of Chapter 2. Green's identity gives

$$E(u) = \int_{\partial A} u\, \partial_n u \, \mathrm{d}s = \int_{\partial_o A} \partial_n u \, \mathrm{d}s = \int_{\partial_o A} *du = p.$$

The inner boundary term is zero. The last equality uses that $*du$ is closed and the outer boundary is homologous to the positive core. Since the boundary values differ, u is nonconstant, so $E(u) > 0$.

U02 and U03 make F single valued. The maximum principle gives $1 < |F| < \mathrm{e}^{2\pi/p}$. A compact subset of the target has log modulus separated from both endpoint values. Its preimage lies where u is separated from zero and one and is therefore relatively compact in A. The preimage is closed there, so F is proper. A nonconstant holomorphic map is open; a proper map into a locally compact target is closed. Connectedness of the target shows F is onto.

It remains to prove that its degree is one. Take smooth collars sufficiently close to the two boundary curves. On each boundary circle the Hopf boundary lemma gives a nonzero normal derivative, so the image of that circle under F traverses the corresponding target circle with positive orientation when the core orientation is used. Its total change of argument is 2π, by the period calculation. Equivalently, F_* sends the generator of $H_1(A; \mathbb{Z})$ to the generator of

the target annulus. For a proper orientation-preserving map between annuli the integer in this homology map is its degree: cut both annuli along an arc transverse to a regular target value and count oriented inverse arcs, or apply the boundary degree identity in relative homology. Thus the degree is one. The local degrees of a holomorphic map are positive integers; a degree-one map has exactly one unramified preimage at each point. Its inverse is holomorphic by the local inverse theorem. □

3.3.1 The normalization discrepancy in the printed source

The source defines $p = \int_\gamma *du$ and writes the multiplier $2\pi/p$ in its exponential. It subsequently gives the target outer radius as $\mathrm{e}^{1/p}$. With those definitions, the outer boundary has $u = 1$, so its modulus is exactly $\mathrm{e}^{2\pi/p}$. The missing factor is therefore determined by direct substitution. It is not a discretionary choice of annular notation.

On a round annulus $A(1, R)$, $u = \log|z|/\log R$ and $v = \arg z/\log R$. The period is $p = 2\pi/\log R$. The corrected formula gives $F = z$ after a unit-modulus factor, and $\mathrm{e}^{2\pi/p} = R$. The printed radius gives $R^{1/(2\pi)}$, which fails this identity unless $R = 1$, the degenerate excluded case.

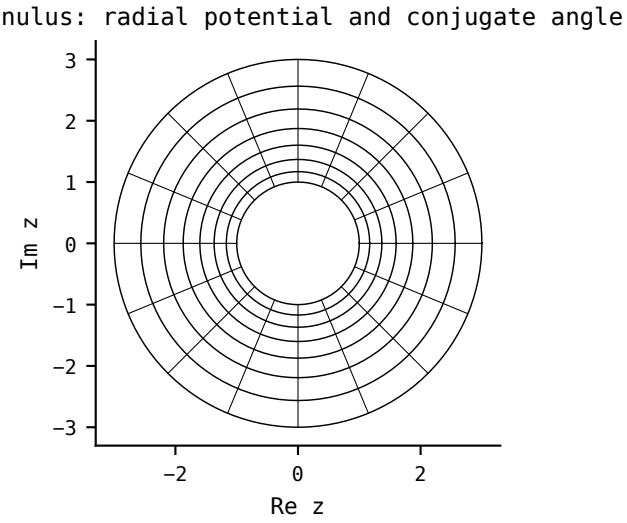


Figure 3.1: Logarithmic coordinates on an annulus. The radial coordinate becomes an interval; the angular coordinate remains periodic. The period is retained in the exponential reconstruction.

3.3.2 Corners, uniqueness and available output

For finitely many admissible corners, solve the continuous Dirichlet problem using the local barriers and apply the construction to smooth interior collars. The period is independent of the collar. Properness follows from the same boundary separation, and degree is computed on an interior core, so boundary differentiability at the corners is not required. The source conclusion therefore persists for the stated piecewise smooth class.

A biholomorphism of round annuli has the form cz or c/z after the radii are matched, as follows by applying uniqueness of the harmonic Dirichlet solution to $\log|f|$. Thus the modulus is a complete conformal invariant of a doubly connected nondegenerate bordered domain. It is not a complete invariant of a domain with three or more boundary components.

Comparative conclusion. A planar field calculation asking only for flux or condenser capacity reduces to the scalar p. Recovering the full conformal coordinate also requires the harmonic potential and its conjugate periods. The theorem permits a reduction in output dimension only when the specified observable depends solely on modulus.

3.4 Source §5.4: relatively compact simply connected domains

Source relation: Source Proposition 5.4, physical pages 116–117. The source's punctured-annulus limit is compared with a Green-function construction that makes nondegeneracy and degree explicit.

Theorem 3.5 (U12: the Green coordinate of a bounded disk)**.** *Let D be a relatively compact simply connected Jordan domain on a Riemann surface, with the boundary regularity specified above. Let $G_D(z,p)$ be its Green function. Then*

$$f(z) = \exp\bigl(-G_D(z,p) - \mathrm{i}G_D^*(z,p)\bigr)$$

patches to a biholomorphism $D \to \mathbb{D}$, with a simple zero at p.

Proof. On $D \setminus \{p\}$, the only homology generator surrounds p. The local expansion $G = -\log|z| + h(z)$ gives period -2π for $*dG$. Consequently the exponential is single valued. Locally take a harmonic conjugate h^*; then

$$f(z) = c\,z\,\exp[-h(z) - \mathrm{i}h^*(z)], \qquad |c| = 1.$$

It extends holomorphically across p, and its derivative there is nonzero. Positivity of G gives $|f| < 1$, and zero boundary values give $|f| \to 1$ at every boundary point. The same compactness argument used for U11 proves properness into $\mathbb{D}$.

A proper nonconstant holomorphic map has constant finite degree. The fibre above zero consists only of p, since the exponential is nonzero elsewhere, and the local expansion shows its multiplicity is one. Thus its degree is one. Surjectivity follows from openness and closedness; positivity of local multiplicity then proves injectivity and a holomorphic inverse. □

3.4.1 What must be supplied to the punctured-annulus proof

The source removes a coordinate disk around p, uniformizes the remaining annulus and takes a normal limit. Compact convergence of bounded holomorphic functions alone does not exclude a constant limit. A complete use of that route requires a normalization and a lower bound at a fixed interior location, or an equivalent capacity argument. The source's references to Euclidean distance also require a declared auxiliary metric when D lies on an abstract surface.

The Green construction resolves these tasks through a fixed pole coefficient. The simple-zero expansion proves nondegeneracy before any global degree conclusion. Properness follows from boundary values, and degree is computed from a known fibre. The proof contains no appeal to the statement that an arbitrary simply connected open surface has already been uniformized.

Corollary 3.6 (U13: Green function and conformal radius)**.** *If $f : D \to \mathbb{D}$ is normalized by $f(p) = 0$, then*

$$G_D(z,p) = -\log|f(z)|.$$

In a local coordinate $z(p) = 0$, write $G_D(z,p) = -\log|z| + H_D(p) + o(1)$. The conformal radius is

$$r_D(p) = \frac{1}{|f'(p)|} = \mathrm{e}^{H_D(p)}.$$

Proof. The two Green functions have the same boundary values and logarithmic pole coefficient, so uniqueness in U07 makes them equal. Expanding $f(z) = f'(p)z + O(z^2)$ gives $H_D(p) = -\log|f'(p)|$, hence the radius formula. □

3.4.2 A domain-monotonicity consequence

For nested regular domains $D \subset E$ and $p \in D$, the function $G_E - G_D$ is harmonic on D after its logarithmic poles cancel, and its boundary values are nonnegative. Hence $G_E \geq G_D$ on D, with strict inequality unless the domains agree in the connected setting. Their regular parts satisfy $r_E(p) \geq r_D(p)$. This furnishes a potential-theoretic interpretation of the normalized radii in the next subsection.

The conformal radius depends on the local coordinate used to normalize derivatives. Ratios at the same marked coordinate and monotonicity under a fixed normalization are invariant statements. An absolute numerical radius in an arbitrary chart is not a physical distance.

3.5 Source §5.5: the open and compact alternatives

Source relation: Source Theorems 5.5 and 5.6, physical page 117. The argument below supplies the surjectivity step after compact convergence.

Let S be a noncompact simply connected Riemann surface, $p \in S$, and z a fixed local coordinate at p. Choose the nested disk exhaustion described in Chapter 2. By U12 each D_n admits a unique map

$$f_n : D_n \longrightarrow \mathbb{D}_{R_n}, \qquad f_n(p) = 0, \quad f_n'(p) = 1.$$

The radius is determined by the derivative normalization.

Lemma 3.7 (U14: monotonicity of normalized radii)**.** *If $D_m \subset D_n$, then $R_m \leq R_n$. If the inclusion is proper, the inequality is strict.*

Proof. The transition map $g = f_n \circ f_m^{-1} : \mathbb{D}_{R_m} \to \mathbb{D}_{R_n}$ fixes zero and has derivative one. Normalize the two radii to unit disks and apply Schwarz's lemma. This gives $R_m/R_n \leq 1$. Equality makes the normalized map a rotation; the derivative condition makes it the identity. Then $f_n(D_m) = \mathbb{D}_{R_n}$, and injectivity of f_n forces $D_m = D_n$. □

Lemma 3.8 (U15: a diagonal normal limit)**.** *A subsequence of f_n converges locally uniformly on S to an injective holomorphic map f with $f(p) = 0$ and $f'(p) = 1$.*

Proof. Fix m. For $n \geq m$, $f_n \circ f_m^{-1}$ is univalent on $\mathbb{D}_{R_m}$, fixes zero and has derivative one. The Koebe growth estimate bounds it uniformly on every smaller concentric disk. Pulling back gives a uniform bound for f_n on every compact subset of D_m. Little Montel supplies a convergent subsequence there. Apply this successively on an increasing collection of compact subdisks exhausting all D_m, and take the diagonal subsequence. The limits agree on overlaps because they are limits of the same subsequence. The patched map is holomorphic. Cauchy's formula preserves its value and derivative at p. An injective normal limit is either injective or constant; the nonzero derivative excludes a constant. □

Local convergence and injectivity have now been proved. They do not by themselves identify $f(S)$. The following quantitative Schwarz estimate supplies the missing image control in the finite-radius case.

Lemma 3.9 (U16: near-extremal Schwarz maps)**.** *Let $h : \mathbb{D} \to \mathbb{D}$ satisfy $h(0) = 0$ and $h'(0) = a \in (0, 1]$. For $|z| \leq r < 1$,*

$$|h(z) - z| \leq r(1 - a)\frac{1 + r}{1 - r}.$$

Proof. Schwarz's lemma makes $q(z) = h(z)/z$ holomorphic on $\mathbb{D}$, with $|q| \le 1$ and $q(0) = a$. Schwarz–Pick gives $|(q-a)/(1-aq)| \le |z|$. Thus $q = (a+\zeta)/(1+a\zeta)$ with $|\zeta| \le r$. Subtraction yields

$$|q-1| = (1-a)\frac{|1-\zeta|}{|1+a\zeta|} \le (1-a)\frac{1+r}{1-r}.$$

Multiplication by $|z| \le r$ gives the result. The case $a = 1$ is the equality case of Schwarz's lemma. □

Lemma 3.10 (U17: surjectivity of the exhaustion limit)**.** *Let $R = \sup_n R_n \in (0, \infty]$. The map f in U15 has image $\mathbb{D}_R$, with $\mathbb{D}_\infty = \mathbb{C}$.*

Proof. Suppose first that $R < \infty$. For fixed $m \le n$, define

$$h_{mn}(w) = \frac{1}{R_n} f_n(f_m^{-1}(R_m w)).$$

It maps $\mathbb{D}$ to $\mathbb{D}$, fixes zero and has derivative $a_{mn} = R_m/R_n$. For $|w| = r$, U16 implies

$$|f_n(f_m^{-1}(R_m w)) - R_m w| \le (R_n - R_m)\, r \left(\frac{1+r}{1-r} + 1\right) = \frac{2r(R_n - R_m)}{1-r}.$$

Take the convergent subsequence and obtain the same inequality with R_n replaced by R. Given $0 < s < R$, choose $r < 1$ and then m sufficiently large that

$$rR_m - s > \frac{2r(R - R_m)}{1-r}.$$

On the circle $|w| = r$, Rouche's theorem then says that $f(f_m^{-1}(R_m w)) - y$ has one zero for every $|y| \le s$, because it is a strict perturbation of $R_m w - y$. Hence $\mathbb{D}_s \subset f(D_m)$. As $s < R$ was arbitrary, $\mathbb{D}_R \subset f(S)$. Conversely each f_n has modulus below R, so $|f| \le R$. Since f is nonconstant, the maximum principle makes $|f| < R$.

If $R = \infty$, the univalent map $f \circ f_m^{-1}$ on $\mathbb{D}_{R_m}$ fixes zero and has derivative one. The scaled Koebe quarter theorem gives $\mathbb{D}_{R_m/4} \subset f(D_m)$. The radii tend to infinity, so every complex number belongs to the image. □

Theorem 3.11 (U18: open simply connected uniformization)**.** *A noncompact simply connected Riemann surface is biholomorphic to $\mathbb{D}$ or $\mathbb{C}$.*

Proof. U15 gives an injective holomorphic map and U17 identifies its image. Its derivative is nonzero at every point because an injective holomorphic map has local degree one. The local inverse theorem gives a holomorphic inverse. A finite-radius image is rescaled to $\mathbb{D}$. □

Theorem 3.12 (U19: compact simply connected uniformization)**.** *A compact simply connected Riemann surface is biholomorphic to $\mathbb{P}^1(\mathbb{C})$.*

Proof. The compact orientable surface classification identifies the underlying surface with a sphere. Remove a point p; the complement is simply connected and noncompact, so U18 makes it biholomorphic to $\mathbb{D}$ or $\mathbb{C}$. If the image is $\mathbb{D}$, the bounded map extends across p by the removable-singularity theorem and gives a nonconstant holomorphic function on a compact surface. Such a function is constant by the maximum principle, a contradiction.

Thus there is a biholomorphism $f : S \setminus \{p\} \to \mathbb{C}$. As $z \to p$, necessarily $|f(z)| \to \infty$: otherwise a sequence approaching p would have images in a compact disk, whose inverse image under the continuous inverse f^{-1} is compact in $S \setminus \{p\}$. The function $1/f$ therefore tends to zero near p after excluding a compact neighborhood of the unique zero of f, and extends holomorphically

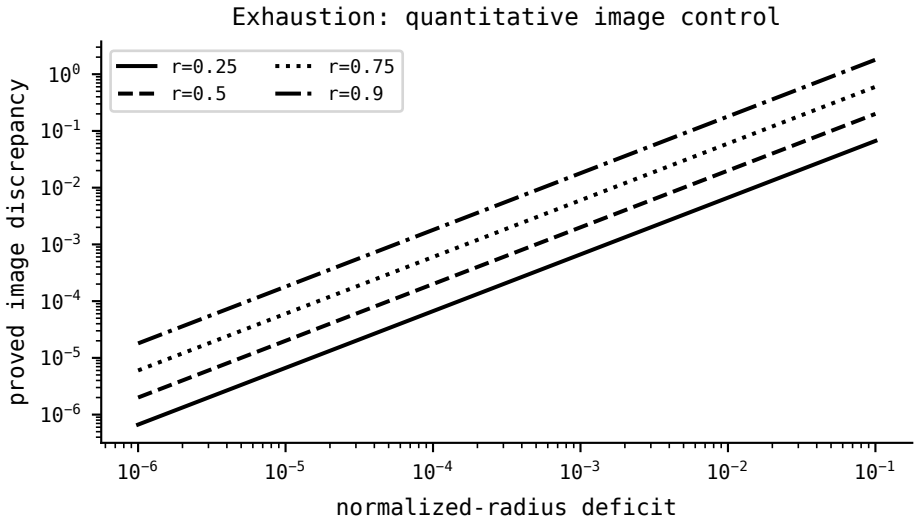


Figure 3.2: Finite-radius exhaustion: the explicitly proved image-error envelope tends to zero as the radius deficit decreases. The display evaluates U17's bound for several fixed interior circles.

with a zero at p. Defining $f(p) = \infty$ gives a continuous holomorphic map to the sphere. It is bijective because the original map is bijective on the complements. Its local degree at p must be one: a higher order would give multiple nearby preimages of a large regular value. Hence it and its inverse are holomorphic everywhere. □

3.5.1 The significance of an infinite radius

An unbounded sequence of normalized radii is not a numerical divergence to be suppressed by rescaling each output independently. It identifies the parabolic conformal type of the marked surface. A finite-radius sequence identifies a hyperbolic type. Neither a finite list of computed radii nor a fitted extrapolation proves which alternative holds without an a priori bound or a certified exhaustion estimate.

The proof also exposes a stability question: the size of the basepoint derivative fixes a scale. A family can degenerate when that derivative vanishes or when the marked point approaches the boundary. A numerical convergence test must therefore record the normalization and a compact interior region on which its estimates are uniform.

3.6 Source §5.6: extension to tame ends

Source relation: Source Lemma 5.7 and Corollary 5.8, physical page 118. The argument uses annular representatives of a proper end map and separates cusp and circle ends.

A tame end has an annular neighborhood. In an ideal conformal completion, a cusp is a missing point modeled by $0 < |z| < \varepsilon$; a circle end is modeled by $r < |z| < 1$ approaching $|z| = 1$. The phrase "proper map of ends" is used here in its local finite-covering sense: sufficiently small target end neighborhoods have an appropriate source component on which the map is proper of finite degree. A weak sequential condition on an arbitrary nonproper holomorphic map is insufficient.

Proposition 3.13 (U20: extension across a cusp)**.** *A nonconstant proper holomorphic map of cusp ends extends across the missing points. In local coordinates it has the form*

$$f(z) = az^d(1 + O(z)), \qquad a \neq 0, \quad d \in \mathbb{N}_{>0}.$$

It is unbranched sufficiently near the puncture away from the puncture itself.

Proof. The target puncture coordinate is bounded on a small source punctured disk. Removability extends the map to the center. Properness toward the chosen end forces its value there to be the target puncture. Nonconstancy gives a finite positive vanishing order d and the expansion. Differentiation yields $f'(z) = az^{d-1}(d + O(z))$, nonzero for all sufficiently small nonzero z. □

A cusp end cannot be properly sent to a circle end by a nonconstant finite-degree end map: a bounded target coordinate would extend to the missing source point with modulus one, contradicting the maximum principle. Conversely, a circle end cannot map properly to a cusp. Indeed $-\log|f|$ would be a harmonic function on a finite-width cylinder tending uniformly to $+\infty$ at one finite endpoint. Its angular mean has zero second derivative and is affine in the cylinder coordinate, which cannot diverge at a finite endpoint.

Proposition 3.14 (U21: extension at a circle end)**.** *A proper holomorphic map of tame circle ends extends continuously, and locally holomorphically in the ideal circular coordinates, to a covering of their boundary circles. Its covering degree is its end degree.*

Proof. Use annular uniformizing coordinates near the two ideal circles and normalize the target circle to $|w| = 1$. Properness toward that end implies $|f(z)| \to 1$ uniformly as the source circle is approached. The function $u = \log|f|$ is harmonic in a sufficiently small collar and has zero boundary values at the circle. Reflection across the circle, written as odd reflection after a local logarithmic coordinate, extends u harmonically. Local conjugates extend as well, and their exponentials extend f; on overlaps they agree with the original holomorphic function, so uniqueness gives a single extension.

Inside the collar u has a fixed strict sign. The Hopf boundary lemma gives a nonzero normal derivative on its smooth boundary. The Cauchy–Riemann equations make the boundary angular derivative nonzero. Thus the boundary restriction is a local diffeomorphism of circles. Compactness makes it a finite covering. Its total argument change equals the integral of $*du$, which is the integer degree induced on a core circle, hence equals the end degree. □

The reflection is in the ideal round coordinate, not a claim of analytic regularity of an arbitrary physical boundary in its original Euclidean embedding. The distinction matters for numerical meshes at re-entrant corners.

Corollary 3.15 (U22: embedding extension)**.** *An embedding that maps a tame circle end properly to a tame circle end extends to a homeomorphism of the ideal circles.*

Proof. The boundary map in U21 is a covering of positive degree. Its degree equals the number of preimages of a nearby regular interior point. Injectivity of the embedding makes that number one. A degree-one circle covering is a homeomorphism. □

3.6.1 Finite annular covers and modulus

For a proper map $F : A(r, R) \to A(r', R')$ preserving the two ends, uniqueness of the harmonic Dirichlet problem gives

$$\log|F(z)| = \log r' + \frac{\log(R'/r')}{\log(R/r)} \log(|z|/r).$$

A conjugate period must be 2π times an integer d. Therefore $\log(R'/r') = d\log(R/r)$ and $F(z) = cz^d$. Reversing the two ends gives cz^{-d}. This proves both the covering classification and

$$\operatorname{mod} A(r', R') = d \operatorname{mod} A(r, R).$$

The formula quantifies the distinction between finite annular collars and punctured disks, whose annular modulus becomes arbitrarily large toward the cusp.

3.7 Source §5.7: orbifolds and the necessary qualifications

Source relation: Source Theorem 5.9, physical pages 118–119; source definition of finite conformal type, physical page 96; orbifold Gauss–Bonnet, physical page 105.

An effective orientable complex orbifold has local charts $z \mapsto z^m$ at a cone point of finite order $m \geq 2$. A puncture is an omitted point, recorded separately; formally its contribution to Euler characteristic is the limit $1 - 1/m \to 1$. For genus g, s punctures and finite cone orders $m_1, \ldots, m_k$, put

$$\chi_{\mathrm{orb}} = 2 - 2g - s - \sum_{j=1}^{k} (1 - 1/m_j).$$

A good orbifold has a manifold orbifold cover. Compact orientable bad orbifolds are the sphere with one finite cone point and the sphere with two unequal finite cone orders. Punctures must not be classified as finite cone points in these exceptions: the plane with one finite cone point is covered by $z \mapsto z^m$ from $\mathbb{C}$.

Proposition 3.16 (U23: analytic uniformization of a good orbifold)**.** *A good Riemann orbifold is the quotient of one of $\mathbb{P}^1$, $\mathbb{C}$ and $\mathbb{D}$ by a discrete group of holomorphic automorphisms with its specified local stabilizers.*

Proof. Take a manifold orbifold covering and then its simply connected covering. Lift the complex coordinates away from the cone points by U01. At a cone point of order m, the covering coordinate is the local root coordinate z, so the complex structure extends through the preimage. The resulting simply connected Riemann surface is uniformized by U08. Deck transformations are holomorphic by the lifted-coordinate argument. A stabilizer of order m is locally conjugate to multiplication by an mth root of unity, giving precisely the prescribed quotient chart. Proper discontinuity follows from the orbifold covering structure. □

Evidence classification. The topological existence of a manifold orbifold cover is the goodness input. The classification of good compact orientable two-orbifolds is a declared topological theorem, represented in the source by Theorems 2.92–2.93. U23 proves the analytic passage for that input; a future formalization must also close the topological covering theorem.

3.7.1 Compact orbifolds without punctures

Theorem 3.17 (U24: compact orbifold curvature trichotomy)**.** *For a compact good orientable Riemann orbifold without punctures, the signs of χ_{orb} are respectively positive, zero and negative in the spherical, Euclidean and hyperbolic cases. A constant-curvature metric normalized to $K \in \{1, 0, -1\}$ satisfies*

$$K \operatorname{area}(O) = 2\pi \chi_{\mathrm{orb}}(O).$$

Proof. U23 gives the uniformizing model. In the spherical case the deck group is finite; average a Hermitian form on the two-dimensional representation of its finite lift and change coordinates to put the group in the round rotation group. In the plane case, a cocompact discrete affine group has no dilation of modulus different from one, since conjugation would create translations approaching the identity. After conjugation it acts by Euclidean motions. In the disk case every holomorphic automorphism preserves the Poincare metric. These metrics descend to orbifold metrics.

Remove small disks around the cone points. Ordinary Gauss–Bonnet on the complement has boundary terms tending to minus the cone angles $-2\pi/m_j$. Moving these terms and comparing with the Euler characteristic of the punctured underlying surface gives

$$\int_O K \, \mathrm{d}A = 2\pi \left(2 - 2g - \sum_j (1 - 1/m_j) \right).$$

The area is finite and positive, so its multiplication by constant K has the same sign as K. This proves the sign classification and the area identity. □

The orbifold Gauss–Bonnet identity is thus an accounting of smooth curvature and missing cone angle. Its application to a noncompact punctured quotient requires control of the end boundary terms and area. They cannot be omitted by assigning the puncture an infinite cone index alone.

3.7.2 A punctured counterexample to the unrestricted sign rule

The source's finite-conformal-type definition includes a compactification with points of infinite index. Under the standard puncture interpretation, the plane is a sphere with one puncture. It has

$$\chi_{\mathrm{orb}}(\mathbb{C}) = 2 - 1 = 1,$$

but its universal covering model is $\mathbb{C}$, not the sphere. The flat plane has infinite area; applying the compact identity $K\,\mathrm{area} = 2\pi\chi$ would already be undefined at $K = 0$ and infinite area. A plane with one cone point of order m similarly has $\chi_{\mathrm{orb}} = 1/m > 0$ and Euclidean uniformization by the finite rotation quotient of $\mathbb{C}$.

These examples expose a necessary scope qualification in the printed sign trichotomy. If the notation for the exceptional signatures were read as including all infinite indices, it would exclude valid good punctured orbifolds as well. The correction is to separate finite cone orders and punctures, and to state the complete finite-type alternatives explicitly.

Proposition 3.18 (U25: finite-type punctured alternatives)**.** *For a good orientable finite-type orbifold with at least one puncture, the Euclidean cases are the plane, the plane with one finite cone point, the twice-punctured sphere, and the plane with two cone points of order two. All other such orbifolds are hyperbolic. In the hyperbolic cases the complete metric has finite area and* $\mathrm{area} = -2\pi\chi_{\mathrm{orb}}$.

Proof. A spherical quotient is compact and has no punctured ends. For a Euclidean quotient, let Λ be the translation subgroup. A discrete orientation-preserving Euclidean motion group has translation rank zero, one or two. Rank two is cocompact, hence excluded by the puncture. At rank zero the group is finite and fixes a common point: two rotations with different centers generate a nontrivial translation or a nondiscrete subgroup. Its quotient is the plane with either no cone or one finite cone point. At rank one, a rotation preserving the translation lattice has linear part 1 or -1. The translation-only quotient is a cylinder, conformally $\mathbb{C}^*$. Adding the half-turn gives the quotient of $\mathbb{C}^*$ by $w \mapsto 1/w$, a plane with two order-two cone points. These exhaust the noncompact Euclidean possibilities.

Every remaining good orbifold has disk universal cover by U23. Its finite conformal type has a compact core and finitely many punctures. A punctured annular end cannot have hyperbolic deck holonomy, whose quotient is a finite-modulus annulus. Its peripheral holonomy is parabolic and gives a cusp. Standard cusp coordinates have finite area, calculated explicitly in Chapter 5. The compact core has finite area as well. Apply Gauss–Bonnet after truncating the cusp ends. Their boundary lengths and geodesic-curvature contributions tend to zero. The cone terms are

those of U24, and each puncture reduces the compactification Euler characteristic by one. This gives area $= -2\pi\chi_{\mathrm{orb}} > 0$. □

The finite-area group in U25 is of the first kind. A gap in its limit set would give a funnel boundary interval and an infinite-area end, incompatible with the finite-area cusp decomposition. Thus the source's first-kind conclusion is appropriate for the finite-area hyperbolic case, but finite topological type alone would not suffice: a finite-modulus annulus is a hyperbolic quotient with a two-point limit set.

3.7.3 Exact signature examples

For triangle signatures, the Euler characteristic is $1/p+1/q+1/r-1$. The triples $(2,3,5)$, $(2,3,6)$ and $(2,3,7)$ give $1/30$, 0 and $-1/42$. These are exact rational distinctions. Floating-point sign testing near zero is unnecessary and can misclassify a Euclidean signature if it uses inconsistent rounding.

For compact Euclidean quotients the cone signatures are $(2,2,2,2)$, $(3,3,3)$, $(2,4,4)$ and $(2,3,6)$, besides the smooth torus. The list follows by solving $\sum(1-1/m_j)=2$, using $m_j \geq 2$ and ordering the m_j. With four terms equality forces all orders to be two. With three terms the equation $1/p+1/q+1/r=1$ gives the three remaining triples by the inequalities $p \leq q \leq r$. A genus-zero surface with at most two finite cones is spherical only when its two orders agree, or it has no cone; the unequal and single-cone compact cases are the bad exceptions.

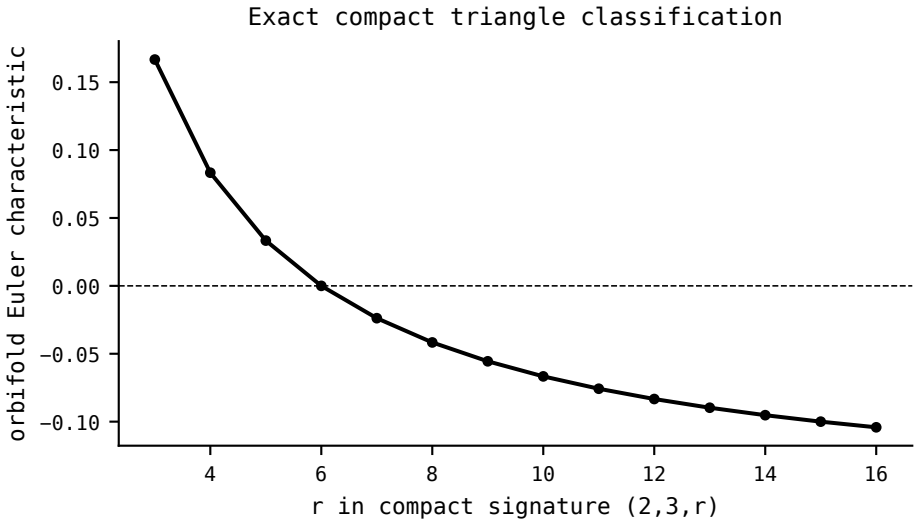


Figure 3.3: Exact reciprocal-sum classification of the compact triangle examples. Punctured Euclidean exceptions are treated separately in the text and are not folded into this compact sign diagram.

Chapter 4

Algebraic geometry, periods and topological invariants

4.1 Local coordinates, local rings and multiplicity

Uniformization is a global classification of analytic curves; its local algebra is the algebra of convergent power series. At a point p, a local coordinate z identifies the local ring with $\mathbb{C}\{z\}$ and its maximal ideal with (z). A nonzero holomorphic germ has the unique factorization $z^m u(z)$, where $u(0) \neq 0$ and m is its vanishing order. Uniqueness follows by comparing the first nonzero Taylor coefficient. The integer m is invariant under a change of coordinate with nonzero derivative.

Proposition 4.1 (U26: finite local fibres)**.** *For a germ $f(z) = z^m u(z)$ with $u(0) \neq 0$, the local fibre algebra $\mathbb{C}\{z\}/(f)$ has complex dimension m. Under composition, local degrees multiply.*

Proof. The germ u is a unit, with convergent reciprocal on a sufficiently small disk. Thus $(f) = (z^m)$. Every class has a unique representative $a_0 + \cdots + a_{m-1}z^{m-1}$, and these m monomials are linearly independent modulo (z^m). For $g(w) = w^n v(w)$, substitution gives

$$g(f(z)) = z^{mn} u(z)^n v(f(z)),$$

whose last factor is a unit. Its order is mn. □

A fibre containing one geometric point can therefore carry nontrivial multiplicity. A numerical root list that merges coincident roots without retaining their local algebra loses information used by degree and ramification. The normalized global maps of §5 have local degree one; the orbifold quotient charts deliberately have degree m.

The finite jet algebra $\mathbb{C}[z]/(z^{n+1})$ represents all Taylor data through order n. Composition is defined when the substituted germ has zero constant term; otherwise truncation before composition can discard terms contributing to low output orders. This is an algorithmic restriction with an algebraic explanation, not a numerical precision issue.

4.2 Divisors and the global degree ledger

For a nonzero meromorphic function f on a compact Riemann surface, its divisor is

$$\operatorname{div}(f) = \sum_p \operatorname{ord}_p(f)[p].$$

Only finitely many terms are nonzero. Cover the finitely many zeros and poles by disjoint coordinate disks and integrate df/f along their boundaries. The remaining compact surface has no singularities of this differential, so Stokes' theorem makes the sum of boundary integrals zero. Since each local integral is $2\pi\mathrm{i}\,\mathrm{ord}_p(f)$,

$$\deg \operatorname{div}(f) = 0.$$

The equality proves that the number of zeros and poles agrees with multiplicity. It is the compact global version of the fibre-count argument used in U12.

For a branched cover $f : S \to T$ of degree d, the canonical divisor relation is

$$K_S = f^*K_T + \sum_p (e_p - 1)[p].$$

Locally, $w = z^{e_p}$ gives $dw = e_p z^{e_p-1} dz$; the extra zero has order $e_p - 1$. Taking degrees yields Riemann–Hurwitz,

$$2g(S) - 2 = d(2g(T) - 2) + \sum_p (e_p - 1).$$

The general degree calculation and its cellular proof are prior dependencies [2, Section 2.2]. In the examples below the formula is applied to explicit smooth compactifications whose branch points are checked directly.

4.3 The torus as a lattice quotient

Choose periods ω_1, ω_2 with $\mathrm{Im}(\omega_2/\omega_1) > 0$. The quotient $\mathbb{C}/\Lambda$ is compact because the closed fundamental parallelogram is compact and maps onto it. The translation action is free and properly discontinuous, so the quotient inherits a Riemann-surface atlas by U01.

The form dz is invariant under translations and descends to a nowhere-vanishing holomorphic differential. Its periods on the two lattice generators are ω_1 and ω_2. Changing the lattice basis by $\left(\begin{smallmatrix} a & b \\ c & d \end{smallmatrix}\right) \in SL_2(\mathbb{Z})$ preserves the lattice and sends a normalized modulus to a fractional-linear transform. The convention for ordering cycles determines whether the transform is $(a\tau+b)/(c\tau+d)$ or its equivalent relabeling; the chosen convention is fixed below.

Proposition 4.2 (U27: modular change and upper-half-plane preservation)**.** *For $\tau \in \mathbb{H}$ and integers a, b, c, d with $ad - bc = 1$, put $\tau' = (a\tau + b)/(c\tau + d)$. Then*

$$\mathrm{Im}\,\tau' = \frac{\mathrm{Im}\,\tau}{|c\tau + d|^2} > 0.$$

The tori with moduli τ and τ' are biholomorphic after a complex rescaling.

Proof. Subtract the conjugate fraction and use $ad - bc = 1$:

$$\tau' - \overline{\tau'} = \frac{(ad - bc)(\tau - \bar{\tau})}{|c\tau + d|^2}.$$

The denominator cannot vanish because τ is nonreal. The two generators $c\tau + d$ and $a\tau + b$ form an oriented integral basis of the same lattice, up to the corresponding ordering convention. Dividing by the first generator gives the normalized lattice generated by 1 and τ'. The division is a holomorphic linear isomorphism. □

The transform preserves complex geometry but changes the displayed basis of cycles. A physical period vector, a numerical period matrix and a homology label must be transformed together. Holding the period vector fixed while changing its cycles produces a spurious discontinuity.

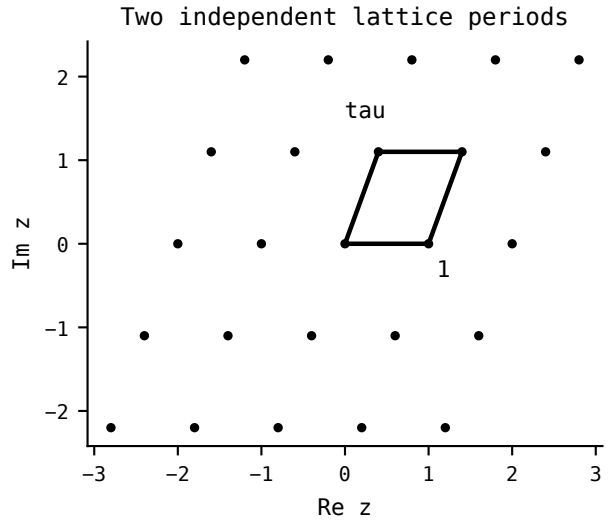


Figure 4.1: A lattice and its fundamental parallelogram. Opposite-edge identifications carry two independent periods; one complex exponential removes only one rank-one period subgroup.

4.4 An algebraic equation from a lattice

For $\Lambda \subset \mathbb{C}$ a rank-two lattice define

$$\wp(z) = \frac{1}{z^2} + \sum_{\omega \in \Lambda \setminus \{0\}} \left(\frac{1}{(z-\omega)^2} - \frac{1}{\omega^2} \right).$$

On a compact set avoiding Λ, the summand is $O(|\omega|^{-3})$. Lattice point counting in annuli gives $O(k)$ lattice points with $k \le |\omega| < k+1$, and $\sum k\, k^{-3}$ converges. Thus the series converges locally uniformly, and derivatives may be taken on smaller compact sets.

Its derivative is the absolutely convergent series $\wp'(z) = -2\sum_{\omega\in\Lambda}(z-\omega)^{-3}$. Reindexing proves that $\wp'$ is periodic. Hence $\wp(z+\omega) - \wp(z)$ is constant. The function $\wp$ is even by pairing ω with $-\omega$; for each primitive lattice-basis generator ω, evaluation at $z = -\omega/2$ is away from the lattice and makes the constant zero. Periodicity for the two basis generators implies periodicity for their integer combinations. Thus $\wp$ is elliptic.

Proposition 4.3 (U28: the Weierstrass differential equation)**.** *Let* $g_2 = 60\sum_{\omega\neq 0}\omega^{-4}$ *and* $g_3 = 140\sum_{\omega\neq 0}\omega^{-6}$*. Then*

$$(\wp')^2 = 4\wp^3 - g_2\wp - g_3.$$

For a nonsingular lattice the resulting cubic is nonsingular, and $z \mapsto (\wp(z), \wp'(z))$ *identifies its smooth projective curve with* $\mathbb{C}/\Lambda$*.*

Proof. Expansion of the defining series gives $\wp = z^{-2} + (g_2/20)z^2 + (g_3/28)z^4 + O(z^6)$. Substitution shows that $(\wp')^2 - 4\wp^3 + g_2\wp + g_3$ has no pole and has zero constant term at the origin. It is elliptic and has no pole anywhere, hence is constant on the compact torus. Its value is zero.

The function $\wp$ has one double pole on the torus and therefore degree two, by the argument principle for a meromorphic function on a compact surface. It is even, so a generic fibre is $\{z, -z\}$. The three nonzero points of order two in $\mathbb{C}/\Lambda$ are zeros of the odd function $\wp'$: at such a point h, periodicity gives $\wp'(-h) = \wp'(h)$, while oddness gives the opposite sign. The derivative has one pole of order three. The equality between the total zero and pole orders consequently shows that these are exactly its three zeros and that each is simple. Their $\wp$-values are distinct: equality at two of them would produce a fibre of total degree at least four, contradicting degree

two. Substitution into the differential equation identifies these three distinct values as the roots of $4x^3 - g_2x - g_3$. The cubic is therefore nonsingular.

The pair $(\wp, \wp')$ separates the generic two-point fibre by oddness. At a half-period the fibre has only that point. Away from half-periods $\wp' \neq 0$, so the first coordinate has nonzero derivative; at a half-period the simple zero of $\wp'$ gives $\wp'' \neq 0$, so the second coordinate has nonzero derivative. At the projective point at infinity, the expansions $\wp = z^{-2} + O(z^2)$ and $\wp' = -2z^{-3} + O(z)$ give the local parameter $-2\wp/\wp' = z + O(z^5)$. The map is thus an injective holomorphic immersion from the compact torus to the smooth cubic. It is open by its local inverse and closed by compactness; the cubic is connected, so it is onto. These properties prove the claimed biholomorphism. □

The analytic-to-algebraic passage is a genus-one statement. For genus at least two, uniformization uses a disk and a nonabelian group. Periods still encode substantial information, but a single doubly periodic function does not uniformize every such surface. The period map and the canonical embedding require additional algebraic geometry.

4.5 Hyperelliptic examples and differential bases

Consider a polynomial $P(x)$ with distinct roots and the affine curve $y^2 = P(x)$. Its normalization has a double cover of the x-sphere. A simple root is a branch point with local coordinate t satisfying $x - a = t^2$. At infinity, parity of the degree determines whether infinity is branched. If $\deg P = 2g+2$, there are $2g+2$ finite branch points and two points over infinity. If $\deg P = 2g+1$, there are $2g + 1$ finite branch points and one branch point at infinity. Riemann–Hurwitz gives genus g in both cases.

Proposition 4.4 (U29: holomorphic differentials on a hyperelliptic curve)**.** *For the smooth compactification of $y^2 = P(x)$ of degree $2g + 1$ or $2g + 2$, the forms*

$$\omega_j = \frac{x^{j-1}dx}{y}, \qquad j = 1, \dots, g,$$

are linearly independent and holomorphic.

Proof. Away from branch points and infinity there are no poles. Near a simple finite branch point, write $x - a = t^2$ and $y = tq(t)$ with $q(0) \neq 0$. Then $dx/y = 2dt/q(t)$ is holomorphic. For even degree, use $s = 1/x$ near each point at infinity; $y \sim cs^{-(g+1)}$ and $x^{j-1}dx/y \sim c's^{g-j}ds$, holomorphic for $j \leq g$. For odd degree use $x = t^{-2}$ and $y \sim ct^{-(2g+1)}$; the form has order $2g - 2j \geq 0$. Finally, a linear relation would imply a polynomial of degree at most $g - 1$ vanishes identically on the open x-plane where $y \neq 0$, hence all coefficients vanish. □

The assertion that these forms exhaust all holomorphic differentials uses the dimension theorem $\dim H^0(K) = g$. That theorem is the Hodge or Riemann–Roch dimension theorem; it is a separately identified foundational result when the complete period matrix is required. The explicit calculations above already prove a g-dimensional independent family and verify the absence of poles, which are the obligations used in the worked curve examples.

For a quartic, $g = 1$ and dx/y is the single holomorphic differential. A choice of two oriented cycles gives periods ω_1, ω_2 and modulus $\tau = \omega_2/\omega_1$. The sign $\operatorname{Im}\tau > 0$ follows from the Riemann bilinear relation with the chosen symplectic orientation, developed next.

4.6 Cut surfaces and the bilinear period identity

Let S be a compact oriented surface of genus g with cycles a_j, b_j of symplectic intersection. Cutting along them gives a polygon. For closed one-forms α, β, choose a primitive A of α on the

cut polygon. Stokes' theorem gives

$$\int_S \alpha \wedge \beta = \int_{\partial \Pi} A\beta.$$

Opposite edges have opposite orientation; their primitive values differ by the corresponding period of α. Pairing their integrals yields

$$\int_S \alpha \wedge \beta = \sum_{j=1}^{g} \left(\int_{a_j} \alpha \int_{b_j} \beta - \int_{b_j} \alpha \int_{a_j} \beta \right).$$

This derivation fixes the sign convention. Reversing the intersection convention reverses both sides' oriented-cycle expression.

For a nonzero holomorphic differential ω, the form $\frac{\mathrm{i}}{2}\omega \wedge \bar{\omega}$ is a nonnegative area density and has positive integral. In genus one, normalize $\int_a \omega = 1$; the identity gives

$$\frac{\mathrm{i}}{2} \int_S \omega \wedge \bar{\omega} = \operatorname{Im} \tau > 0.$$

For a basis of normalized differentials, the same identity gives symmetry of the period matrix and positive definiteness of its imaginary part. Those are stringent consistency checks on a numerically computed period matrix, although floating-point satisfaction alone does not prove exact normalization.

4.7 Degeneration and the logarithmic period scale

On the Legendre curve $y^2 = x(1-x)(1-mx)$, $0 < m < 1$, a real half-period is the complete elliptic integral

$$K(m) = \int_0^{\pi/2} \frac{d\theta}{\sqrt{1 - m \sin^2 \theta}}.$$

Here m is the parameter, not its square root. As $m \uparrow 1$, the contribution near $\theta = \pi/2$ has the form

$$\int_0^{c} \frac{ds}{\sqrt{(1-m) + s^2}},$$

up to uniformly bounded multiplicative and additive corrections. Its antiderivative is $\operatorname{arsinh}(s/\sqrt{1-m})$, establishing logarithmic divergence. A topological cycle is pinching while the dual period grows logarithmically. Merely relabeling a root branch does not remove this conditioning.

The precise classical leading form $K(m) \sim \log(4/\sqrt{1-m})$ requires estimating the complementary regular integral. The logarithmic order, which suffices for the conditioning argument here, follows directly from two-sided comparison in a small endpoint interval and a bounded remainder away from it. The numerical figure reports the exact integral evaluation and the leading approximation separately.

4.8 Quotient topology and information that coordinates do not erase

A simply connected coordinate cover removes local multivaluedness by enlarging the domain. It does not erase the deck group from the underlying problem. A function on the quotient is represented upstairs by an invariant function; a section of a line bundle can instead transform by a character. These are different descent conditions.

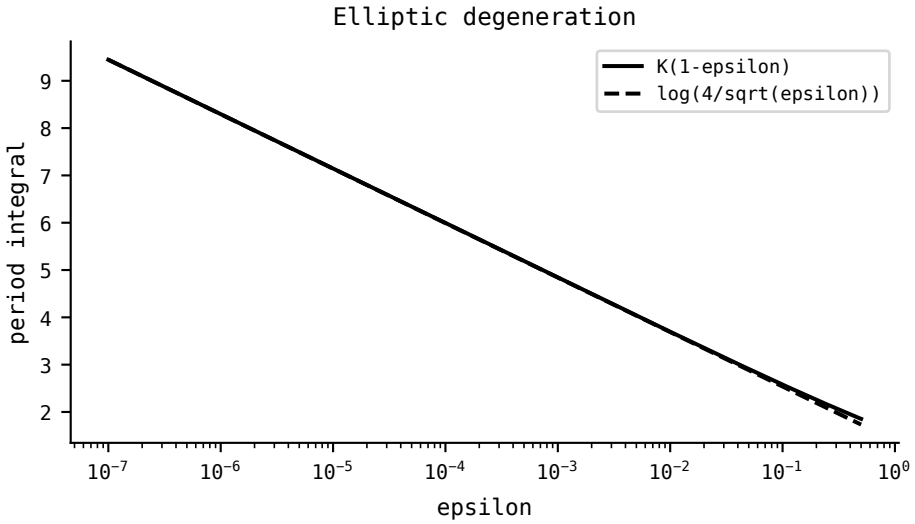


Figure 4.2: The complete elliptic integral and its logarithmic leading scale near a degenerating branch pair. Numerical evaluations illustrate the stated limit; they are not used to prove the asymptotic.

For a lattice cover, the invariance condition is $f(z + \lambda) = f(z)$. For a flat line bundle it is $f(z + \lambda) = \chi(\lambda) f(z)$, where $\chi : \Lambda \to \mathbb{C}^*$ is a homomorphism. Its consistency requires $\chi(\lambda + \mu) = \chi(\lambda)\chi(\mu)$. A numerically fitted phase at each edge of a fundamental polygon must obey the corresponding cocycle constraints; independent edge fits need not descend to a global object.

For a punctured genus-zero surface with at least two punctures besides infinity, the fundamental group is free and nonabelian. Integrals of closed scalar one-forms record only its abelianization. A continuation problem with nonabelian monodromy requires the full group word or its permutation representation. This is the topological reason that several independent winding numbers can be insufficient for a distributed branch-tracking algorithm.

Chapter 5

Harmonic, functional and Fourier analysis

5.1 Conformal energy and the correct transformed equation

Proposition 5.1 (U30: invariance of two-dimensional Dirichlet energy)**.** *Let $f : U \to V$ be a conformal diffeomorphism and $u : V \to \mathbb{R}$ have finite Dirichlet energy. Then*

$$\int_U |\nabla(u \circ f)|^2 \,\mathrm{d}A = \int_V |\nabla u|^2 \,\mathrm{d}A.$$

For smooth u, $\Delta(u \circ f) = |f'|^2(\Delta u) \circ f$.

Proof. The real derivative of a holomorphic conformal map is $Df = |f'|Q$ with Q orthogonal and orientation preserving. The chain rule gives $|\nabla(u \circ f)|^2 = |f'|^2|\nabla u|^2 \circ f$. The Jacobian is $|f'|^2$, so change of variables proves the energy identity. Differentiating twice, the cross terms cancel by the Cauchy–Riemann equations and the coordinate functions of f are harmonic, giving the Laplacian identity. Smooth approximation extends the energy identity to finite-energy Sobolev functions. □

A homogeneous Laplace equation is preserved. A Poisson equation $-\Delta u = s$ becomes $-\Delta(u \circ f) = |f'|^2 s \circ f$. An eigenproblem becomes a weighted eigenproblem. A constant-mass Helmholtz equation generally becomes variable-coefficient after conformal mapping. Keeping the old source, eigenvalue weight or mass term would change the physical problem.

5.2 The logarithmic cylinder

Write $z = r\mathrm{e}^{t+\mathrm{i}\theta}$, $0 < t < L$, with $\theta \in \mathbb{R}/(2\pi\mathbb{Z})$. The annular Euclidean metric is $r^2\mathrm{e}^{2t}(dt^2 + d\theta^2)$. U30 makes its energy

$$E(u) = \int_0^L \int_0^{2\pi} (|u_t|^2 + |u_\theta|^2) \,\mathrm{d}\theta \,\mathrm{d}t.$$

Thus harmonicity is $u_{tt} + u_{\theta\theta} = 0$. The geometry has been flattened in the energy, but the physical area weight $r^2\mathrm{e}^{2t}$ remains in an L^2 norm or a transient diffusion equation.

For boundary data $a(\theta)$ at $t = 0$ and $b(\theta)$ at $t = L$, use the Fourier convention

$$a_n = \frac{1}{2\pi} \int_0^{2\pi} a(\theta)\mathrm{e}^{-\mathrm{i}n\theta} \,\mathrm{d}\theta, \qquad a(\theta) = \sum_{n \in \mathbb{Z}} a_n \mathrm{e}^{\mathrm{i}n\theta}.$$

The zero mode is $u_0(t) = a_0 + (b_0 - a_0)t/L$. For $n \neq 0$,

$$u_n(t) = a_n \frac{\sinh(|n|(L-t))}{\sinh(|n|L)} + b_n \frac{\sinh(|n|t)}{\sinh(|n|L)}.$$

Finite sums can be checked by direct differentiation. For boundary data in $H^{1/2}$, the energy formula below controls the series and establishes convergence in the energy norm. This is the appropriate function space for a finite-energy harmonic extension.

Theorem 5.2 (U31: exact annular Dirichlet-to-Neumann symbol)**.** *Let $v_n = (a_n, b_n)^{\mathsf{T}}$. The harmonic extension has energy*

$$E(u) = 2\pi \sum_{n\in\mathbb{Z}} v_n^* D_n v_n,$$

where

$$D_0 = \frac{1}{L}\begin{pmatrix} 1 & -1 \\ -1 & 1 \end{pmatrix}, \qquad D_n = |n| \begin{pmatrix} \coth(|n|L) & -\operatorname{csch}(|n|L) \\ -\operatorname{csch}(|n|L) & \coth(|n|L) \end{pmatrix} \quad (n \neq 0).$$

Each D_n is positive definite for $n \neq 0$. Its eigenvalues are $|n|\tanh(|n|L/2)$ and $|n|\coth(|n|L/2)$.

Proof. For one mode $w = u_n$, integration by parts and $w'' = n^2 w$ give

$$\int_0^L (|w'|^2 + n^2|w|^2)\,\mathrm{d}t = \bar{w}(L)w'(L) - \bar{w}(0)w'(0).$$

Differentiate the explicit hyperbolic-sine interpolation at the two endpoints. Its outward derivatives are $(-w'(0), w'(L)) = D_n v_n$. Fourier orthogonality multiplies the modal expression by 2π, proving the finite-sum identity. The $n = 0$ calculation is direct. The eigenvectors $(1, 1)$ and $(1, -1)$ give eigenvalues $|n|(\coth x - \operatorname{csch} x)$ and $|n|(\coth x + \operatorname{csch} x)$. The half-angle identities convert these to the stated positive quantities. Monotone convergence of the nonnegative modal energies and completion establish the formula for finite-energy boundary data. □

The symbol is a flux-weighted boundary operator. Physical unit-normal derivatives in the original annulus include the boundary radii. Omitting that distinction gives a dimensionally incorrect capacitance or heat-flux formula. The zero eigenvalue of D_0 is the common constant boundary mode; it represents the invariance of energy under an additive constant.

5.3 A complete error budget for Fourier truncation

Suppose the boundary coefficients satisfy $|a_n| + |b_n| \leq M\mathrm{e}^{-\sigma|n|}$, $\sigma > 0$. For $0 \leq t \leq L$, the two hyperbolic-sine interpolation factors lie between zero and one. Truncation to $|n| \leq N$ therefore has the uniform bound

$$\left\| u - u^{(N)} \right\|_\infty \leq 2M \sum_{n>N} \mathrm{e}^{-\sigma n} = \frac{2M\mathrm{e}^{-\sigma(N+1)}}{1 - \mathrm{e}^{-\sigma}}.$$

No estimate on a sampled residual is needed once the coefficient envelope is established. Conversely, a finite list of sampled boundary values does not itself prove this envelope. An analyticity witness or a separately verified coefficient estimate is required.

For an interior cylinder $\delta \leq t \leq L - \delta$, the interpolation factors are at most $\mathrm{e}^{-|n|\delta}/(1 - \mathrm{e}^{-2|n|L})$. This gives additional exponential attenuation, with the denominator bounded below by $1 - \mathrm{e}^{-2L}$ for $|n| \geq 1$. Interior evaluation can therefore use a smaller retained bandwidth than uniform boundary evaluation. The requested output norm determines which truncation is justified.

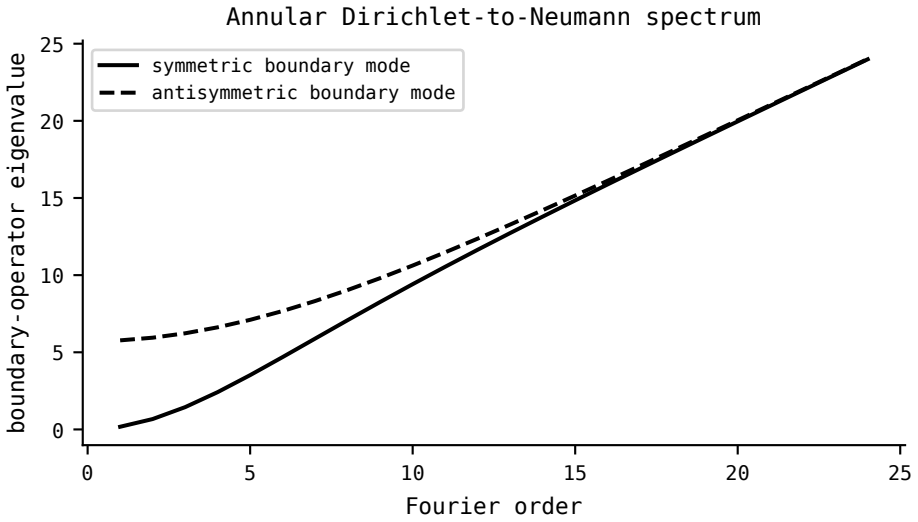


Figure 5.1: Eigenvalues of the annular boundary operator for several Fourier modes. The symmetric and antisymmetric boundary combinations have different thin-collar asymptotics.

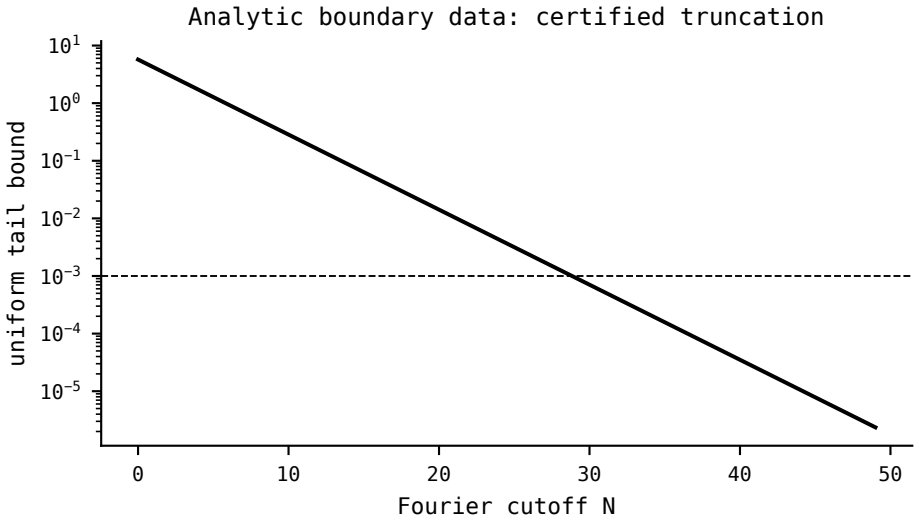


Figure 5.2: A geometric Fourier-tail envelope for analytic boundary data with $M = 1$ and strip parameter 0.3. The tolerance line is an illustrative target.

The energy error has the exact modal expression

$$E(u - u^{(N)}) = 2\pi \sum_{|n|>N} v_n^* D_n v_n.$$

An upper bound follows from $\|D_n\| \le |n| \coth(L/2)$ for $|n| \ge 1$ and the geometric coefficient envelope. The resulting series $\sum nq^n$ has a closed rational sum. This provides a second certificate in a derivative-sensitive norm.

5.4 Harmonic measure and optimal error allocation

For a regular domain D and point p, the map sending continuous boundary data g to its harmonic extension evaluated at p is positive, linear, and has value one on the constant function one. The Riesz representation theorem therefore gives a probability measure ω_p on the boundary. For the round annulus and constant values on each boundary component, U11 gives the two weights $1 - u(p)$ and $u(p)$.

If errors on boundary components are bounded by $\varepsilon_0, \varepsilon_1$, the interior error is at most

$$(1 - u(p))\varepsilon_0 + u(p)\varepsilon_1.$$

This is sharp for sign-aligned constant errors. Equal tolerances are not automatically optimal when the costs of reducing the two errors differ. For a cost model $C = c_0 \log(1/\varepsilon_0) + c_1 \log(1/\varepsilon_1)$ and an active weighted-error constraint, elementary Lagrange multipliers give $\varepsilon_j = c_j/(\lambda w_j)$, restricted to the admissible tolerance range. The weights are geometric probabilities, while the c_j encode the chosen numerical representation.

Proposition 5.3 (U32: weighted error-allocation optimum)**.** *Let $w_j, c_j > 0$ and minimize $\sum_j c_j \log(1/\varepsilon_j)$ over $\varepsilon_j > 0$ subject to $\sum_j w_j \varepsilon_j \le E$. With no additional upper bounds, the unique minimizer is*

$$\varepsilon_j^* = \frac{E c_j}{w_j \sum_k c_k}.$$

Proof. The objective is strictly convex because its Hessian is diagonal with positive entries c_j/ε_j^2. It decreases in each coordinate, so the constraint is active at a minimizer. The Lagrange equations are $-c_j/\varepsilon_j + \lambda w_j = 0$. Summing $w_j \varepsilon_j = c_j/\lambda$ gives $\lambda = (\sum c_j)/E$. The displayed point is feasible and satisfies these equations. Convexity implies global optimality, and strict convexity implies uniqueness. □

When costs are integer precision bits, this continuous solution is only a relaxation. Rounding requires a discrete feasibility check and a lower-bound argument. The earlier PHI precision-allocation theorem supplies an example of that additional step [2, 3].

5.5 Hyperbolic annular metrics and cusp limits

The strip $0 < t < L$ with periodic coordinate θ maps locally to the upper half-plane by an exponential. Pulling back $|dw|/\operatorname{Im} w$ gives

$$ds_A = \frac{\pi}{L \sin(\pi t/L)} \sqrt{dt^2 + d\theta^2}.$$

The closed curve $t = L/2$ has length $2\pi^2/L$. It is a geodesic because the transverse derivative of the conformal factor vanishes there. The inversion $t \mapsto L - t$ is an isometry fixing that curve. In terms of modulus, its length is $\pi/\operatorname{mod} A$.

Proposition 5.4 (U33: cusp completeness and finite area)**.** *On $0 < |q| < 1$, the metric*

$$ds = \frac{|dq|}{|q| \log(1/|q|)}$$

has curvature -1, is complete toward the puncture, and has area $2\pi/\log(1/\varepsilon)$ on $0 < |q| < \varepsilon$.

Proof. Use $q = \mathrm{e}^{2\pi \mathrm{i} z}$ with $z = x + \mathrm{i}y$, $y > 0$, and the quotient x mod 1. The metric $|dz|/y$ pulls back to the displayed expression. Its curvature is -1 by the half-plane calculation. A radial path has length integral $\int_0^\varepsilon dr/(r \log(1/r))$, which diverges. Any path approaching the puncture has length at least the variation of $\log \log(1/r)$, so completeness is not limited to radial paths. Area integration gives

$$2\pi \int_0^\varepsilon \frac{dr}{r \log^2(1/r)} = \frac{2\pi}{\log(1/\varepsilon)}.$$

□

A cusp can have arbitrarily small area near its end and infinite distance to the puncture. This distinction is important when truncating a hyperbolic computational domain: small omitted area does not imply that all spectral or scattering effects of the omitted end are negligible.

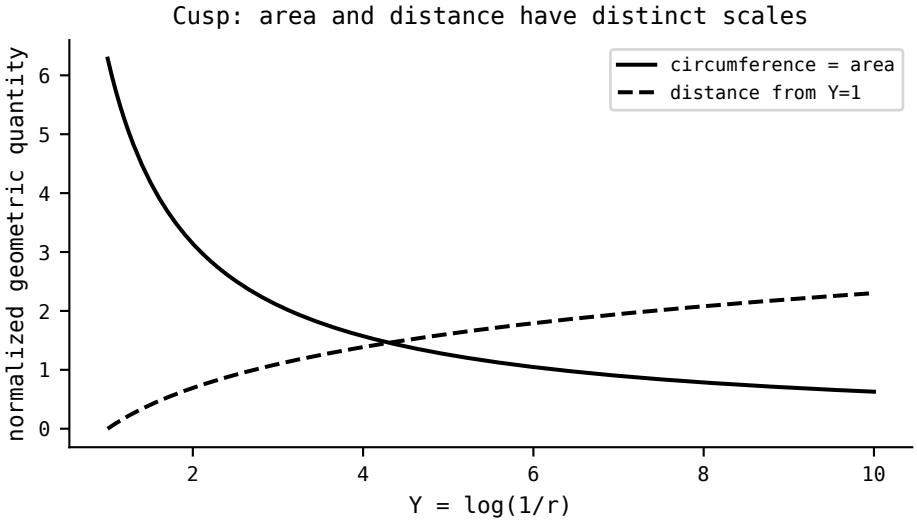


Figure 5.3: Cusp circumference, area and radial distance use different scales. The circumference and remaining area decrease as inverse logarithms, while the distance diverges as a logarithm of a logarithm.

5.6 Conformal pullback on Bergman and Dirichlet spaces

Let $A^2(D)$ denote the holomorphic functions square integrable for Euclidean area. For a biholomorphism $f : U \to V$, define

$$(T_f g)(z) = g(f(z)) f'(z).$$

Change of variables gives $\|T_f g\|_{A^2(U)} = \|g\|_{A^2(V)}$, and $T_{f^{-1}}$ is the inverse. Thus the derivative-weighted pullback is unitary. The unweighted composition map generally is not: it changes the area density.

For a holomorphic scalar function g, the Dirichlet seminorm $\int |g'|^2 dA$ is invariant under unweighted composition with a biholomorphism. Constants are its nullspace. A Hilbert norm is

obtained by adding a basepoint value, after specifying how the basepoint is transported. This is the correct setting for comparing approximation errors after uniformization.

The Bergman kernel transforms by

$$K_U(z,w) = f'(z)\overline{f'(w)}K_V(f(z),f(w)).$$

To verify this formula, substitute it into the reproducing integral, change variables, and use the reproducing property on V. Uniqueness of the reproducing kernel gives the result. On the disk, the orthogonal basis $\sqrt{(n+1)/\pi}\,z^n$ sums to $K_{\mathbb{D}}(z,w) = 1/[\pi(1-z\bar{w})^2]$.

5.7 The exact finite-rank model

For Hardy-space restriction $T_r g(z) = g(rz)$, the monomial basis diagonalizes the operator with singular values $1, r, r^2, \ldots$. The previously established exact result is

$$\inf_{\operatorname{rank} A \le N} \|T_r - A\| = r^N,$$

over bounded complex-linear competitors [2, Section 7.8]. Its upper bound is truncation. Its lower bound uses a nonzero vector in the kernel of a rank-N map on the first $N+1$ monomials. That vector has T_r norm at least r^N times its original norm.

The normalized uniformizing chart transfers this approximation problem to an interior region of a general simply connected surface. What is preserved depends on the transported Hilbert norm. Claiming the same optimum for unweighted point samples in the original physical domain would introduce a different admissible information class. The present use is an operator-norm theorem with a declared pullback norm.

5.8 Spectral heat on a flat quotient

For the flat torus with coordinates $z = x + \tau y$, $0 \le x, y < 1$, put $a = \operatorname{Re}\tau$, $b = \operatorname{Im}\tau > 0$. The metric matrix and inverse are

$$G = \begin{pmatrix} 1 & a \\ a & a^2+b^2 \end{pmatrix}, \qquad G^{-1} = \frac{1}{b^2}\begin{pmatrix} a^2+b^2 & -a \\ -a & 1 \end{pmatrix}.$$

The Fourier mode $\mathrm{e}^{2\pi\mathrm{i}(mx+ny)}$ has eigenvalue

$$\lambda_{mn} = \frac{4\pi^2}{b^2}|m\tau - n|^2.$$

The heat solution is therefore

$$u(t,x,y) = \sum_{m,n} c_{mn}\mathrm{e}^{-\kappa t\lambda_{mn}}\mathrm{e}^{2\pi\mathrm{i}(mx+ny)}.$$

For L^2 data, Parseval proves uniqueness and contraction: $\|u(t)\|_2 \le \|u(0)\|_2$. The nonconstant part decays at least as $\mathrm{e}^{-\kappa t\lambda_1}$, where λ_1 is the first positive eigenvalue. A long thin torus can have a small spectral gap. Genus alone gives no quantitative mixing time.

5.9 Residual certificates for elliptic solves

For a positive-definite discrete or continuous coercive operator A, the exact solution of $Au = b$ and an approximate $\widehat{u}$ satisfy $A(u-\widehat{u}) = r = b - A\widehat{u}$. If $A \succeq \alpha I$ in the chosen Hilbert norm, then

$$\|u - \widehat{u}\| \le \frac{\|r\|}{\alpha}.$$

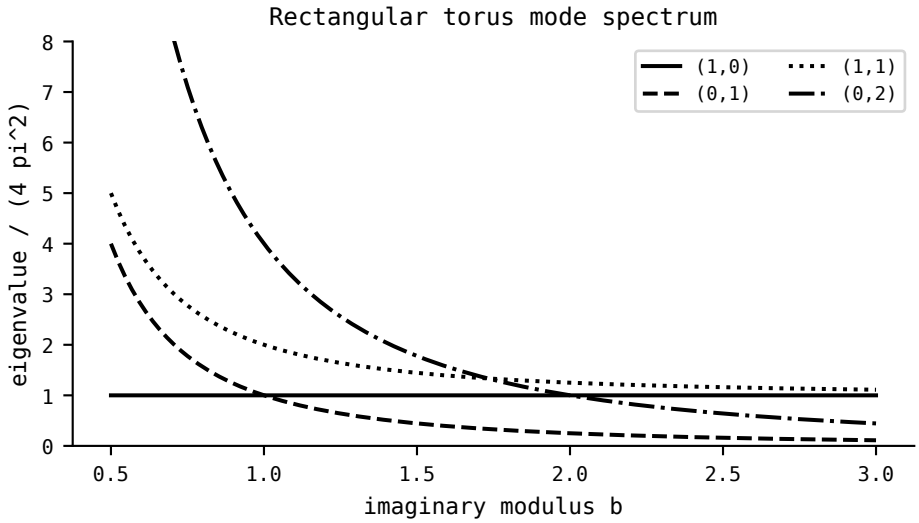


Figure 5.4: Selected torus eigenvalues under variation of the imaginary modulus. The diagram records a geometric dependence absent from a purely topological genus classification.

For the energy norm, $\|u - \widehat{u}\|_A^2 = \langle r, A^{-1} r \rangle$. A small residual without a lower spectral bound does not give a small forward error.

A conformal map may simplify the stiffness operator while complicating the mass matrix. The lower bound must use the transformed inner product. If a spectral gap is estimated from floating-point eigenvalues, an enclosure or a separate coercivity inequality is required for a rigorous certificate. The verification chapter supplies exact rational examples of the finite version and records the continuous theorem separately.

Chapter 6

Nuclear, high-energy and M/string-theory applications

6.1 The analytical role of a physical model

Uniformization supplies canonical complex coordinates and the constraints required to descend functions to a quotient. It does not determine an interaction Hamiltonian, a scattering potential, a quantum anomaly or a compactification spectrum. Each application in this chapter begins with a specified mathematical representation of the physical model, derives the geometric consequence and states the additional physical assumptions needed to interpret it.

The examples use nonrelativistic threshold surfaces, algebraic spectral curves and classical two-dimensional actions. Their derived identities are exact within the stated models. Numerical plots use dimensionless normalized parameters. No nuclear experiment, particle measurement, brane construction or string vacuum has been simulated or experimentally validated by this document.

6.2 Nuclear scattering: one square-root threshold

For a nonrelativistic two-body channel with threshold E_0 and reduced mass $\mu > 0$, choose

$$k^2 = \frac{2\mu}{\hbar^2}(E - E_0).$$

The square root gives two energy sheets. In the k coordinate the threshold is a single regular point and $E = E_0 + \hbar^2 k^2/(2\mu)$. A model amplitude $T(k) = 1/(\alpha + \beta k^2 - \mathrm{i}k)$ is meromorphic in k, with poles determined by a quadratic. Its real-energy interpretation still depends on the physical sheet and the boundary value convention.

Proposition 6.1 (U34: threshold regularization and its conditioning)**.** *For $k \neq 0$, $dk/dE = \mu/(\hbar^2 k)$. Thus the energy-to-momentum coordinate is ill-conditioned near threshold. An analytic function $T(k)$ can be regular at $k = 0$ while dT/dE diverges like $1/k$ when $T'(0) \neq 0$.*

Proof. Differentiate $k^2 = 2\mu(E - E_0)/\hbar^2$. The chain rule gives $dT/dE = T'(k)\mu/(\hbar^2 k)$. If $T'(0) \neq 0$, continuity supplies a nonzero limiting numerator. This proves the stated inverse-square-root growth in the energy coordinate. The regularity of T in k and the conditioning of the coordinate conversion are independent assertions. □

A threshold fit should therefore compare residuals in the physical observable and errors after transforming back to energy. Meromorphic pole fitting in k can eliminate an artificial branch-cut

bookkeeping burden, but it cannot improve the conditioning of an intrinsically threshold-sensitive energy estimate without additional information.

6.3 Two thresholds: an explicit rational uniformization

Absorb equal kinetic prefactors into normalized momenta and let

$$k_1^2 = E - E_1, \qquad k_2^2 = E - E_2, \qquad \Delta = E_2 - E_1 > 0.$$

Then $k_1^2 - k_2^2 = \Delta$. Define $w = k_1 + k_2$. Since $(k_1 - k_2)w = \Delta$, $w \neq 0$ at finite momenta and

$$k_1 = \frac{1}{2}\left(w + \frac{\Delta}{w}\right), \qquad k_2 = \frac{1}{2}\left(w - \frac{\Delta}{w}\right), \qquad E = E_1 + \frac{1}{4}\left(w + \frac{\Delta}{w}\right)^2.$$

Every rational expression in E, k_1, k_2 becomes rational in w. The four sheet changes are generated by

$$w \mapsto -w, \qquad w \mapsto \frac{\Delta}{w},$$

with their product $w \mapsto -\Delta/w$. These transformations make sheet tracking algebraic.

Proposition 6.2 (U35: two-channel inverse identities)**.** *The displayed map gives a rational parametrization of the smooth compactification of $k_1^2 - k_2^2 = \Delta$. Its sheet transformations preserve E, and the thresholds correspond to $w = \pm\sqrt{\Delta}$ and $w = \pm i\sqrt{\Delta}$.*

Proof. Substitution gives $k_1^2 - k_2^2 = \Delta$ identically. Conversely, $w = k_1 + k_2$ reconstructs both momenta because their difference is Δ/w. The parametrization extends to the two points at infinity in the projective conic using $w = 0$ and $w = \infty$ as local coordinates. The formula for E is unchanged by the two displayed involutions. Setting $k_2 = 0$ gives $w^2 = \Delta$ and $E = E_2$; setting $k_1 = 0$ gives $w^2 = -\Delta$ and $E = E_1$. □

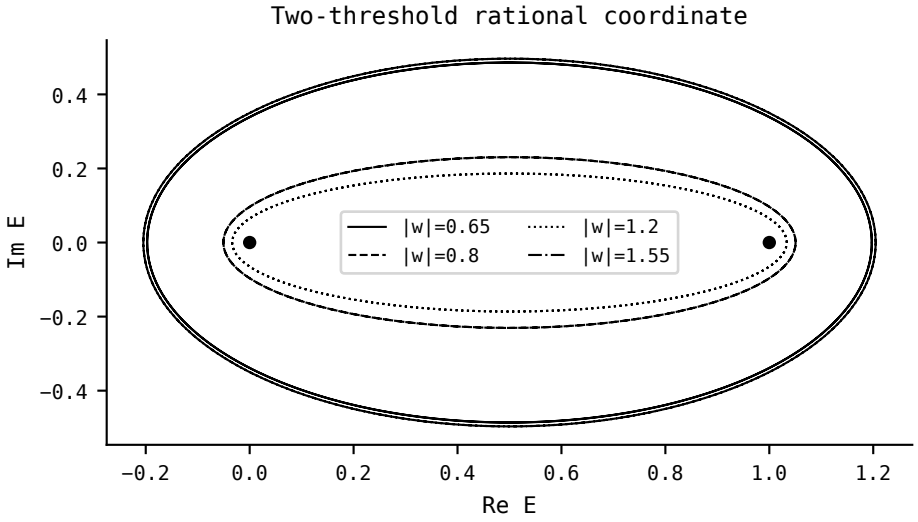


Figure 6.1: Image of coordinate circles under the exact two-threshold energy map with normalized threshold separation one. The marked critical points account for the four threshold-sheet junctions.

Comparative conclusion. For repeated evaluations of a rational model amplitude, the uniformizing coordinate removes repeated square-root sign selection and replaces it with explicit

involutions. This is an exact representation advantage. The total numerical cost still includes inversion of the energy map, boundary-value selection and propagated uncertainty. No universal scattering-fit speedup follows from the change of variable.

Realistic amplitudes may also have logarithmic cuts, left-hand cuts, additional channels and long-range singularities. The rationalization theorem applies to the stated algebraic square roots. It does not establish that every physical amplitude is rational on the resulting sphere.

6.4 Three and more thresholds: a genus obstruction

For n distinct thresholds, consider the algebraic extension generated by independent square roots $k_j = \sqrt{E - E_j}$. Its generic degree over the energy sphere is 2^n. At each finite threshold, half of the local sheets pair into ramification points of order two. At infinity all square roots change sign together, again giving 2^{n-1} simple ramification points. Riemann–Hurwitz gives the complete genus calculation.

Theorem 6.3 (U36: genus of the independent-threshold surface)**.** *For the smooth compactification of the connected independent-square-root cover with $n \geq 2$ distinct thresholds,*

$$g = 1 + 2^{n-2}(n-3).$$

In particular, two thresholds give genus zero, three give genus one, and four give genus five.

Proof. The extension has degree 2^n: no nonempty product of distinct linear factors $E - E_j$ is a square in $\mathbb{C}(E)$, since it has an odd valuation at each included threshold. Each of the $n+1$ branch values, including infinity, has 2^{n-1} points of ramification index two. Thus the ramification sum is $(n+1)2^{n-1}$. Riemann–Hurwitz yields

$$2g - 2 = -2 \cdot 2^n + (n+1)2^{n-1} = 2^{n-1}(n-3).$$

Solving for g gives the formula. □

The three-threshold surface requires a torus coordinate and elliptic functions. An attempted global rational parameter would make its function field rational and force genus zero, contradicting U36. The higher-channel genus increase is an objective obstruction to extending the two-channel rational trick unchanged. The cited multichannel analysis uses a torus and Weierstrass functions in the three-channel setting [9]. Here the genus obstruction is derived independently from the branch data.

The surface formula is also a useful resource estimate. Its sheet count grows exponentially even before any nonlinear fit is performed. Symmetry, channel degeneracies or an observable invariant under a sheet subgroup can reduce the representation size, but each reduction has a separate invariance obligation.

6.5 Bound states, virtual states and resonant poles

For a short-range scalar model, a pole at $k = \mathrm{i}\kappa$, $\kappa > 0$, gives negative relative energy $-\hbar^2\kappa^2/(2\mu)$ on the decaying branch. A pole at $k = -\mathrm{i}\kappa$ lies on the other sheet at the same real energy. The coordinate alone does not assign the same physical state to these two poles. A resonance model places poles off the imaginary axis with a time and outgoing-wave convention determining the relevant half-plane.

For a concrete rational amplitude $T(k) = 1/(k^2 + \mathrm{i}ak + b)$, compute both roots exactly. Checking the roots in the denominator, their sheet labels and the chosen time convention gives a

complete algebraic verification. A small denominator residual at a double pole does not give a linear root-error bound. The discriminant $-a^2 - 4b$ is an independent conditioning diagnostic.

The annular and end theory enters when continuing a pole around a parameter loop. If the loop surrounds a discriminant zero, the two roots can exchange. A spectral observable symmetric in the roots remains single valued. Branch labeling is then topological data, while the physical observable may not require that label. The numerical interface should expose the distinction.

6.6 High-energy amplitudes and elliptic cuts

A quartic maximal-cut model has an integral of the form

$$I = \oint_\gamma \frac{R(x)\,dx}{\sqrt{(x-a_1)(x-a_2)(x-a_3)(x-a_4)}}$$

with distinct a_j and a rational numerator R. The curve is genus one by U29's branch count. Its cycles, periods and branch collisions belong to elliptic geometry. Even when the full amplitude contains additional integrations or regularization, this cut already prevents a global reduction to a single rational coordinate in x.

Choose a Mobius transformation sending three branch points to $0, 1, \infty$. The fourth becomes their cross-ratio m. The differential transforms to a scalar multiple of $dt/\sqrt{t(1-t)(1-mt)}$. This is a direct change-of-variables calculation: the denominator powers from the four linear factors cancel the square of the Mobius derivative in the required way. The remaining complex modulus cannot be removed by another normalization fixing $0, 1, \infty$.

The computational consequence is a reduction of redundant coordinate parameters, not elimination of the elliptic period. Differentiation in m produces a finite differential system after reducing rational differentials modulo exact forms. Such Picard–Fuchs systems are natural targets for symbolic and interval verification. A complete scattering amplitude still requires its original contour, causal prescription, regulator and subtraction conditions.

6.7 Classical string worldsheets and Weyl scaling

Let $X : \Sigma \to M$ be a map from a two-dimensional surface with metric h to a target with metric G. The classical sigma-model energy is

$$S[X,h] = \frac{1}{4\pi\alpha'} \int_\Sigma \sqrt{\det h}\, h^{ab} G_{\mu\nu}(X) \partial_a X^\mu \partial_b X^\nu \, \mathrm{d}^2\sigma.$$

Under $h \mapsto \mathrm{e}^{2\omega} h$, the square-root determinant contributes $\mathrm{e}^{2\omega}$ and the inverse metric contributes $\mathrm{e}^{-2\omega}$. Their product is unchanged.

Proposition 6.4 (U37: dimensional criterion for classical Weyl invariance)**.** *For the corresponding quadratic gradient action on a d-dimensional source, Weyl rescaling multiplies its integrand by $\mathrm{e}^{(d-2)\omega}$. The scalar gradient action is classically Weyl invariant in dimension two. A scalar mass term acquires a factor $\mathrm{e}^{d\omega}$ if the field is held fixed.*

Proof. A $d \times d$ metric determinant scales by $\mathrm{e}^{2d\omega}$, so its square root scales by $\mathrm{e}^{d\omega}$. The inverse metric scales by $\mathrm{e}^{-2\omega}$. The gradient action contains exactly one inverse metric, giving $\mathrm{e}^{(d-2)\omega}$. A mass term without inverse metrics receives only the determinant factor. □

Uniformization therefore gives a canonical constant-curvature representative for a compact worldsheet conformal class, with moduli and marked points retained. It does not eliminate

integration over moduli, ghost contributions, boundary conditions or quantum anomalies in a string path integral. Those are separate ingredients in the cited string-theory construction [6]. The classical calculation U37 remains valid independently of the quantization procedure.

For a three-dimensional membrane worldvolume the factor is e^{ω}, so the same quadratic action is not Weyl invariant. This is an explicit dimensional obstruction to applying the two-dimensional uniformization argument directly to an arbitrary membrane theory or to eleven-dimensional spacetime. Two-dimensional curves can still enter an M-theory construction as internal geometric data, as in the next section.

6.8 A brane-curve model and exact period differentiation

A dimensionless genus-one model motivated by algebraic curves in supersymmetric gauge constructions is

$$t + t^{-1} = 2(v^2 - u), \qquad y = t - (v^2 - u), \qquad y^2 = (v^2 - u)^2 - 1.$$

The physical interpretation of such curves is imported from the specified gauge/brane framework [7, 8]. The mathematical consequences below are derived for this displayed curve and require no claim that it describes all M-theory compactifications.

For $u \neq \pm 1$, the quartic has four distinct roots and the curve has genus one. Let

$$\lambda = v\frac{dt}{t} = \frac{2v^2\,dv}{y}.$$

The second equality follows by differentiating $t+t^{-1} = 2(v^2-u)$ at fixed u and using $t-t^{-1} = 2y$.

Proposition 6.5 (U38: derivative of a period modulo an exact differential)**.** *For a locally transported cycle avoiding the degenerations $u = \pm 1$,*

$$\frac{d}{du}\oint_\gamma \lambda = \oint_\gamma \frac{dv}{y}.$$

Proof. Differentiating at fixed v gives

$$\partial_u \lambda = \frac{2v^2(v^2-u)}{y^3}\,dv.$$

On the other hand,

$$d\left(\frac{v}{y}\right) = \left(\frac{1}{y} - \frac{2v^2(v^2-u)}{y^3}\right)dv.$$

Thus $\partial_u\lambda = dv/y - d(v/y)$. On a locally constant homology class the derivative of the period is the period of this parameter derivative. The integral of an exact single-valued meromorphic differential along a closed cycle avoiding its poles is zero, proving the identity. □

The period derivatives are controlled by the holomorphic differential dv/y. Their ratio is a torus modulus after a symplectic cycle normalization. U27 establishes positivity of its imaginary part and the correct transformation under a cycle-basis change. The nonlinear physical coupling interpretation requires the cited supersymmetric model; the period identity itself is a theorem about an explicit algebraic family.

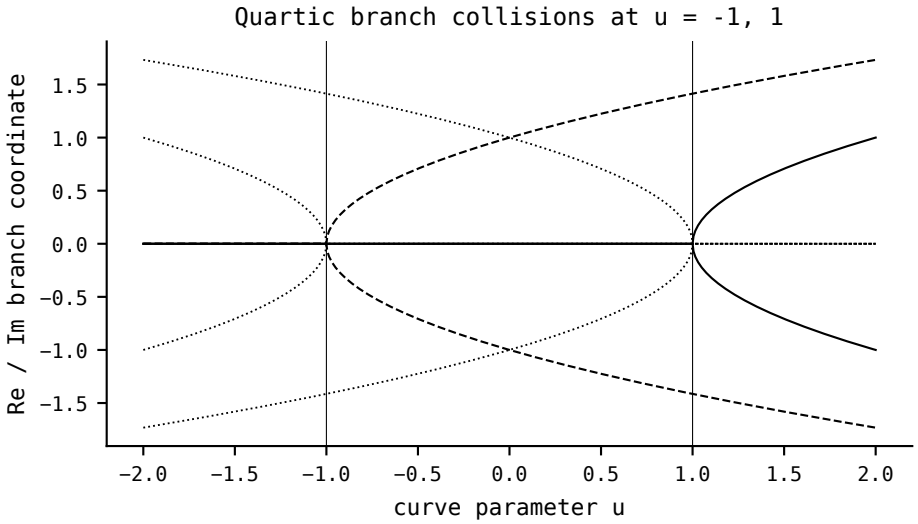


Figure 6.2: Branch points of the displayed quartic family as the real parameter varies. Collisions at the marked critical parameter values change the smooth-curve hypothesis of the period calculation.

6.9 Cylinders, punctures and conditional conformal-field identities

The map $z = \exp(2\pi w/L)$ sends a cylinder $w \bmod \mathrm{i}L$ to a punctured plane. It preserves the complex structure and converts translations in w to dilations in z. Its Schwarzian is

$$\{z, w\} = \frac{z'''}{z'} - \frac{3}{2}\left(\frac{z''}{z'}\right)^2 = -\frac{1}{2}\left(\frac{2\pi}{L}\right)^2.$$

This is an exact differentiation identity. If a conformal field theory is supplied with the stress-tensor transformation law

$$T_w(w) = \left(\frac{dz}{dw}\right)^2 T_z(z) + \frac{c}{12}\{z, w\},$$

then a plane state with $\langle T_z \rangle = 0$ has $\langle T_w \rangle = -c(2\pi/L)^2/24$. The conclusion is conditional on that quantum transformation law and on the state; it is not derived from classical uniformization alone.

Similarly, a primary-field covariance law converts a known plane two-point function into a cylinder expression with hyperbolic sines. The exponential coordinate computes the geometric factors. Operator content, central charge, anomaly cancellation and state selection remain independent field-theoretic information.

6.10 What can be certified in these applications

The exact identities of U34–U38 admit rational or symbolic checks after the stated polynomial and differential relations are included. A branch permutation can be checked in a finite permutation group. A discriminant enclosure can separate the parameter path from a degeneracy. Period quadrature requires contour-distance, integrand and tail bounds; a sampled period without those bounds remains a numerical diagnostic.

A complete physical certificate must identify the model and the observable. For a nuclear amplitude this includes channel thresholds, sheet and unitarity conventions. For a field-theory

curve it includes the differential, cycles and parameter domain. For a worldsheet action it includes source dimension, target data and quantization status. A theorem about one of these objects cannot be substituted for another merely because both are described by a Riemann surface.

Chapter 7

Thermodynamics and computational mathematical physics

7.1 Steady conduction through a conformal annulus

Consider a homogeneous two-dimensional conducting region of thickness d, conductivity $k > 0$, and two boundary components held at constant temperatures $T_0 < T_1$. In steady state without volumetric sources, $\Delta T = 0$. Let u be the annular harmonic coordinate of U11. Then

$$T = T_0 + (T_1 - T_0)u.$$

The total heat current from the hot boundary to the cold boundary is

$$Q = kd(T_1 - T_0)\operatorname{cap} A = \frac{kd(T_1 - T_0)}{\operatorname{mod} A}.$$

For the round annulus this is $2\pi kd(T_1 - T_0)/\log(R/r)$. The result is independent of the angular shape after conformal equivalence only under the stated two-dimensional homogeneous and steady assumptions.

The thermal resistance is $\operatorname{mod} A/(kd)$. It increases with logarithmic separation in the round geometry. The formula concerns total heat current, not the local maximum flux, which depends on the derivative of the conformal map and can become large near corners. Thus two conformally equivalent shapes can have equal total resistance and very different local stress on a material interface.

Proposition 7.1 (U39: exact entropy-production identity)**.** *Under this steady homogeneous model with $T > 0$, the total entropy production is*

$$\dot{S} = kd \int_A \frac{|\nabla T|^2}{T^2}\,\mathrm{d}A = Q\left(\frac{1}{T_0} - \frac{1}{T_1}\right) \geq 0.$$

Proof. Since $\Delta T = 0$, $\operatorname{div}(\nabla T/T) = -|\nabla T|^2/T^2$. Integrate and apply the divergence theorem. The hot boundary has outward derivative whose integral is $Q/(kd)$; the cold boundary has the negative of that integral by flux conservation. Multiplication by the constant reciprocal temperatures on the boundaries gives $-kd\int_{\partial A} \partial_n T/T = Q(1/T_0 - 1/T_1)$. Positivity follows from $Q > 0$ and $T_1 > T_0 > 0$. □

The formula verifies the sign of entropy production independently of the coordinate representation. Temperature-dependent conductivity, anisotropy, radiation, phase change and internal heat sources produce different equations. Their effects cannot be absorbed into a conformal modulus without a new derivation.

7.2 Transient diffusion retains a weight

The physical heat equation in the annulus is $\rho c\,\partial_t T = k\Delta_z T$. In logarithmic coordinates $z = re^{s+i\theta}$ it becomes

$$\rho c\, r^2 e^{2s} \partial_t T = k(T_{ss} + T_{\theta\theta}).$$

The variable mass factor is essential. Dropping it changes the decay rates. In a finite-element formulation the stiffness matrix may simplify under the coordinate change while the mass matrix acquires this weight.

Separation $T(s,\theta,t) = R(r)e^{in\theta-\lambda t}$ in physical polar radius gives Bessel's equation

$$R'' + \frac{1}{r}R' + \left(\frac{\rho c\lambda}{k} - \frac{n^2}{r^2}\right)R = 0.$$

The two boundary conditions determine a transcendental eigenvalue equation. An annular harmonic solution is a zero-frequency calculation; it is not a complete transient eigensolution.

Comparative conclusion. Uniformization removes geometric complexity from the steady energy problem. For transient diffusion it transports the geometry into a weight. Efficiency must therefore be measured on the resulting weighted generalized eigenproblem, with the same physical time scale and norm.

7.3 A posteriori energy control for a diffusion step

For backward Euler with a positive mass matrix M and semidefinite stiffness matrix K, the discrete update is

$$(M + \Delta t K)u^{n+1} = Mu^n + \Delta t f^{n+1}.$$

For homogeneous forcing, multiply by $(u^{n+1})^{\mathsf{T}}$ and use $2\langle a, a-b\rangle_M = \|a\|_M^2 - \|b\|_M^2 + \|a-b\|_M^2$. This yields

$$\left\|u^{n+1}\right\|_M^2 - \|u^n\|_M^2 + \left\|u^{n+1}-u^n\right\|_M^2 + 2\Delta t\left\|u^{n+1}\right\|_K^2 = 0.$$

It proves contraction in the mass norm for every positive time step. A numerical solver residual adds a term that can be bounded by dual norms. The positivity of M and K must be checked in the actual discretization; a nonconforming or incorrectly weighted assembly may fail those assumptions.

This discrete identity is suitable for an exact matrix certificate. It also provides a physical diagnostic: a growing mass norm under zero forcing signals a violation of the declared model or numerical solve, not a new instability of the exact backward-Euler scheme.

7.4 Gaussian fields and finite determinants

For a finite-dimensional real Gaussian field with energy $H(x) = \frac{1}{2}x^{\mathsf{T}}Ax$, $A \succ 0$, the partition function is

$$Z(\beta) = \int_{\mathbb{R}^n} e^{-\beta H(x)}\,dx = \left(\frac{2\pi}{\beta}\right)^{n/2}(\det A)^{-1/2}.$$

An orthogonal diagonalization reduces the integral to n one-dimensional Gaussian integrals. The covariance is $\beta^{-1}A^{-1}$. If A varies differentiably with a parameter s,

$$\frac{d}{ds}\log Z = -\frac{1}{2}\operatorname{tr}(A^{-1}A').$$

The identity follows from differentiating the determinant, or directly by differentiating under the integrable Gaussian integral and evaluating the quadratic expectation.

On a discrete periodic surface, Fourier modes can diagonalize a translation-invariant A, reducing determinant and covariance calculations to scalar mode operations. A massless Laplacian has a constant zero mode; its Gaussian integral diverges. Pinning the mean or adding a mass is part of the model specification. Removing the zero eigenvalue without recording the constraint changes the measure.

An infinite product over continuum eigenvalues requires a regularization and renormalization convention. The finite determinant identity does not authorize an unqualified substitution of an infinite-dimensional determinant. The present verification suite uses finite matrices and states their dimension explicitly.

7.5 Poisson summation and the heat-trace duality

For $t > 0$, the Gaussian Fourier transform is

$$\int_{\mathbb{R}} \mathrm{e}^{-\pi t x^2} \mathrm{e}^{-2\pi \mathrm{i} \xi x} \, \mathrm{d}x = t^{-1/2} \mathrm{e}^{-\pi \xi^2 / t}.$$

One proof differentiates the transform in ξ, integrates by parts and solves the resulting first-order ODE; its value at zero is the real Gaussian integral. Periodize the Gaussian and integrate its Fourier coefficients over a period. Absolute convergence permits termwise integration and gives the Jacobi identity

$$\sum_{n \in \mathbb{Z}} \mathrm{e}^{-\pi t n^2} = t^{-1/2} \sum_{n \in \mathbb{Z}} \mathrm{e}^{-\pi n^2 / t}.$$

In two dimensions, apply the identity along a lattice basis and retain its covolume and dual metric. The result relates a heat trace on a flat torus to a rapidly converging dual-lattice sum.

Proposition 7.2 (U40: a certified Gaussian-tail rule)**.** *For $a > 0$ and integer $N \geq 1$,*

$$\sum_{n > N} \mathrm{e}^{-a n^2} \leq \int_N^\infty \mathrm{e}^{-a x^2} \, \mathrm{d}x \leq \frac{\mathrm{e}^{-a N^2}}{2aN}.$$

Proof. The summand is decreasing on $[0, \infty)$, so each term is bounded by the preceding unit interval's integral. For $x \geq N$, $1 \leq x/N$. Therefore the integral is at most $N^{-1} \int_N^\infty x \mathrm{e}^{-a x^2} dx = \mathrm{e}^{-a N^2}/(2aN)$. □

The primal or dual sum can be selected by comparing their rigorously bounded term counts at the requested tolerance. This is an error-controlled algorithmic choice. A physical interpretation as a thermal partition function requires the appropriate spectrum, degeneracies and energy units; the theta identity alone does not select them.

7.6 Liouville's equation and constant curvature

For $g = \mathrm{e}^{2\varphi}(dx^2 + dy^2)$, direct computation of the Levi-Civita connection gives

$$K = -\mathrm{e}^{-2\varphi} \Delta \varphi.$$

Thus constant curvature K_0 is the nonlinear equation $\Delta\varphi + K_0 \mathrm{e}^{2\varphi} = 0$. For the disk metric $\varphi = \log 2 - \log(1 - r^2)$, differentiation gives $\Delta\varphi = 4/(1 - r^2)^2 = \mathrm{e}^{2\varphi}$, hence $K = -1$.

The curvature equation is a local differential expression. Its global solvability must respect Gauss–Bonnet, cone angles, completeness and normalization. A small discretized Liouville residual does not prove those global conditions. Conversely, a correctly uniformized quotient supplies an exact solution with its topology already specified.

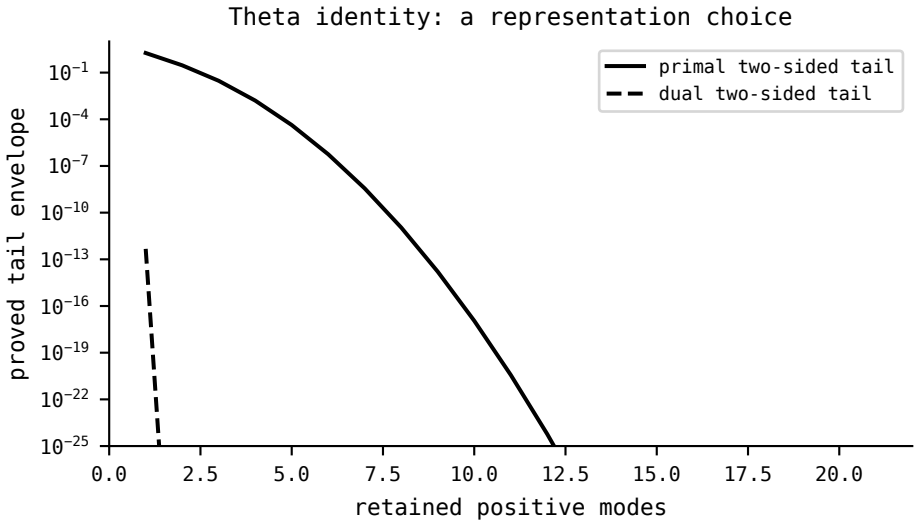


Figure 7.1: The primal and dual Gaussian sums converge at different rates for the same exact quantity. The plotted certified tail envelopes determine a representation choice at a fixed tolerance.

For a smooth perturbation $\varphi + \varepsilon\psi$, the curvature variation is

$$\delta K = -\mathrm{e}^{-2\varphi}\Delta\psi - 2K\psi.$$

This follows by differentiating the two factors. It supplies a linearized conditioning operator for a nonlinear curvature solve. Its kernel can contain normalization directions; numerical optimization should remove or constrain those normalization directions before interpreting its conditioning.

7.7 Energy minimization, discretization and best approximation

Let $V \subset H^1$ be an affine space of fixed traces and $V_h \subset V$ a finite-dimensional conforming subspace. The exact harmonic minimizer u and discrete minimizer u_h satisfy Galerkin orthogonality. For every $v_h \in V_h$,

$$\|u - u_h\|_E \leq \|u - v_h\|_E .$$

To prove it, write $u - v_h = (u - u_h) + (u_h - v_h)$ and use orthogonality of the two terms in the energy inner product. The identity gives the sum of squared norms, so the desired inequality follows.

This is an attained optimum within the declared approximation subspace. It does not make one mesh globally optimal among all discretizations of equal storage. Such a comparison needs an admissible mesh class, approximation lower bounds and the cost of assembly and solution. The same distinction applies to spectral truncation and finite-rank kernels.

7.8 Inverse problems and conformal nonidentifiability

Suppose an experiment measures only the total steady conductance between two equipotential boundary components. U11 shows that the output depends on the conformal modulus and material constants. Infinitely many differently shaped domains have the same modulus. The observable cannot uniquely recover their Euclidean geometry.

A proof is obtained by taking a nontrivial univalent conformal deformation of a round annulus and transporting the boundary conditions. Capacity is unchanged by U30, while Euclidean

curvature and local boundary shape change. Thus any algorithm returning a unique shape from that single conductance has inserted an additional prior or constraint. Measurement noise is not the only obstruction; the noiseless map is already noninjective.

Additional boundary measurements can distinguish more geometry, but their identifiability requires a separate inverse theorem. The monograph uses this example to keep explanatory efficiency distinct from information loss: a scalar invariant is sufficient for one forward observable and insufficient for a general inverse reconstruction.

7.9 A computational-physics acceptance specification

A reproducible computation based on a uniformizing coordinate should record the original field equation; source, boundary and initial conditions; the coordinate map and its normalization; transformed coefficients and measures; the finite representation; solver error; and the error of the map itself. Each term has a separate place in the final uncertainty budget.

For a transported field $u \circ f$, a map perturbation $\widehat{f}$ and field approximation $\widehat{u}$ give

$$|u(f(z)) - \widehat{u}(\widehat{f}(z))| \leq \|u - \widehat{u}\|_{\infty,V} + \sup_{V} |\nabla \widehat{u}|\, |f(z) - \widehat{f}(z)|,$$

provided the segment or a controlled connecting path stays in the valid domain. If it does not, replace the Euclidean segment estimate with a path-length bound. Near a singular boundary, the derivative factor can dominate. Reporting only the spectral approximation error can therefore conceal the principal source of physical error.

Chapter 8

Logical complexity, algorithms, parallelism and cryptography

8.1 What a computational uniformization problem contains

The input to a computation cannot be an unspecified Riemann surface. Typical finite encodings are a triangulated surface with metric data, algebraic equations with branch information, a polygon with edge identifications, a boundary parametrization with regularity bounds, or a finite atlas with transition maps. Each encoding supplies different algorithms and permits different certificates.

A computational task must also identify its output. Possible outputs include a conformal type, a normalized map on a compact subset, a modulus, a period matrix, a field value, an operator action or a topological monodromy label. The existence theorem does not identify the bit complexity of every one of these tasks. An input domain specified by an arbitrary oracle can conceal undecidable or noncomputable information; the finite precision model must be part of any algorithmic theorem.

The following comparisons use explicit finite matrices, finite graphs, rational certificates or analytic classes with quantitative regularity. Their bounds are consequently stated for those representations. The source theorem supplies their geometric organization, while each algorithm has its own proof.

8.2 Logical complexity as a dependency problem

A source proof compressed to a few lines can invoke several substantial theorems. Counting those lines assigns zero cost to the hidden dependencies. A more useful formal representation is a directed graph whose vertices are exact propositions and whose edges identify hypotheses or imported results. An application of a theorem contributes an edge only when its hypotheses have been discharged in the new setting.

For annular uniformization, the relevant graph contains Dirichlet existence, closedness of the conjugate form, period quantization, properness and degree one. Computing a few equipotential curves does not replace the degree proof. For global uniformization, the graph contains finite-disk uniformization, normalized radius monotonicity, compact convergence, injectivity and surjectivity. U17 is a distinct obligation because injectivity of a limit does not imply that it fills the proposed target.

Logical compression becomes meaningful when a single invariant discharges an explicitly defined family of obligations. For example, positivity of a Bernstein coefficient list proves a

polynomial inequality at every point of an interval. The finite input is a coefficient list; the conclusion has a universal real quantifier. The reduction is justified by the basis theorem, not by claiming that the continuum has been exhaustively sampled.

8.3 Typed certificates and soundness

Definition 8.1 (Certificate interface)**.** A checker is a total function $\mathrm{check} : \mathcal{D} \times \mathcal{C} \to \{\mathrm{true}, \mathrm{false}\}$ with a soundness assertion

$$\mathrm{check}(d, c) = \mathrm{true} \Longrightarrow P(d).$$

The input interpretation, certificate format and proposition P are part of the interface.

The source data d should use an exact representation when the conclusion is exact. Rational coefficients, integer permutations and algebraic interval endpoints are suitable finite objects. A decimal string interpreted as a rational is different from a floating-point value rounded from that decimal. The delivered certificate programs make that interpretation explicit.

Proposition 8.2 (U41: exact Bernstein positivity)**.** *If*

$$p(t) = \sum_{k=0}^{n} b_k \binom{n}{k} t^k (1-t)^{n-k}, \qquad b_k \geq \eta,$$

then $p(t) \geq \eta$ *for every* $0 \leq t \leq 1$*.*

Proof. Every basis function is nonnegative on the interval. The binomial theorem says their sum is $(t + (1-t))^n = 1$. Hence $p(t) - \eta$ is a nonnegative linear combination of nonnegative functions. □

A subdivision certificate additionally lists subintervals covering the full requested interval, exact transformed coefficients on each subinterval and the asserted lower bounds. Soundness requires checking the affine substitution, every coefficient inequality and interval coverage. A gap between two subintervals invalidates the certificate even when every individual coefficient list is positive.

8.3.1 Certificates of nonexistence and corrected statements

The same mechanism can establish impossibility. A positive lower bound for $|F|^2$ on a parameter interval excludes a zero there. A genus calculation excludes a rational uniformizing parameter. A finite permutation witness disproves the assertion that two continuation loops commute. Each is a fully specified logical output, not a failure to find a positive construction.

A checker that accepts a deliberately weakened or changed target statement can still be mathematically sound for the wrong problem. Source-concordance review therefore precedes proof checking. The formalization register records the source proposition and any corrected proposition as separate entries where they differ.

8.4 Modal algorithms and exact arithmetic counts

For a periodic grid with N points, define the cyclic shift S and the screened cycle Laplacian

$$A_N = \alpha I + 2I - S - S^{-1}, \qquad \alpha > 0.$$

The Fourier vectors are eigenvectors with eigenvalues

$$\lambda_k = \alpha + 4\sin^2(\pi k/N) > 0.$$

Thus $A_N x = b$ is solved by a forward transform, N scalar divisions and an inverse transform.

Theorem 8.3 (U42: Fourier solution of the screened cycle system)**.** *The Fourier algorithm returns the unique exact solution. In a radix-two arithmetic model with $N = 2^m$, its transform work is $O(N \log N)$ and depth is $O(\log N)$. A dense elimination implementation has $O(N^3)$ setup work and $O(N^2)$ storage.*

Proof. The cyclic shift acts on the kth Fourier vector by a root of unity. Substitution gives the displayed positive eigenvalues. Since the Fourier matrix is invertible, division by these eigenvalues and transformation back solves the system uniquely. A radix-two transform splits into two half-size transforms and $N/2$ butterflies. The recurrence $W(N) = 2W(N/2) + cN$ gives $W(N) = cN \log_2 N + O(N)$. Parallel butterflies at each level give $D(N) = D(N/2) + O(1) = O(\log N)$. The dense Gaussian-elimination work and dense-array storage counts follow from summing the squared trailing matrix sizes and counting N^2 entries. □

A cyclic tridiagonal direct solver has $O(N)$ work and is a strong conventional baseline for this particular system. U42 does not prove FFT superiority over that solver. The Fourier representation is especially useful when repeated operator functions or multiple periodic dimensions make the modal basis reusable. The benchmark records the implemented baselines and does not present the dense comparison as a lower bound on all conventional methods.

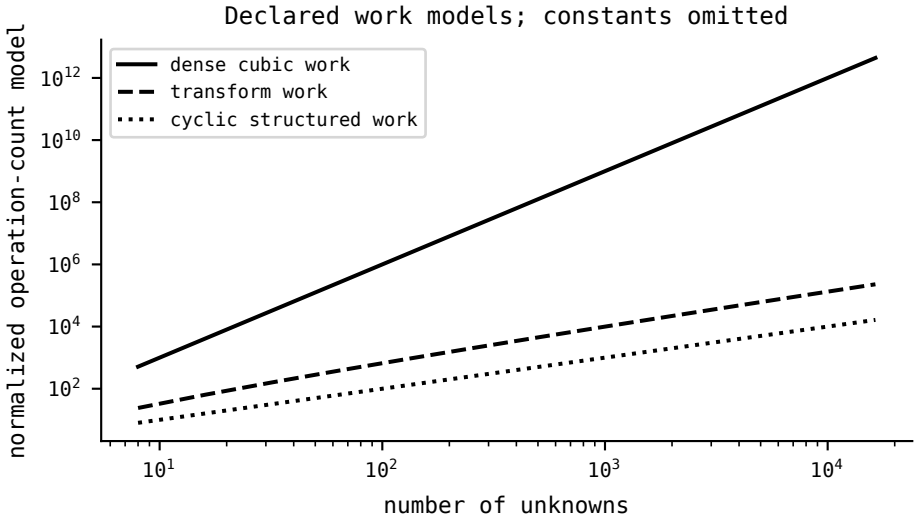


Figure 8.1: Declared operation-count growth for dense elimination, a transform solve and a cyclic structured solve. These are model curves; observed timings are recorded separately.

8.5 Two-dimensional periodic operators

For an $n \times n$ rectangular periodic grid, $N = n^2$ unknowns, the five-point screened Laplacian is a Kronecker sum. A two-dimensional Fourier transform diagonalizes it. Its work is $O(N \log n)$ and storage $O(N)$. A generic dense matrix representation has $N^2 = n^4$ entries, so forming it would discard sparsity before any solve begins.

The appropriate comparisons include sparse direct factorization, multigrid and iterative methods with preconditioners. Their performance depends on the operator, geometry, tolerance

and repeated-use pattern. A uniformized physical surface can produce variable coefficients or a mass weight that breaks exact translation invariance. Then the Fourier operator can serve as a preconditioner, but the remaining variable-coefficient solve must be analyzed.

For a positive coefficient $a(x)$ satisfying $0 < a_- \le a(x) \le a_+$, the energy forms obey

$$a_- \int |\nabla v|^2 \le \int a|\nabla v|^2 \le a_+ \int |\nabla v|^2.$$

This yields a spectral-equivalence condition number bound a_+/a_- for the constant-coefficient preconditioner on the trace-zero or mean-zero space. It is a proved quantitative benefit when that ratio is bounded. A narrow conformal neck can make coefficient ratios or low spectral gaps unfavorable; uniformization is not automatically a well-conditioned preconditioner.

8.6 Parallel work, depth and communication

Work and depth characterize an ideal dependency graph. A real distributed FFT also moves data. Under a latency–bandwidth model, a message carrying m scalars costs $\alpha_{\text{net}} + \beta_{\text{net}} m$. A staged all-to-all decomposition may therefore have communication time of the form

$$T_{\text{comm}} = r\alpha_{\text{net}} + \beta_{\text{net}} V,$$

where r is the number of dependent communication rounds and V the per-process communicated volume under the chosen decomposition.

A proof of $O(\log N)$ arithmetic depth does not eliminate these rounds. Likewise, an asymptotic work reduction can lose on small grids because setup and communication dominate. A reproducible high-performance comparison records process count, decomposition, precision, transform planning, network model, all communication and the norm of the returned residual.

Uniformizing a surface may create a periodic coordinate domain and make transform methods available. If the geometric map itself costs C_{map} and a transformed solve saves ΔC per query, the break-even query count is at least $\lceil C_{\text{map}}/\Delta C \rceil$ when $\Delta C > 0$. The bound is an exact statement for the declared affine cost model. It says nothing about a different workload or an unmeasured communication regime.

8.7 Distributed averaging and spectral gaps

Consider $x^{(t+1)} = Px^{(t)}$, where P is a symmetric stochastic matrix on a connected finite graph and all eigenvalues other than the constant eigenvalue one have modulus at most $\rho < 1$. Orthogonal diagonalization gives

$$\left\| x^{(t)} - \bar{x}\mathbf{1} \right\|_2 \le \rho^t \left\| x^{(0)} - \bar{x}\mathbf{1} \right\|_2 .$$

A sufficient number of rounds for error at most ε is

$$t \ge \frac{\log(\left\| x^{(0)} - \bar{x}\mathbf{1} \right\|_2 / \varepsilon)}{-\log \rho}.$$

The mean is preserved because $\mathbf{1}^{\mathsf{T}} P = \mathbf{1}^{\mathsf{T}}$. The spectral estimate proves a finite-dimensional mixing guarantee.

On a cycle, a local averaging matrix has a gap of order N^{-2}, so local consensus can require quadratically many rounds at a fixed relative error. A direct global reduction uses a different communication primitive. Calling the transform or global-reduction approach “faster” without naming that primitive would compare different network models.

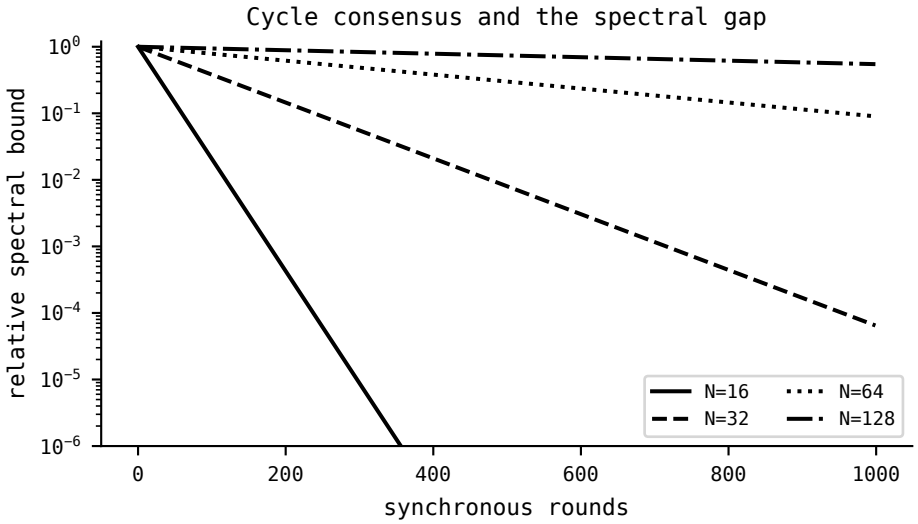


Figure 8.2: Exact spectral envelopes for symmetric averaging on cycles of different sizes. The dependence on graph size is a communication-round statement, independent of wall-clock network measurements.

8.8 Branch continuation as a distributed state machine

A continuation state should include the parameter location, branch value, certified domain, normalization and source-version identifier. A transition along a path segment is accepted only when a local inverse or continuation certificate establishes existence and uniqueness on that segment. If a worker returns a result for an earlier domain version, the result must be rejected or explicitly translated.

Proposition 8.4 (U43: compositional branch safety)**.** *Suppose every accepted transition has a postcondition matching the next transition's precondition, and each transition preserves a declared invariant I. Then every finite accepted execution preserves I. If local branch continuation is unique on each segment, the composed value is the continuation along the concatenated path.*

Proof. Induct on the execution length. The empty execution has the initial invariant. If it holds after k transitions, the postcondition–precondition match permits transition $k+1$, whose preservation theorem gives the invariant afterward. Uniqueness of the local analytic continuation makes the value at each joint the initial value for the next segment, so induction also identifies the composition with continuation along the concatenated path. □

This proves safety. Liveness additionally requires termination of certificate search or a sufficient refinement rule, fair scheduling and a path that stays a positive distance from singularities. An infinite refinement sequence approaching a branch collision need not terminate. A temporal-logic claim must distinguish "every accepted result is valid" from "every requested result is eventually returned."

8.8.1 An exact noncommutativity witness

Let two continuation generators act on three sheets by $a = (12)$ and $b = (23)$. Their commutator $aba^{-1}b^{-1}$ is nonidentity, although its abelianized winding counts are zero. The finite permutation computation is a certificate that scalar winding counters alone do not determine the final sheet. A distributed implementation must retain the permutation action or a sufficiently rich homotopy label.

The issue is mathematical, not a race-condition artifact. Parallel paths that are homotopic relative to endpoints have the same continuation under the usual uniqueness hypotheses. Paths with different monodromy can return different branches even when every local numerical step is correct.

8.9 Temporal logic and finite-model verification

For a branch service, a safety specification can be expressed as: every published state has a matching version and a checked path certificate. A liveness specification can state: every admissible request is eventually answered, assuming fair scheduling, finite certificate-search bounds and absence of permanent worker failure. These are propositions about an explicitly defined transition system.

Finite-state model checking can enumerate all executions up to the state-space closure, proving a safety invariant for that finite abstraction. An unbounded real-parameter system requires an abstraction theorem connecting concrete states to the finite model. Bounded execution checking proves no violation within the bound; it does not establish all-time liveness. The mathematical abstraction, the temporal formula and the checker result belong in separate fields of the verification register.

The present release supplies exact finite checks of permutation composition and version-independent algebraic invariants. It supplies no model-checker proof of an operational distributed service. The prospective proof routes identify where such a development can reuse the local continuation and composition lemmas.

8.10 Cryptography: complex tori and finite fields

A complex elliptic curve is analytically $\mathbb{C}/\Lambda$ and algebraically a nonsingular cubic. Cryptographic arithmetic usually takes place over a finite field. The finite group of points is not a topological quotient of $\mathbb{C}$ used as a real-number computation. Reduction requires an integral algebraic model and a prime of good reduction; group sizes, subgroup orders and security assumptions are additional arithmetic data.

For $E : y^2 = x^3 + ax + b$ over a field of characteristic different from two and three, the discriminant condition is $4a^3 + 27b^2 \neq 0$. Point addition follows from intersecting the secant line with the cubic. If the line through $P = (x_1, y_1)$ and $Q = (x_2, y_2)$ has slope s, comparison of the cubic's root sum gives

$$x_3 = s^2 - x_1 - x_2, \qquad y_3 = -y_1 + s(x_1 - x_3).$$

For doubling, $s = (3x_1^2 + a)/(2y_1)$ when the denominator is nonzero. Vertical lines and the point at infinity are separate cases. These formulas can be checked exactly in finite fields; complex floating-point evaluation is not their specification.

Proposition 8.5 (U44: public multiplication is not encryption)**.** *On a known cyclic group of order m, the map $P \mapsto [n]P$ is publicly invertible whenever* $\gcd(n, m) = 1$*. A publicly known translation $P \mapsto P + Q$ is also publicly invertible.*

Proof. Bezout's identity gives integers u, v with $un + vm = 1$. Since $[m]P = 0$, multiplication by u inverts multiplication by n. Translation is inverted by adding $-Q$. □

A conformal map's visual complexity therefore supplies no encryption proof. Public uniformization data can be useful in curve construction, period computation or complex multiplication, but cryptographic security requires an explicit game, key distribution and reduction to an identified computational assumption. This volume makes no novel security claim.

8.11 A finite arithmetic example and a transfer boundary

Take $E : y^2 = x^3 - x$ and a prime $p > 2$. The reduction is nonsingular because $4(-1)^3 = -4$ is nonzero. An exact point count can enumerate $x \in \mathbb{F}_p$, determine the number of square roots of $x^3 - x$, and add the point at infinity. This costs $O(p)$ residue tests in the direct enumeration model. A faster point-counting algorithm has its own arithmetic theory; the complex torus coordinate alone does not establish its complexity.

At $p = 5$, the values $x = 0, 1, 4$ give one root each, $x = 2$ gives two roots, and $x = 3$ gives two roots. Together with infinity, there are eight points. The exact checker reproduces this count and checks the nonsingularity condition. This is an illustrative finite certificate, not a cryptographically sized instance.

8.12 Algorithm optimization with a certificate cost

Let two algorithms return the same output with the same tolerance. Suppose one computes a candidate quickly but needs an expensive checker, while the other is slower and returns a cheaply verifiable certificate. The relevant total is

$$C_{\text{total}} = C_{\text{construction}} + C_{\text{checking}} + C_{\text{data preparation}}.$$

A published speedup excluding required certificate construction is incomplete for a proof-carrying workflow. Similarly, a checker that assumes exact input coefficients while the actual input is uncertain proves the wrong instance.

For annular capacity, a useful certificate contains a primal test potential and a dual divergence-free flux. The primal energy bounds capacity from above. A normalized dual flux gives a reciprocal-energy lower bound by Cauchy–Schwarz. Their gap can quantify the quality of the approximate uniformization without requiring a visually perfect map. The next chapter derives that pair in engineering form.

Chapter 9

Engineering models and dual certificates

9.1 A common mathematical interface

An engineering application of uniformization begins with a planar or surface-supported model whose geometry is part of the input. The transformed problem must retain its constitutive coefficients, units and boundary data. For a purely digital task, finite algebra and verification semantics supply the relevant connection when no surface geometry is present.

The principal interfaces considered here are electrostatics and conduction; circuits and passive response; signals and periodic computations; control and embedded realizations; machines and power networks; computational geometry; and scientific software. Mechanical, chemical, environmental and general professional tasks receive a relevant mathematical subproblem only when one can be specified. An ideal mathematical model is not a certification of a physical installation or device.

9.2 Planar electrostatics and capacitance

For a homogeneous dielectric cross-section with permittivity ϵ, conductor voltage difference V and translational invariance along the device axis, the electrostatic potential is $V\,u$ with u as in U11. The energy per unit axial length is

$$W' = \frac{\epsilon}{2}\int_A |\nabla(V\,u)|^2\,\mathrm{d}A = \frac{1}{2}C'V^2, \qquad C' = \epsilon\,\mathrm{cap}\,A = \frac{\epsilon}{\mathrm{mod}\,A}.$$

For concentric radii r, R, $C' = 2\pi\epsilon/\log(R/r)$. The coordinate map changes the field components and local stress but preserves the unweighted two-dimensional Dirichlet energy. Axial fringing, spatially varying permittivity and three-dimensional geometry require additional terms.

A capacitance estimate based only on a boundary-node count has no theorem-level error interpretation. A conformal or variational estimate can instead use energy upper and lower bounds. The following pair is particularly useful because it does not require knowing the exact solution.

Theorem 9.1 (U45: primal–dual condenser certificate)**.** *Let u be the unit-voltage harmonic potential on a smooth annular conductor domain. For any admissible test potential v with the same boundary values,*

$$\mathrm{cap}\,A \le \int_A |\nabla v|^2\,\mathrm{d}A.$$

For any square-integrable divergence-free flux field j carrying total flux one from one boundary component to the other,

$$\frac{1}{\int_A |j|^2 \,\mathrm{d}A} \le \operatorname{cap} A.$$

Both bounds are attained by $v = u$ and $j = \nabla u / \operatorname{cap} A$ with the corresponding orientation.

Proof. The upper bound is U05. For the lower bound, integration by parts and the unit-voltage boundary trace give $\int_A j \cdot \nabla u \,\mathrm{d}A = 1$ after orienting the flux. Cauchy–Schwarz yields $1 \le (\int |j|^2)(\int |\nabla u|^2) = (\int |j|^2) \operatorname{cap} A$. The exact flux field is divergence-free and has total flux one because the total flux of ∇u is $\operatorname{cap} A$. Substituting it makes equality hold. □

The field j must be divergence-free in the required weak sense, with its flux verified. A numerical vector field that approximately satisfies conservation gives a modified bound with a residual term, not the exact reciprocal inequality. Exact rational fluxes on a finite network provide a tractable certificate model.

9.3 An exact network analogue

On a finite undirected network with conductances $c_e > 0$, write the energy as $E(v) = \sum_e c_e (v_i - v_j)^2$ for fixed terminal potentials zero and one. Its unique interior minimizer solves the weighted graph Laplace equation. A unit terminal flow f_e with zero divergence at interior vertices has dissipation $\sum_e f_e^2 / c_e$.

The same summation-by-parts and Cauchy–Schwarz argument gives

$$\frac{1}{\sum_e f_e^2 / c_e} \le C_{\mathrm{eff}} \le E(v).$$

At the exact potential, $f_e = c_e (v_i - v_j) / C_{\mathrm{eff}}$ gives equality. This is the discrete Dirichlet–Thomson duality. The verification suite uses rational conductances and exact elimination, so the certificate values are rational and independently reproducible.

The network is an analogue of the continuum variational problem. Establishing convergence of a mesh's effective conductance to the continuum capacity requires a conforming discretization or a separate homogenization theorem. Agreement of one graph with a closed-form annulus is a diagnostic and cannot establish all-mesh convergence.

9.4 Corners and field singularities

In a wedge of opening angle α, homogeneous Dirichlet harmonic modes are

$$u(r, \theta) = r^{\pi/\alpha} \sin(\pi\theta/\alpha).$$

Their gradient scales as $r^{\pi/\alpha - 1}$. A re-entrant angle $\alpha > \pi$ produces an unbounded gradient near the corner. The energy density integrates as

$$\int_0^{\varepsilon} r^{2\pi/\alpha - 2} r \,\mathrm{d}r = \frac{\varepsilon^{2\pi/\alpha}}{2\pi/\alpha},$$

which is finite for every finite positive α.

Thus a convergent energy calculation can coexist with diverging meshwise maximum field. The local conformal map $w = z^{\pi/\alpha}$ explains both facts and fixes the branch on the wedge. A certificate for total energy is not a certificate for the peak field at a geometrically singular ideal corner.

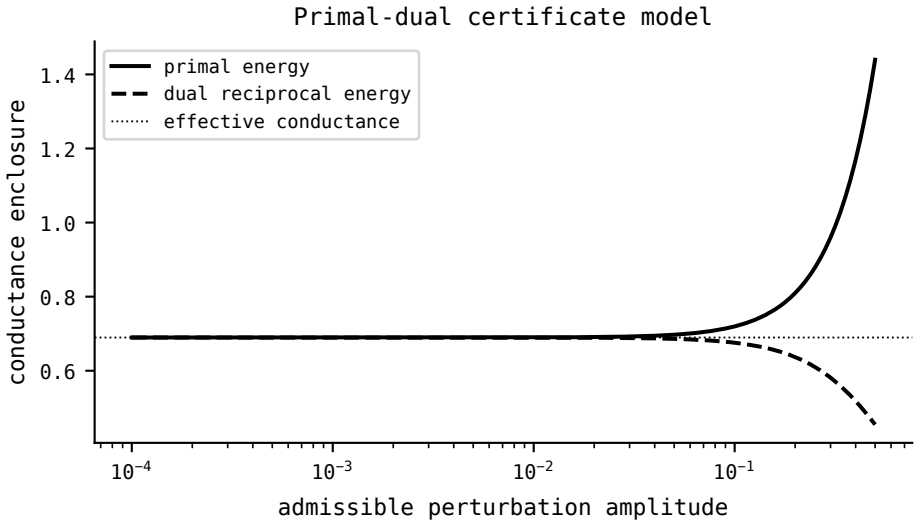


Figure 9.1: Illustrative primal–dual energy model with reference conductance $20/29$: $P = C + 3\varepsilon^2$ and $R = 1/C + 3\varepsilon^2$. The graph depicts these declared model curves; the exact path certificate is a separate calculation.

The same geometry appears in steady conduction and some scalar potential-flow models. Elasticity and full vector electromagnetism have additional field components and constitutive structure. The scalar wedge formula is not a complete solution of those vector systems.

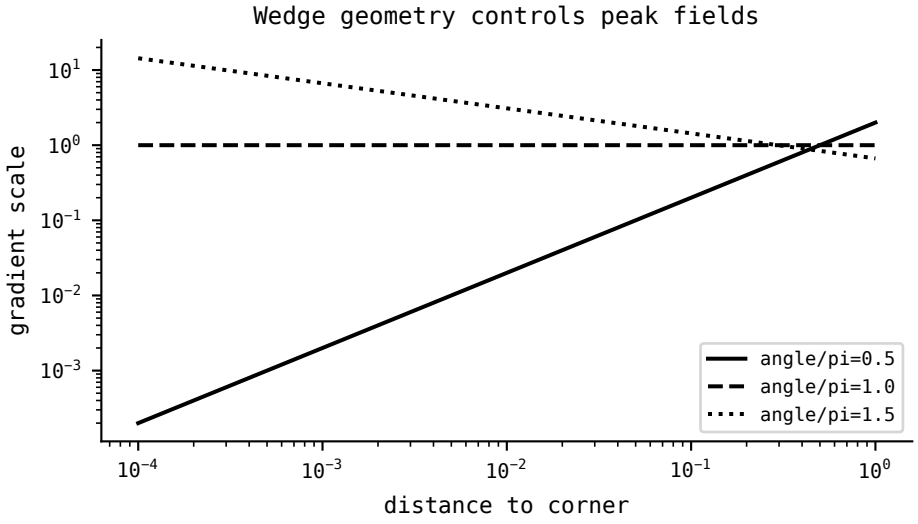


Figure 9.2: Exact gradient exponents for three wedge angles. The re-entrant case has an unbounded ideal peak field despite finite local energy.

9.5 Circuit response as a half-plane function

For a passive scalar impedance in its appropriate analytic domain, the condition $\operatorname{Re} Z \geq 0$ maps under

$$\Gamma = \frac{Z - Z_0}{Z + Z_0}, \qquad Z_0 > 0,$$

to the disk condition $|\Gamma| \le 1$. Indeed,

$$1 - |\Gamma|^2 = \frac{4Z_0 \operatorname{Re} Z}{|Z + Z_0|^2}.$$

The inverse is $Z = Z_0(1+\Gamma)/(1-\Gamma)$ where $\Gamma \neq 1$. This is an exact Mobius equivalence of pointwise feasible sets; analyticity and realization hypotheses must accompany it for a frequency-dependent physical network.

Uniformization and the disk geometry support interpolation and sensitivity estimates. A finite set of values inside the disk does not prove that an interpolating rational response stays in the disk between samples. A Pick-matrix criterion or a constructive Schur representation can provide a continuum statement, subject to its hypotheses. The earlier PHI circuit analyses develop the corresponding finite interpolation examples [4].

9.6 Control, stability domains and discrete implementations

The Cayley map $z = (1 + s)/(1 - s)$ sends the open left half-plane in s to the open disk in z after the sign convention is fixed. Direct computation gives

$$1 - |z|^2 = \frac{-4 \operatorname{Re} s}{|1 - s|^2}.$$

A bilinear discretization introduces a time-scale factor, usually $s = (2/T)(z - 1)/(z + 1)$. The stability-domain relation is a theorem about the transformed scalar pole location. Internal state stability after pole-zero cancellation, actuator saturation and fixed-point rounding are additional obligations.

For a stable ideal recurrence $x_{n+1} = ax_n$, $|a| < 1$, rounding to a finite state grid can create a nonzero fixed point whenever a grid state lies in its own rounding cell after multiplication. A complete digital stability analysis therefore studies the finite transition map. Uniformization organizes the ideal domain; it does not remove machine arithmetic.

9.7 Machines, drives and power-network calculations

Complex coordinates efficiently represent rotating two-axis quantities. A rotation $z \mapsto \mathrm{e}^{\mathrm{i}\theta} z$ preserves the Euclidean norm, while a time-dependent rotation introduces an extra $\mathrm{i}\dot{\theta} z$ term in the transformed differential equation. Omitting that term changes the dynamics. A conformal map more general than a rotation usually changes the metric and constitutive relation, so it cannot be treated as a lossless coordinate relabeling of a machine model without a derivation.

Power-flow equations include complex conjugates and are not holomorphic in the original voltage variables. One may construct an analytic embedding in an auxiliary parameter and solve its branch problem. A certificate must then distinguish the desired operating branch, ensure the model constraints, and bound truncation and continuation error. The existence of an analytic continuation is not a proof of feasibility at every load parameter.

The source-section connection is the distinction between local invertibility and global branch selection. A network solver may return a small residual on an unintended branch, just as a continuation algorithm may return the wrong sheet after a nontrivial loop. The relevant acceptance test includes state constraints and the branch history.

9.8 Signals, transforms and finite observables

Periodic signals on a uniformized torus have two frequency indices determined by its lattice. Signals on an annular boundary have one periodic angular coordinate and a separate radial propagation operator. A function periodic in an arbitrary physical coordinate need not remain uniformly sampled after a nonlinear conformal map.

If a physical boundary parameter s is replaced by $\theta = \theta(s)$, quadrature weights change by $ds/d\theta$. Applying an FFT to values equally spaced in s and interpreting them as equally spaced in θ creates a sampling error independent of transform implementation. A complete numerical pipeline records the parametrization, Jacobian, interpolation and error of resampling.

Finite Fourier observables can be certified by an analyticity envelope or by a proved discrete algebraic identity. These are different methods: the former controls truncation of a continuum representation; the latter exactly solves a finite transform problem. The code and theorem register retain the distinction.

9.9 Computational geometry and conformal meshes

A smooth conformal map is locally angle preserving. A piecewise affine map between triangle meshes is generally not conformal on every triangle unless its local derivative is a similarity. Discrete conformal theories use explicitly different definitions, such as vertex scale factors or circle patterns. Their variational formulations have established literature [10]; a discrete map must be evaluated under the definition actually implemented.

For a triangle map with real derivative J, a quantitative distortion measure is $\sigma_{\max}(J)/\sigma_{\min}(J)$ when $\det J > 0$. The determinant condition prevents a folded or degenerate element from appearing acceptable merely because an unoriented ratio is small. Global injectivity also requires compatibility and boundary information; positive local determinants alone can fail on a globally overlapping mesh.

A practical certificate can combine positive orientation, a boundary homeomorphism, degree one and verified local nondegeneracy. The proof mirrors U11's properness-and-degree construction. Its finite-mesh form still requires exact predicates or a controlled rounding analysis for element orientation.

9.10 Software, electronics and the remaining engineering subjects

For software engineering, compilers, databases and operating systems, uniformization is not a general replacement for the native semantics. Its useful contributions are specialized numerical contracts, branch-aware interfaces and certificate architecture. For digital logic and embedded systems, the core verification objects are bit-vector transformations, state transitions, timing and memory. Their analysis can reuse exact algebra and invariants without pretending that every transition system is a Riemann surface.

For materials, chemistry and thermal processes, a planar diffusion or potential model can admit the conformal treatment derived above. Reaction terms, nonlinear kinetics and evolving boundaries require new equations. For graphics, the coordinate map can aid parameterization, with distortion and sampling costs retained. For communication and general professional work, no direct uniformization theorem is asserted; the relevant transferable practice is precise specification and evidence separation.

Each application is indexed by its governing mathematical model, its admissible regime and

the observable that the calculation certifies.

Chapter 10

Quantitative closure, computability and additional structural proofs

10.1 What a finite presentation can establish about uniformization type

A Riemann surface can be presented by charts, transition functions and an exhaustion. Such a presentation contains more information than a list of numerical samples, but the representation still matters. A classification theorem asserts the existence of a conformal model. It need not supply a terminating procedure that identifies the model from arbitrary finite observations of the presentation.

Consider the particularly simple surfaces obtained as unions of concentric disks. A presentation supplies a strictly increasing sequence of positive rational radii R_n and exact inclusions $D_{R_n} \subset D_{R_{n+1}}$. The union is D_R, where $R = \sup_n R_n \in (0, \infty]$. The only classification question is whether R is finite. Every finite prefix is compatible with both possibilities: continue with increments 2^{-k} to obtain a finite limit, or with increments one to obtain an infinite limit. This is an information-theoretic obstruction that already occurs before general surfaces enter the problem.

Theorem 10.1 (U46: no total classification procedure for arbitrary computable exhaustions)**.** *There is no algorithm which, from every program computing a strictly increasing positive rational disk exhaustion, always terminates and correctly decides whether the union is conformally a disk or the plane.*

Proof. For a program M and its input, define $R_0 = 1$ and, for $k \geq 1$,

$$R_k - R_{k-1} = \begin{cases} 1, & M \text{ has not halted within its first } k \text{ steps}, \\ 2^{-k}, & M \text{ has halted within those steps}. \end{cases}$$

A bounded simulation computes each increment exactly, so this is a computable, strictly increasing rational sequence. If M never halts, $R_k = 1 + k$ and the union is $\mathbb{C}$. If M first halts after a finite number of steps, there are finitely many unit increments followed by a convergent geometric tail, so the union is a bounded round disk. A total classifier would decide whether M halts.

For completeness, the latter decision is impossible by diagonalization. If a total algorithm $H(P, x)$ decided whether program P halts on input x, define a program $Q(x)$ which runs forever when $H(x, x)$ reports halting and halts immediately otherwise. Apply it to its own code q. Each possible value of $H(q, q)$ contradicts the prescribed behavior of $Q(q)$. Thus H, and hence the supposed conformal-type classifier, cannot exist. □

The theorem concerns program-described exhaustions without a supplied bound on their limit. It does not obstruct classification for an algebraic curve of known genus, a finite polygon with a certified group action, or an exhaustion carrying an independently proved radius bound. It specifies exactly which missing information causes the failure. A numeric implementation that terminates after a large number of steps has not escaped the obstruction unless its admissible input class is narrower.

A useful positive certificate for disk type is a finite rational B together with a proof that $R_n \le B$ for all n. A useful positive certificate for plane type is a computable witness $n(m)$ with $R_{n(m)} > m$ for every integer m. Checking one value of either relation is insufficient; the universal certificate can be represented by an inductive argument or a proved formula. These conclusions make the nonconstructive and quantitative parts of uniformization compatible without conflating them.

10.2 Finite observation and the need for an analytic envelope

The same distinction controls recovery of a holomorphic function. Suppose an algorithm samples a function at points $z_1, \dots, z_n$ in a domain. Define $p(z) = \prod_{j=1}^{n}(z - z_j)$. Every pair f and $f + cp$ yields the same observed values for arbitrary $c \in \mathbb{C}$. If the target point z_* is different from the sample points, their values there differ by $cp(z_*)$, with arbitrarily large magnitude as c varies.

Proposition 10.2 (U47: finite samples do not certify unrestricted analytic recovery)**.** *From finitely many exact values of an otherwise unrestricted holomorphic function, no finite uniform bound on the error at an unsampled point follows. The assertion remains true for a deterministic adaptive sampling algorithm that always uses finitely many samples.*

Proof. The nonadaptive assertion follows from the polynomial construction above. For an adaptive algorithm, answer zero to each successive query until it terminates. Let $z_1, \dots, z_n$ be the resulting transcript. Every function cp vanishes at all queried points, so the algorithm follows exactly the same branches and produces the same answer for these functions. At the unsampled target point their true values are unbounded. Any proposed finite error bound fails for a sufficiently large $|c|$. □

A norm constraint changes the problem. If $|f| \le M$ on a larger certified domain, the perturbation cp cannot be scaled arbitrarily while remaining admissible. Cauchy estimates then connect unobserved derivatives to M and geometric clearance. For an H^2 ball, the prior public finite-rank theorem gives an exact optimality statement. For an analytic strip, geometric Fourier tails give sample or coefficient requirements. The bound, domain and norm are therefore input specifications, not conclusions extracted from a visually smooth graph.

An important consequence for adversarial verification is that a certificate must contain or reference the envelope. A checker that accepts a finite sample plot as proof of global nonvanishing is unsound on the unrestricted function class. Polynomial degree bounds can supply a different envelope through algebraic completeness: enough exact values determine the polynomial, after which an exact root or positivity certificate can be checked.

10.3 Uniform conditioning from energy equivalence

A smooth coordinate change transforms a differential equation and its function-space norms together. For the conformal change $z = F(w)$, the Dirichlet numerator is unchanged in two dimensions, whereas the L^2 denominator becomes weighted by $J(w) = |F'(w)|^2$. This gives explicit spectral comparison when the Jacobian has certified upper and lower bounds.

Proposition 10.3 (U48: conformal spectral comparison under bounded Jacobian)**.** *Let $F : U \to V$ be a conformal isomorphism between bounded regular domains, and suppose $0 < j_- \le |F'|^2 \le j_+ < \infty$. Write $\lambda_k(U)$ and $\lambda_k(V)$ for Dirichlet eigenvalues, counted with multiplicity. Then*

$$\frac{\lambda_k(U)}{j_+} \le \lambda_k(V) \le \frac{\lambda_k(U)}{j_-}.$$

Proof. Under pullback, the Rayleigh quotient on V is

$$\mathcal{R}_V(v) = \frac{\int_U |\nabla v|^2}{\int_U |v|^2 |F'|^2}.$$

The denominator is between $j_- \int_U |v|^2$ and $j_+ \int_U |v|^2$. Hence $\mathcal{R}_U(v)/j_+ \le \mathcal{R}_V(v) \le \mathcal{R}_U(v)/j_-$. The pullback is a linear bijection on the relevant zero-trace energy spaces, using the stated Jacobian bounds. Apply the min–max characterization by taking the supremum over each k-dimensional subspace and then its infimum over all such subspaces. Both inequalities survive these operations. □

The min–max characterization used here follows from the compact self-adjoint spectral decomposition of the Dirichlet resolvent. It is a declared functional-analytic prerequisite when the whole spectrum is discussed. For $k = 1$, the same calculation applies directly to the infimum defining the first Rayleigh value, without requiring higher eigenspaces. No claim is made when the boundary map has unbounded derivative or when a corner sends j_- to zero.

For a finite element system with stiffness matrices A and B satisfying $a_- x^* B x \le x^* A x \le a_+ x^* B x$, the identical argument gives

$$\operatorname{spec}(B^{-1/2} A B^{-1/2}) \subset [a_-, a_+], \qquad \kappa_2(B^{-1/2} A B^{-1/2}) \le a_+/a_-.$$

This is a preconditioner certificate, provided both matrices represent the same constrained subspace. A hidden constant nullspace must first be removed or handled by a compatible pseudoinverse. Comparing an invertible screened operator with an unscreened singular Laplacian without this projection changes the problem.

10.4 A complete contraction estimate for preconditioned descent

Let A be positive definite and B a positive definite preconditioner. Consider $x_{k+1} = x_k - \omega B^{-1}(A x_k - b)$. In the B-scaled coordinate, the error obeys $e_{k+1} = (I - \omega M) e_k$ with $M = B^{-1/2} A B^{-1/2}$.

Proposition 10.4 (U49: optimal constant step for a spectral interval)**.** *If $\operatorname{spec}(M) \subset [a, b]$, $0 < a \le b$, then the step $\omega_* = 2/(a + b)$ minimizes $\max_{t \in [a,b]} |1 - \omega t|$ over real ω, with value $q_* = (b - a)/(b + a)$. Consequently $\|e_k\|_2 \le q_*^k \|e_0\|_2$ for that step.*

Proof. The absolute value of an affine function is convex, so its maximum on the interval is attained at an endpoint. For $\omega < 0$ the value exceeds one and cannot minimize. For $\omega \ge 0$, the maximum of $|1 - \omega a|$ and $|1 - \omega b|$ is minimized when the two endpoint errors have opposite signs and equal magnitude; solving $1 - \omega a = -(1 - \omega b)$ gives ω_*. Before that crossing the first endpoint controls and decreases; after it the second endpoint controls and increases. Thus the minimizer is global. Orthogonal spectral diagonalization bounds $\|I - \omega_* M\|_2$ by q_*. Iteration proves the error estimate. □

For an accuracy ratio $\varepsilon \in (0,1)$ and $a < b$, the sufficient iteration count is

$$k \geq \frac{\log(1/\varepsilon)}{-\log q_*}.$$

If $a = b$, one step is exact in exact arithmetic. The theorem is an optimum within the family of constant-step stationary iterations and the declared spectral interval. Conjugate gradients, multilevel methods or direct transforms are different competitor families. The calculation is useful because it makes a geometry-dependent condition bound into an explicit temporal-complexity bound without claiming that a measured runtime has been minimized.

10.5 Communication-round bounds from a finite spectrum

Take a cycle with $N \geq 3$ vertices and a lazy averaging matrix $P = \frac{1}{2}I + \frac{1}{4}(S + S^{-1})$. Its eigenvectors are Fourier characters and its eigenvalues are $\lambda_k = \frac{1}{2} + \frac{1}{2}\cos(2\pi k/N) = \cos^2(\pi k/N)$. On the mean-zero subspace the maximal absolute eigenvalue is $\rho_N = \cos^2(\pi/N)$.

Proposition 10.5 (U50: exact worst-case consensus contraction)**.** *For every mean-zero vector x, $\|P^t x\|_2 \leq \rho_N^t \|x\|_2$. Equality is attained by a nonzero first Fourier mode. Thus the least number of synchronous rounds guaranteeing relative error at most ε is*

$$t_* = \left\lceil \frac{\log(1/\varepsilon)}{-\log \rho_N} \right\rceil.$$

Proof. Diagonalize P in the orthonormal Fourier basis. The zero-frequency coefficient vanishes. Squared norms are sums of $|\widehat{x}_k|^2 \lambda_k^{2t}$, bounded by $\rho_N^{2t}\|x\|_2^2$. A vector supported in $k = 1$ attains equality. Therefore fewer than the displayed number of rounds fail on that vector, and the displayed number works for all vectors. □

The asymptotic relation $-\log \rho_N \sim \pi^2/N^2$ follows by Taylor expansion of cosine and logarithm at zero. Hence the rounds scale as $N^2 \log(1/\varepsilon)$ for this topology and fixed update rule. The result does not transfer to asynchronous schedules without a specified delay/fairness model. A global Fourier transform may compute the averaged limit immediately in an arithmetic model while requiring communication unavailable to a nearest-neighbour network. The locality of information exchange is part of the competitor class.

10.6 Branch certificates as invariants of a path subdivision

Let $F(z,t)$ be holomorphic in z and continuous in a real path parameter $t \in [0,1]$. Suppose a subdivision $0 = t_0 < \cdots < t_m = 1$ has disks B_j and verified conditions: each $F(\cdot,t)$ has exactly one zero in B_j for $t \in [t_j, t_{j+1}]$; no zero lies on its boundary; and consecutive disks share a smaller certified region containing the endpoint zero. The local implicit functions then join to a unique continued branch along the path.

Proposition 10.6 (U51: soundness of a chained continuation certificate)**.** *Under the preceding conditions, the local zero branches form one continuous function on $[0,1]$. If F is jointly holomorphic on the corresponding complex parameter neighborhoods and $\partial_z F \neq 0$ at the zeros, the branches are holomorphic there and agree on every overlap reached by the chain.*

Proof. On each interval, isolate the unique zero in its disk. Compactness and absence of boundary zeros imply continuity: for any convergent parameter sequence, every convergent subsequence of roots has a root of the limiting function as its limit, and uniqueness forces that limit to

be the selected root. A smaller compact disk around the limiting root supplies the requisite local compactness. At a common endpoint, the shared-region certificate identifies the two roots. A finite gluing induction produces a continuous branch on the whole path. In the holomorphic setting, the implicit-function theorem gives local holomorphic branches. Their equality follows from uniqueness of the zero in the overlapping isolating region, and then from analytic continuation on each relevant connected overlap. □

The theorem establishes soundness for an accepted chain. It does not prove that a particular subdivision strategy always finds such a chain. A completeness theorem needs a lower separation margin, a derivative bound and a computable modulus of variation. Branch collisions violate those hypotheses. For a loop, the endpoint can be a different root of the initial polynomial, even though every step is uniquely continued. The certificate must retain that permutation when the base surface is not simply connected.

10.7 Why certificate termination needs quantitative input

Suppose f is continuously differentiable on a path of length L, with $|f| \geq \delta > 0$ and derivative along arc length bounded by M. A segment of length h satisfies $|f(z)-f(z_0)| \leq Mh$. If $h < \delta/M$, its image lies in a disk avoiding zero and can be certified by a centre-radius witness.

Proposition 10.7 (U52: a sufficient nonvanishing subdivision bound)**.** *For $M > 0$, a uniform partition into $n > 2LM/\delta$ pieces makes every image segment lie in a disk of radius less than half the guaranteed centre modulus. Consequently a disk-based local nonvanishing test accepts every segment, provided its arithmetic bounds are exact or outward certified. If $M = 0$, one nonzero value certifies the whole connected path.*

Proof. Each segment has length at most $L/n < \delta/(2M)$. The mean-value integral bound gives image radius less than $\delta/2$. Since the centre modulus is at least δ, the disk avoids zero with positive margin. For $M = 0$, the path derivative is zero and the image is constant. □

The factor two is a convenient strict margin, not an optimal subdivision constant. The bound proves a termination guarantee for a class with supplied δ, M, L. A certificate generator receiving no nonvanishing margin may continue refining indefinitely near an actual zero. An axis-only separating test can also fail for an image lying on the diagonal, although a rotated witness succeeds. Soundness, mathematical nonvanishing, geometric adequacy of the witness class and algorithmic termination remain four separate obligations.

10.8 Formal statement fidelity and nonvacuous comparison

A verifier proves its encoded proposition. If a precondition is inconsistent, every conclusion follows logically, including a false-looking speed claim. Thus a conditional theorem used in a comparison must have a demonstrably inhabited admissible class. A concrete exact input is often the simplest witness; a family result can provide a stronger witness.

The uniformization inputs make this especially important. A quotient group must act properly discontinuously; an ordinary surface quotient additionally requires freeness. A claimed sphere quotient by a nontrivial free holomorphic group has no instance. A harmonic conjugate assumed globally single-valued on a condenser annulus with nonzero period also has no instance. Such preconditions would trivialize the main geometric obligations.

A useful formal interface distinguishes four objects: the declared input class $\mathcal{A}$, a representation relation $\mathsf{Rep}(d, a)$, a mathematical output relation $\mathsf{Sol}(a, y)$ and a finite checker $\mathsf{Check}(d, c)$. Its

soundness assertion is

$$\forall d, c, a, \quad \mathsf{Rep}(d, a) \wedge \mathsf{Check}(d, c) \Longrightarrow \mathsf{Sol}(a, \mathsf{decode}(c)).$$

For a uniqueness claim, prove that all admissible outputs coincide. For an approximation claim, the relation contains the norm and tolerance. For a cost claim, count the operations of the concrete algorithm producing the specified output. This prevents a fast scalar summary from being compared with an algorithm obliged to return an entire field or matrix.

The theorem register in the following chapter uses these distinctions. Entries with an external geometric or physical premise retain that premise; exact computational checks are linked only to the assertions they actually evaluate. Formal scripts are not marked accepted unless a checker has executed and its output has been inspected.

Chapter 11

Solved investigations: geometry and analysis

The following investigations specify mathematical questions with complete solutions under the stated premises. They supplement the nine source results with independent examples, counterexamples and quantitative consequences. Their numbering is local to this monograph. Each investigation has one principal location; later lecture routes refer to it without reproducing its solution. Numerical approximations are displayed only after the exact relation determining them.

11.1 Conformal type and period structure

Investigation 11.1 (I01: identical topology, different conformal type)**.** The plane and the unit disk are homeomorphic. Prove that no biholomorphism connects them, and identify the extra information absent from a topological presentation. Give a concrete homeomorphism and explain why it is not holomorphic.

Solution. The radial map $h(z) = z/(1 + |z|)$ maps $\mathbb{C}$ bijectively to $\mathbb{D}$, with continuous inverse $w \mapsto w/(1 - |w|)$. Thus both spaces have the same topology. If a biholomorphism $f : \mathbb{C} \to \mathbb{D}$ existed, it would be a bounded entire function and hence constant by Liouville's theorem, contradicting injectivity. The radial map depends on $\bar{z}$ through $|z|$; for $z \neq 0$, its real differential scales the radial direction by $(1 + |z|)^{-2}$ and the tangential direction by $(1 + |z|)^{-1}$. These scales are unequal, so the differential is not a complex similarity. Consequently the map fails conformality away from the origin.

The missing datum is the complex structure, not an additional topological handle or boundary component. Both surfaces are simply connected and noncompact. The disk supports the complete curvature -1 Poincare metric, while the plane has no biholomorphic disk coordinate. U46 further shows that an arbitrary computable exhaustion cannot always be classified by a terminating algorithm. A topology-only test may correctly identify simple connectivity yet leave precisely this analytic alternative unresolved. The proof uses a qualitative invariant—bounded entire functions—and does not require solving a differential equation for a candidate coordinate map. Its cost advantage is logical reduction, not a measured execution-time improvement.

Investigation 11.2 (I02: measured condenser period and radius uncertainty)**.** An annular condenser has normalized boundary potential zero and one. A certified calculation encloses its conjugate period by $p \in [1/2, 51/100]$. Determine an enclosure for the outer radius of its normalized round-annulus model and quantify sensitivity in logarithmic coordinates.

Solution. U11 gives $L = \log R = 2\pi/p$. Since this is strictly decreasing on positive p,

$$\frac{200\pi}{51} \le L \le 4\pi, \qquad \exp(200\pi/51) \le R \le \exp(4\pi).$$

The enclosure width in L is $4\pi - 200\pi/51 = 4\pi/51$. The multiplicative radius uncertainty is therefore at most $\exp(4\pi/51)$. A small absolute period uncertainty can generate substantial relative uncertainty in a large radius because exponentiation amplifies the logarithmic interval. Differentiating gives $dL/dp = -2\pi/p^2$ and $d\log L/d\log p = -1$. Thus the relative condition number for recovering L from p is exactly one; that for recovering R is L.

A numerically suitable representation stores L and postpones exponentiation. This preserves the annulus modulus $L/(2\pi)$ and capacity $2\pi/L$ without creating a huge coordinate radius. The conclusion is a representation/conditioning result. It does not imply that every operation on the logarithmic cylinder is cheaper, because periodicity and transformed boundary data remain necessary. The exact endpoints above are also suitable for an interval checker, whereas a central estimate and an unspecified number of decimal digits would not certify either inequality.

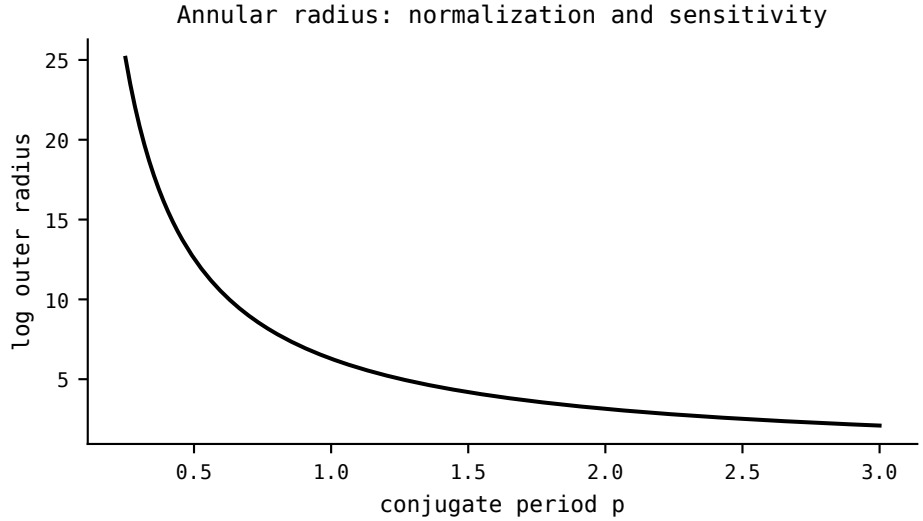


Figure 11.1: The exact relation between the conjugate period and the logarithmic outer radius. Small periods produce strong radius sensitivity.

Investigation 11.3 (I03: a degree constraint from annular modulus)**.** Let $A = A(1, \mathrm{e}^3)$ and $B = A(1, \mathrm{e}^6)$. Determine all possible positive degrees of a finite unbranched holomorphic covering $A \to B$. Construct such a map and count the lifts of one ordinary target point.

Solution. A finite annular covering of degree d multiplies the modulus by d, so $6/(2\pi) = d\,3/(2\pi)$ and $d = 2$. The map $F(z) = z^2$ has this degree and maps the boundary radii correctly. Every $w \in B$ has the two roots $\pm\sqrt{w}$, whose moduli lie strictly between 1 and e^3. No root is critical because $F'(z) = 2z \neq 0$ on A.

To justify necessity without presupposing a formula for every covering, lift to logarithmic strips. The induced homomorphism on the fundamental group sends a positive generator to d generators. Harmonic boundary potentials pull back from B to A, and their conjugate periods are multiplied by d. With capacity reciprocal to modulus, this is exactly the displayed relation. Equivalently, the energy of a pulled-back potential is d times its target energy. Hence the degree follows from one scalar conformal invariant. Enumerating possible branched formulas would be unnecessary and could include maps that fail properness.

The induced map on fundamental groups is multiplication by two. It is injective, not surjective, and its image has index two. A global single-valued inverse would split the covering into degree

one and contradict that index. Local square-root formulas remain valid on simply connected target patches.

Investigation 11.4 (I04: proper annulus self-maps with fixed modulus)**.** Classify the finite proper unbranched holomorphic self-maps of $A(r, R)$, where $0 < r < R < \infty$. Distinguish maps preserving each boundary component from maps interchanging them.

Solution. Modulus multiplicativity forces the degree to equal one, so every such map is an automorphism. Let $u(z) = \log(|z|/r)/\log(R/r)$. If F preserves the boundary components, uniqueness of the Dirichlet problem gives $u \circ F = u$. Thus $|F(z)/z| = 1$ everywhere. The holomorphic function $F(z)/z$ has constant modulus and is constant by the open mapping theorem. Therefore $F(z) = \mathrm{e}^{\mathrm{i}\theta} z$.

If the components are exchanged, then $u \circ F = 1 - u$, whence $|F(z)z| = rR$. The holomorphic function $F(z)z$ is constant of that modulus, giving $F(z) = rR\mathrm{e}^{\mathrm{i}\theta}/z$. Each displayed formula is a conformal self-map, so the list is complete. The reciprocal formula reverses the winding of a circle when expressed with a fixed ambient counterclockwise orientation, while it remains an orientation-preserving holomorphic map of the surface. Boundary orientation and ambient circle orientation must therefore be distinguished.

The classification has reduced a functional search to one real phase and one discrete choice. The reduction is exact because properness and boundary correspondence are part of the input. Without properness, many non-surjective holomorphic maps into the same annulus may exist and this parameter count would be unjustified.

Investigation 11.5 (I05: two incommensurable conjugate periods)**.** On a multiply connected domain suppose a locally defined holomorphic function H has additive monodromy i around one generator and $\mathrm{i}\sqrt{2}$ around another. Can $\exp(aH)$ be single-valued for a nonzero real constant a? State the general criterion for finitely many imaginary periods.

Solution. Single-valuedness requires $a = 2\pi m$ and $a\sqrt{2} = 2\pi n$ for integers m, n. If $a \neq 0$, then $m \neq 0$ and $\sqrt{2} = n/m$, a contradiction. Thus no such nonzero real a exists. For periods $\mathrm{i}p_1, \ldots, \mathrm{i}p_k$, the general criterion is $ap_j \in 2\pi\mathbb{Z}$ for all j. When one period is nonzero, this requires all nonzero period ratios to be rational with a common denominator after finitely many ratios are reduced.

The annulus construction works because its first homology has rank one. On a general surface the period subgroup can have higher rank. A scalar exponential can remove a cyclic imaginary lattice; it does not remove arbitrary period data. A vector of periods, a lattice quotient or a section with an automorphy factor may be the appropriate output. The impossibility proof prevents using an annular formula as a global multi-hole coordinate without a compatibility test.

A numerical ratio close to a rational does not establish exact commensurability. Finite-precision fitting must state whether it constructs an approximate local chart or certifies a genuinely single-valued map. The latter requires exact period relations or rigorous bounds strong enough to identify the relevant integers under a separately specified separation hypothesis.

Investigation 11.6 (I06: cusp extension and an essential singularity)**.** Compare $f(z) = z^4$ and $g(z) = \exp(1/z)$ near the puncture of $0 < |z| < 1$. Explain which admits the local finite-degree extension used in §5.6 and why the other is not a counterexample to that extension theorem.

Solution. The first map extends holomorphically to zero, with a zero of order four. For every sufficiently small target punctured disk, its preimage component at zero is a punctured disk and the restriction is a four-sheeted covering. Its local fibre algebra is $\mathbb{C}\{z\}/(z^4)$ and has dimension four.

For g, along the positive real sequence $z_n = 1/n$, $g(z_n) = \mathrm{e}^n \to \infty$; along $z_n = -1/n$, $g(z_n) = \mathrm{e}^{-n} \to 0$; and along $z_n = 1/(2\pi\mathrm{i}n)$, $g(z_n) = 1$. Thus the puncture is not sent to one

well-defined target end. The proper end-map premise fails. In particular, infinitely many points tending to the puncture map to the compact singleton $\{1\}$, contradicting properness into $\mathbb{C}^*$ for any collar containing those points.

The failure is geometric, not a numerical difficulty evaluating an exponential. A source end-extension theorem can be applied only after its induced-end and finite/proper behavior has been established. Merely being holomorphic on a punctured domain is insufficient. The three explicit sequences give a finite analytical witness to that failure, and the repeated value sequence identifies the violated compact-preimage condition directly.

11.2 Moduli, compactification and quotient geometry

Investigation 11.7 (I07: changing the lattice basis)**.** For $\tau = \frac{1}{2} + \mathrm{i}$, compute the transformed modulus $\tau' = -1/\tau$. Verify positive imaginary part and identify the linear rescaling of lattices. Determine how an ordered period vector must change.

Solution. Multiplying by the conjugate yields $\tau' = (-\frac{1}{2}+\mathrm{i})/(5/4) = -2/5+(4/5)\mathrm{i}$. Its imaginary part is $4/5 > 0$, agreeing with $\operatorname{Im}\tau/|\tau|^2$. The lattice $\mathbb{Z}+\mathbb{Z}\tau$ has the ordered basis $(\tau, -1)$, whose oriented area is unchanged. Dividing that basis by τ gives $(1, -1/\tau)$, so multiplication by $1/\tau$ induces the biholomorphism to the normalized new torus.

If (a, b) are the old cycles, the new ordered cycles are $(b, -a)$. A differential with periods (A, B) has periods $(B, -A)$ in the new basis. Holding (A, B) fixed after changing cycles would not represent the same differential. The modular transformation preserves the surface while changing its numerical coordinate description.

For algorithms, choosing a well-scaled fundamental parallelogram can improve convergence of lattice sums. Any such improvement must include the cost of the basis change and the transformation of periods, characters and boundary data. The present calculation proves geometric equivalence and a precise data-transformation rule; it does not claim a measured speedup for a particular lattice-sum implementation.

Investigation 11.8 (I08: compact triangle signatures)**.** Classify the compact orientable triangle orbifolds with signatures $(2, 3, 5)$, $(2, 3, 6)$ and $(2, 3, 7)$, and compute the area of the last one in curvature -1 normalization.

Solution. Their Euler characteristics are respectively

$$\frac{1}{2}+\frac{1}{3}+\frac{1}{5}-1 = \frac{1}{30}, \quad \frac{1}{2}+\frac{1}{3}+\frac{1}{6}-1 = 0, \quad \frac{1}{2}+\frac{1}{3}+\frac{1}{7}-1 = -\frac{1}{42}.$$

All are good compact triangle signatures. U24 gives spherical, Euclidean and hyperbolic types in that order. In the hyperbolic case Gauss–Bonnet gives $-\text{area} = 2\pi\chi$, hence area $= \pi/21$ for the orientation-preserving quotient. A single reflection triangle has half this area, $\pi/42$, because the oriented triangle orbifold is the double of the reflection fundamental region.

This factor two is independent of the annular 2π normalization. Both arise from geometry, but one is a quotient index and the other is the angular period of an exponential. Retaining the convention avoids a common area mismatch. Exact rational arithmetic determines the sign without floating-point uncertainty even for signatures close to Euclidean. The computational task is finite here because the signature and the goodness hypothesis are given. It is not a classification procedure for arbitrary program-described surfaces.

Investigation 11.9 (I09: a puncture changes the Euler-sign inference)**.** Compute the ordinary Euler characteristics of $\mathbb{C}$, $\mathbb{C}^*$ and the thrice-punctured sphere. Identify their uniformizing covers and explain why the compact curvature-sign rule cannot be applied unchanged to all three.

Solution. Compactifying each surface adds respectively one, two and three punctures to a sphere. Thus $\chi = 1, 0, -1$. The plane covers itself; the exponential covers $\mathbb{C}^*$ by $\mathbb{C}$; the thrice-punctured sphere has the disk as universal conformal cover. In the last case its complete finite-area cusp metric satisfies area $= -2\pi\chi = 2\pi$.

The plane has positive ordinary Euler characteristic but is parabolic, so positivity alone does not imply a spherical universal cover for a noncompact surface. Gauss–Bonnet on an exhaustion includes boundary terms, and a complete flat plane has infinite area with a boundary contribution at infinity. Dropping that contribution is invalid. For the finite-area punctured hyperbolic case, cusp limits allow the stated area formula; those end assumptions are substantive.

The counterexample is directly relevant to the interpretation of source Theorem 5.9 when finite conformal type includes punctures. The corrected compact theorem remains valid. The noncompact Euclidean list and finite-area hyperbolic case require their own classification statements. A public proof must preserve this distinction even when all three surfaces are drawn on the same compactified sphere.

Investigation 11.10 (I10: translation and dilation quotients of the half-plane)**.** Compare $\mathbb{H}/\langle z \mapsto z + 1\rangle$ and $\mathbb{H}/\langle z \mapsto az\rangle$ for $a > 1$. Give explicit quotient coordinates and identify the end geometry.

Solution. For translation, $q = \exp(2\pi \mathrm{i} z)$ is invariant and maps the quotient bijectively to $0 < |q| < 1$. If two points have equal q, their difference is an integer, proving injectivity on the quotient. As $\operatorname{Im} z \to \infty$, $q \to 0$ and the quotient has a cusp. Pulling back $|dq|/(|q| \log(1/|q|))$ gives $|dz|/\operatorname{Im} z$.

For dilation, let $\zeta = \log z = s + \mathrm{i}\theta$, $0 < \theta < \pi$. Dilation acts by $s \mapsto s + \log a$. Therefore $w = \exp(2\pi \mathrm{i}\zeta/\log a)$ has radii $\mathrm{e}^{-2\pi^2/\log a} < |w| < 1$. It is a finite round annulus with modulus $\pi/\log a$. Its core closed geodesic has length $\log a$: the vertical line through the imaginary axis projects to the dilation axis, and the hyperbolic length from i to $a\mathrm{i}$ is $\int_1^a dy/y = \log a$.

The parabolic versus hyperbolic group element is encoded in the quotient's conformal modulus and end structure. Both quotients are topological cylinders. Their different conformal types cannot be inferred from that topology alone. The explicit coordinates also provide exact test cases for branch and metric implementations.

11.3 Harmonic observables and spectral calculations

Investigation 11.11 (I11: a cubic Fourier mode on an annulus)**.** On $A(1, 2)$ prescribe inner boundary value zero and outer boundary value $\cos(3\theta)$. Find the harmonic solution and its Dirichlet energy.

Solution. Write $t = \log r$, $L = \log 2$. The separated solution is

$$u(r, \theta) = \frac{\sinh(3 \log r)}{\sinh(3 \log 2)} \cos(3\theta) = \frac{r^3 - r^{-3}}{8 - 1/8} \cos(3\theta).$$

Its radial logarithmic coefficient solves $v'' - 9v = 0$ with $v(0) = 0, v(L) = 1$, so it is harmonic and has the required boundary values. Uniqueness follows from the maximum principle. In cylinder coordinates the energy is

$$E = \pi \int_0^L (v'^2 + 9v^2)\, \mathrm{d}t = \pi[vv']_0^L = 3\pi \coth(3 \log 2) = \frac{65\pi}{21}.$$

Here $\coth(3 \log 2) = (64 + 1)/(64 - 1) = 65/63$. The energy is exact, and the missing factor π would correspond to a different Fourier normalization.

A two-dimensional mesh solve is unnecessary for this single-mode specification. Evaluation at m requested points costs $O(m)$ elementary operations once the coefficient is known, which is optimal in the output-size sense. For arbitrary boundary data, coefficient acquisition and truncation must be included, so this example does not establish an unconditional linear-time PDE algorithm.

Investigation 11.12 (I12: least energy for a prescribed circulation)**.** Among smooth closed real one-forms on $A(1, \mathrm{e}^L)$ with period p around a positive circle, find the minimum squared norm $\int_A |\alpha|^2$ and its minimizer. Use the Euclidean metric; the form norm and area transform together.

Solution. In logarithmic coordinates, write $\alpha = a(t,\theta)\,\mathrm{d}t + b(t,\theta)\,\mathrm{d}\theta$. Conformal invariance gives energy $\int_0^L \int_0^{2\pi} (a^2 + b^2)\,\mathrm{d}\theta\,\mathrm{d}t$. Closedness implies $\partial_t b = \partial_\theta a$, so the angular integral of b is independent of t and equals p. By Cauchy–Schwarz,

$$\int_0^{2\pi} b(t,\theta)^2\,\mathrm{d}\theta \geq \frac{p^2}{2\pi}.$$

Integration in t gives $E \geq Lp^2/(2\pi)$. Equality requires $a = 0$ almost everywhere and $b = p/(2\pi)$ for every t, so the minimizer is $\alpha = (p/2\pi)\,\mathrm{d}\theta$. It is smooth and closed and has the required period, proving attainment and uniqueness in the smooth class.

The result is a concrete one-dimensional Hodge component extracted from a continuum of possible forms. Exact forms with zero period contribute additional orthogonal energy after the corresponding projection. This provides a period-based error diagnostic: a locally small residual does not certify that a computed form has the correct global circulation. The lower bound is global over the declared class, not an observation from one discretization.

Investigation 11.13 (I13: two boundary modes and thin-annulus conditioning)**.** For the annular Dirichlet-to-Neumann block at order $n \geq 1$, compare symmetric data $(1, 1)$ and antisymmetric data $(1, -1)$. Determine the condition number of the block and its behavior as $nL \to 0$.

Solution. The block is $n \begin{pmatrix} \coth(nL) & -\operatorname{csch}(nL) \\ -\operatorname{csch}(nL) & \coth(nL) \end{pmatrix}$. The displayed vectors are orthogonal eigenvectors, with eigenvalues $\lambda_s = n\tanh(nL/2)$ and $\lambda_a = n\coth(nL/2)$. Both are positive. Their ratio is $\coth^2(nL/2)$. Since $\tanh x = x + O(x^3)$ and $\coth x = x^{-1} + O(x)$,

$$\lambda_s \sim n^2 L/2, \quad \lambda_a \sim 2/L, \quad \kappa \sim 4/(n^2 L^2).$$

The poor condition number has a geometric interpretation: equal boundary values create a slowly varying mode, whereas opposite boundary values force a steep cross-annulus gradient. Dividing by the mean and difference eigenvalues gives an exact diagonal preconditioner for this block. Any implementation must retain the separate zero-frequency block, which has a constant nullspace before boundary differences are fixed.

The proof uses a two-dimensional invariant subspace in coefficient space and yields an exact condition number. A visual plot of the field could reveal steep gradients but would not identify this quantitative distinction between symmetric and antisymmetric data.

Investigation 11.14 (I14: optimally allocating unequal boundary tolerances)**.** Suppose two independent boundary approximations cost $-\log \varepsilon_1$ and $-3\log \varepsilon_2$, and the interior error bound is $\frac{1}{4}\varepsilon_1 + \frac{3}{4}\varepsilon_2 \leq \delta$. Determine the cost-minimizing positive allocation.

Solution. The cost decreases as either tolerance increases, so the constraint is active. A Lagrange multiplier gives $1/\varepsilon_1 = \lambda/4$ and $3/\varepsilon_2 = 3\lambda/4$, hence $\varepsilon_1 = \varepsilon_2 = 4/\lambda$. The active constraint gives both equal to δ. The apparent symmetry of the answer is caused by matching cost and harmonic

weights: the second approximation is three times as expensive but contributes three times as strongly to the bound.

Strict convexity of $-\log\varepsilon_1 - 3\log\varepsilon_2$ on the positive quadrant makes the stationary point the unique global minimum on the convex feasible segment. To prove sufficiency directly, set $x = \varepsilon_1/\delta$, $y = \varepsilon_2/\delta$, so $(x + 3y)/4 \le 1$. Weighted arithmetic–geometric mean gives $x^{1/4}y^{3/4} \le 1$, hence $-\log x - 3\log y \ge 0$, with equality only at $x = y = 1$.

This example explains why unequal geometric weights need not imply unequal tolerances. A heuristic based only on geometric importance would miss the cost coefficients. Additional upper bounds on tolerances lead to an active-set problem; the unconstrained formula must then be clipped and reoptimized over the remaining variables.

Investigation 11.15 (I15: a torus heat evolution with two exact rates)**.** On the rectangular torus $\mathbb{R}^2/(\mathbb{Z} \times 2\mathbb{Z})$, solve $u_t = \Delta u$ with $u(0, x, y) = \cos(2\pi x) + 2\sin(\pi y)$. Determine the exact L^2 norm and the long-time dominant component.

Solution. The two modes are Laplacian eigenfunctions with eigenvalues $4\pi^2$ and π^2. Thus

$$u(t, x, y) = \mathrm{e}^{-4\pi^2 t}\cos(2\pi x) + 2\mathrm{e}^{-\pi^2 t}\sin(\pi y).$$

They are orthogonal over the fundamental rectangle, each having squared norm one because its mean square is one half and the area is two. Hence $\|u(t)\|_2^2 = \mathrm{e}^{-8\pi^2 t} + 4\mathrm{e}^{-2\pi^2 t}$. Differentiating this expression agrees with $-2\|\nabla u(t)\|_2^2$, proving the energy identity for the solution. The sine component dominates because its decay exponent is smaller.

The calculation displays the role of the modulus: changing the vertical period changes only the corresponding frequencies. A coordinate rescaling to a unit square changes the operator to $\partial_x^2 + \frac{1}{4}\partial_{y'}^2$, not the ordinary square Laplacian. Uniformization and normalization therefore simplify geometry while preserving a metric-dependent operator. The exact modal solution is an appropriate regression test for a periodic solver and its time-step interpretation.

Investigation 11.16 (I16: boundary and coordinate error in a composed observable)**.** Let u be harmonic on a domain V, $F : U \to V$ conformal, and $\widetilde{F}$ an approximate coordinate map with $\|F - \widetilde{F}\| \le \eta$ on a compact set K. Suppose the connecting segments lie in a region where $\|\nabla u\| \le M$, and a boundary-data approximation changes the exact harmonic field by at most ε throughout that region. Bound the final observable error.

Solution. Let $\widetilde{u}$ denote the exact harmonic extension of the approximate boundary values, with $\|u - \widetilde{u}\|_\infty \le \varepsilon$ supplied by the maximum principle. Then

$$|u(F(w)) - \widetilde{u}(\widetilde{F}(w))| \le |u(F(w)) - u(\widetilde{F}(w))| + |u(\widetilde{F}(w)) - \widetilde{u}(\widetilde{F}(w))| \le M\eta + \varepsilon.$$

The first estimate follows by integrating the gradient along the connecting segment. A pointwise gradient bound only at $F(w)$ would not suffice. If the field is represented by the real part of a holomorphic function bounded by B in disks of radius d around the connecting segments, Cauchy's estimate supplies $M \le B/d$ with the corresponding convention for the analytic representative.

The error budget separates coordinate construction from field approximation. Decreasing the field discretization error below $M\eta$ gives little improvement until the map is refined. Conversely, an exceptionally accurate conformal map can be wasted on poorly controlled boundary data. This is a quantitative stopping criterion, subject to the stated compact-region and segment hypotheses.

Investigation 11.17 (I17: a conformal radius from an explicit Green function)**.** For $a \in \mathbb{D}$, verify the Green function $G(z, a) = -\log\left|\frac{z-a}{1-\bar{a}z}\right|$ and compute the conformal radius of $\mathbb{D}$ at a. Determine the ratio to the Euclidean distance from a to the boundary.

Solution. The fraction is a disk automorphism sending a to zero. Its modulus is one on the unit circle and less than one inside, so G is positive, has zero boundary values, and is harmonic away from a. Near a,

$$G(z,a) = -\log|z-a| + \log(1-|a|^2) + o(1).$$

Thus the conformal radius is $1-|a|^2$. It also equals the reciprocal modulus of the automorphism derivative at a, confirming U13. The Euclidean boundary distance is $1-|a|$, giving ratio $1+|a| \in [1,2)$.

The general Koebe bound permits a factor up to four; the disk has stronger geometry and a sharper exact ratio. Using the universal bound is valid but loses information. This distinction between validity and sharpness is part of the adversarial method: a nonoptimal constant is not a false theorem. The formula supplies an exact reference for Green-function regular-part extraction, especially near the boundary where subtracting two logarithmic singular terms can be numerically delicate.

Investigation 11.18 (I18: fixed-area tori and a sharp first-eigenvalue comparison)**.** A rectangular flat torus has side lengths a and $1/a$, so its area is one. Determine its first positive Laplacian eigenvalue and the value of a maximizing that eigenvalue among rectangular tori.

Solution. Its eigenvalues are $4\pi^2(m^2/a^2 + n^2a^2)$ for integers (m,n). The first positive one is $4\pi^2\min(a^2, a^{-2})$, attained by a unit mode along the longer side. Since $\min(a^2,a^{-2}) \le 1$ with equality precisely at $a=1$, the square torus uniquely maximizes this value within the rectangular family, with optimum $4\pi^2$.

This proof includes the lower bound determining the first mode: every nonzero integer pair has either $|m| \ge 1$ or $|n| \ge 1$, so its eigenvalue is no smaller than the displayed minimum. It also proves the global maximum over all positive rectangular aspect ratios. It does not optimize over all flat tori; oblique lattices form a larger competitor class. The spectral gap controls mean-zero heat decay and Poincare constants, so the same geometric choice affects several observables. The family restriction must be retained whenever the optimum is cited.

11.4 Branch surfaces in mathematical physics

Investigation 11.19 (I19: four sheets in one rational coordinate)**.** Use $k_1^2 = E$ and $k_2^2 = E-4$. At $E = 25/4$, enumerate the four sheets and the corresponding values of $w = k_1 + k_2$. Verify the inverse formula on all four.

Solution. The momentum pairs are $(5/2, 3/2)$, $(5/2, -3/2)$, $(-5/2, 3/2)$ and $(-5/2, -3/2)$, giving $w = 4, 1, -1, -4$. The inverse formulas

$$k_1 = \tfrac{1}{2}(w + 4/w), \qquad k_2 = \tfrac{1}{2}(w - 4/w)$$

recover these four pairs exactly. Negating k_2 sends $w \mapsto 4/w$; negating k_1 sends $w \mapsto -4/w$; negating both sends $w \mapsto -w$. Their compositions commute because the sheet group is $\mathbb{Z}/2 \times \mathbb{Z}/2$ in this two-independent-square-root model.

The branch values occur at $k_1 = 0$ or $k_2 = 0$, namely $E = 0, 4$. In the w-plane these are respectively $w = \pm 2\mathrm{i}$ and $w = \pm 2$. The apparent four-sheeted energy description becomes a rational map of one sphere, since the compactified surface has genus zero. Pole fitting in w therefore avoids arbitrary energy-plane cut labels, but the inverse map and physical sheet conditions must accompany the fitted function. The algebra does not establish unitarity or a physical scattering model by itself.

Investigation 11.20 (I20: a genus obstruction to rational uniformization)**.** For distinct thresholds $a_1, \dots, a_n$, consider the normalized compact curve with function field

$\mathbb{C}(E)(\sqrt{E-a_1},\dots,\sqrt{E-a_n})$. Compute the genus for $n=3$ and $n=4$, and decide whether a one-to-one rational parameterization by the sphere can exist.

Solution. Each square class is independent: a nonempty product of distinct factors has odd valuation at at least one a_j and cannot be a square in $\mathbb{C}(E)$. The degree is therefore 2^n. At each finite threshold the inertia index is two and the contribution to ramification is 2^{n-1}. At infinity simultaneous sign reversal gives another inertia group of order two, with the same contribution. Riemann–Hurwitz yields

$$2g-2=-2^{n+1}+(n+1)2^{n-1}=2^{n-1}(n-3),\quad g=1+2^{n-2}(n-3).$$

Hence $g=1$ for three thresholds and $g=5$ for four. A biholomorphic rational parameterization by the sphere would force genus zero, contradicting these values. For $n=3$, an elliptic lattice coordinate is available after uniformization; for $n=4$, the universal cover is the disk and a nonabelian quotient group is required.

The obstruction is topological and algebraic. Increasing the degree of a trial rational function does not remove it if the desired output is a globally one-to-one coordinate. Rational approximants to a selected observable on a compact region remain possible and have a different specification. This prevents a successful local approximation from being reported as global uniformization.

Chapter 12

Solved investigations: physics, algorithms and certificates

12.1 Fields, energy and transformed physical equations

Investigation 12.1 (I21: a pole and a ramified observation coordinate)**.** Let $E(w) = (w+1/w)^2/4$ and $A(w) = 1/(w-2)$. Determine the local behavior of A as a function of E near $w = 2$, and contrast it with a pole located at the ramification point $w = 1$.

Solution. At $w = 2$, $E = 25/16$ and $E'(w) = (w + 1/w)(1 - w^{-2})/2$, so $E'(2) = 15/16 \neq 0$. The inverse function theorem gives $w - 2 = (16/15)(E - 25/16) + O((E - 25/16)^2)$ and therefore

$$A = \frac{15/16}{E - 25/16} + O(1).$$

The pole remains simple but its residue changes by the Jacobian. At $w = 1$, expansion gives $E(w) = 1 + (w-1)^2 + O((w-1)^3)$. A pole $1/(w-1)$ thus becomes a branch singularity proportional to $(E-1)^{-1/2}$ on a chosen local sheet.

A residue measured in the energy coordinate cannot be transferred unchanged to a uniformizing coordinate. At a ramification point there may not even be a meromorphic energy-plane germ. This is the same local-ring distinction as a multiplicity-two fibre. The analytic calculation supplies both a leading coefficient and a diagnostic for when ordinary pole fitting is ill-posed. A small least-squares residual against energy samples does not establish that the assumed pole model has the correct local singularity.

Investigation 12.2 (I22: singular parameters of an illustrative brane curve)**.** For $y^2 = (v^2 - u)^2 - 1$, determine all parameter values at which finite branch points collide. For nonsingular parameters compute the parameter derivative of the period of $\lambda = 2v^2\,\mathrm{d}v/y$ over a continuously transported closed cycle.

Solution. The four branch points satisfy $v^2 = u + 1$ or $v^2 = u - 1$. Within each pair a collision occurs precisely when $u = -1$ or $u = 1$. A point belonging to both pairs would require $u + 1 = u - 1$, which is impossible. Thus these are the only finite collision parameters. Away from them the compactification is a genus-one curve.

At fixed v, $\partial_u y = -(v^2 - u)/y$. Consequently $\partial_u \lambda = 2v^2(v^2 - u)\,\mathrm{d}v/y^3$. Direct differentiation of v/y gives

$$\frac{\mathrm{d}v}{y} - \mathrm{d}\left(\frac{v}{y}\right) = \frac{2v^2(v^2-u)}{y^3}\,\mathrm{d}v = \partial_u \lambda.$$

The integral of the exact differential around a closed cycle is zero. Therefore the derivative of the transported period is $\oint \mathrm{d}v/y$, with the cycle transported in a region avoiding the discriminant.

The motion of a representative contour contributes an exact-variation term and leaves this closed-cycle relation unchanged.

The relation identifies a period derivative with a holomorphic period. Physical interpretations as charges or effective couplings need the relevant external theory and normalization. In particular, the calculation alone does not prove confinement, a BPS spectrum or a global statement about M theory. It provides a fully specified geometric mechanism used by such models.

Investigation 12.3 (I23: why a membrane does not inherit the string Weyl calculation)**.** For a d-dimensional parameter space with metric h, determine the Weyl scaling of $S = \frac{1}{2}\int \sqrt{h}\, h^{ab}\partial_a X \partial_b X$. What happens at $d = 2$ and $d = 3$? How does a mass term change the two-dimensional conclusion?

Solution. Under $h_{ab} \mapsto \mathrm{e}^{2\omega} h_{ab}$, the determinant scales by $\mathrm{e}^{2d\omega}$ and the inverse metric by $\mathrm{e}^{-2\omega}$. Thus the kinetic density scales by $\mathrm{e}^{(d-2)\omega}$. It is invariant for $d = 2$, even for variable ω, because no derivative of h appears in this expression. At $d = 3$ it gains a factor e^{ω} and is not invariant in general. Hence the two-dimensional uniformization argument for a worldsheet does not directly classify a membrane worldvolume.

A term $\frac{1}{2}m^2 \int \sqrt{h}\, X^2$ scales by $\mathrm{e}^{d\omega}$, so in two dimensions it breaks this classical Weyl invariance unless the mass or field transformation is changed as part of a different model. Quantum regularization can add further anomalies; none is inferred from the classical scaling calculation. The dimensional factor is an exact obstruction to extending a useful string-theory representation by terminology alone.

The comparison is therefore a model-validity result. The invariant two-dimensional kinetic term can be evaluated in a conformal representative with its global moduli retained. The three-dimensional term cannot be simplified by discarding the Weyl factor without changing the action being extremized.

Investigation 12.4 (I24: heat current through a logarithmic annulus)**.** A homogeneous planar conducting layer of thickness d occupies $A(1, \mathrm{e}^2)$. Its thermal conductivity is $k > 0$, and its boundary temperatures are $T_i > T_o > 0$. Compute the steady temperature, heat current and total entropy production.

Solution. The unique steady solution is $T(r) = T_i + (T_o - T_i)\log r/2$. The outward radial heat flux density is $-kT'(r) = k(T_i - T_o)/(2r)$. Multiplying by the circumference and thickness gives the constant current $Q = \pi k d(T_i - T_o)$. The normalized capacity is π, which recovers the same result from the condenser formulation.

The local entropy-production density is $k|\nabla T|^2/T^2$ times thickness. Its integral can be calculated directly:

$$\dot{S} = 2\pi k d \int_1^{\mathrm{e}^2} \frac{(T_i - T_o)^2}{4rT(r)^2}\,\mathrm{d}r = Q\left(\frac{1}{T_o} - \frac{1}{T_i}\right) \geq 0.$$

The substitution $\mathrm{d}T = -(T_i - T_o)\,\mathrm{d}r/(2r)$ gives the equality. Positivity follows from the ordering and strict positivity of temperatures. Celsius values cannot be inserted into the reciprocal-temperature formula without conversion to absolute temperature.

The calculation is exact within steady, isotropic, temperature-independent conduction. Contact resistance, radiative exchange, anisotropy and volumetric sources change either the boundary conditions or equation. Uniformization supplies geometric reduction for the stated model; it does not identify the conductivity or validate those constitutive assumptions experimentally.

Investigation 12.5 (I25: a Robin coefficient under conformal pullback)**.** Suppose u satisfies $\partial_{n_z} u + \beta(z)u = g(z)$ on a smooth boundary arc of V. Let $z = F(w)$ be conformal and $v = u \circ F$. Derive the boundary condition in the w coordinate, including the metric factor.

Solution. At the boundary, a conformal derivative rotates and scales tangent and normal vectors by $|F'(w)|$. The chain rule therefore gives $\partial_{n_w} v = |F'|\,\partial_{n_z} u \circ F$ when outward normals correspond. Multiply the original equation by $|F'|$ to obtain

$$\partial_{n_w} v + |F'|\,\beta(F(w))v = |F'|\,g(F(w)).$$

Thus a constant Robin coefficient is generally variable after pullback. Dirichlet data compose without this factor; Neumann flux density acquires it; integrated flux remains invariant because arc length transforms inversely in the paired expression.

This is an important limit of boundary simplification. A round coordinate boundary need not carry constant transformed material coefficients. A solver which leaves β unchanged solves a different boundary-value problem unless $|F'| = 1$ on the boundary or the coefficient definition already includes the factor. The formula gives a direct implementation test using a linear scaling $F(w) = aw$: the coefficient must become $|a|\beta$, while the normal derivative has the corresponding reciprocal physical scale.

Investigation 12.6 (I26: a reaction term is not conformally invariant)**.** Transform $-\Delta_z u + q(z)u = f(z)$ on V under $z = F(w)$. State precisely when a harmonic coordinate reduction remains valid and derive a coercive finite-dimensional comparison for positive transformed coefficients.

Solution. The Laplacian transforms as $\Delta_w(u \circ F) = |F'|^2(\Delta_z u) \circ F$. Hence, with $v = u \circ F$,

$$-\Delta_w v + |F'|^2 q(F(w))v = |F'|^2 f(F(w)).$$

Only the homogeneous equation with $q = f = 0$ becomes an unweighted harmonic equation. Even a constant nonzero q becomes variable when the conformal scale varies. The weak form has unchanged gradient energy and a weighted zero-order integral, which agrees with the direct transformation.

If $q \geq 0$ and the Dirichlet space has a Poincare inequality, the bilinear form is coercive. In a common basis its matrix is $A = K + M_q$, where K is stiffness and M_q the weighted mass. If $q|F'|^2$ is enclosed between q_- and q_+, then $K + q_- M \preceq A \preceq K + q_+ M$. These are verifiable spectral bounds for a chosen preconditioner, not an assertion that the mass term can be ignored. The same distinction governs diffusion-reaction models in mathematical physics and engineering chemistry.

Investigation 12.7 (I27: an exact finite Gaussian partition function)**.** Let $A = \alpha I + 2I - S - S^{-1}$ on a four-cycle, $\alpha > 0$, and define $Z(\beta) = \int_{\mathbb{R}^4} \exp[-\beta x^T A x/2]\,\mathrm{d}x$. Compute Z and the mean quadratic energy.

Solution. Fourier diagonalization gives eigenvalues $\alpha, \alpha+2, \alpha+4, \alpha+2$. Thus $\det A = \alpha(\alpha+2)^2(\alpha+4)$. An orthogonal real diagonalization preserves Lebesgue measure and separates the four Gaussian integrals, giving

$$Z(\beta) = \left(\frac{2\pi}{\beta}\right)^2 [\alpha(\alpha+2)^2(\alpha+4)]^{-1/2}.$$

Differentiating $-\partial_\beta \log Z$ yields $\mathbb{E}[x^T A x/2] = 2/\beta$. Positive α is essential for a finite integral. At $\alpha = 0$, the constant mode has zero energy and its integral diverges; one may instead constrain the mean or define a quotient measure, but that is another model.

The result verifies a finite determinant and a thermodynamic identity with no infinite regularization. Replacing the four-cycle by a continuum surface requires an infinite-dimensional measure or regularized determinant, whose existence and normalization must be established separately. The simple example is therefore a positive control for exact mode factoring and a negative control against silently discarding zero modes.

Investigation 12.8 (I28: a theta transformation with a certified tail)**.** Let $\Theta(t) = \sum_{n\in\mathbb{Z}} \mathrm{e}^{-\pi t n^2}$ and $t = 1/16$. Compare summing in the original representation with using $\Theta(t) = t^{-1/2}\Theta(1/t)$. Give an explicit absolute tail bound after keeping only $n = 0$ in the dual sum.

Solution. The dual representation is $\Theta(1/16) = 4\Theta(16)$. Its omitted tail is $8\sum_{n=1}^{\infty} \mathrm{e}^{-16\pi n^2}$. Since $n^2 \geq 1 + 3(n-1)$ for integers $n \geq 1$,

$$0 < \Theta(1/16) - 4 \leq \frac{8\mathrm{e}^{-16\pi}}{1 - \mathrm{e}^{-48\pi}}.$$

This is below 1.2×10^{-21}, with that decimal comparison independently certifiable by rational enclosures for the exponential. The symbolic bound is the primary result. The original representation has much slower term decay because its exponent is $-\pi n^2/16$.

The gain is caused by a proved identity and a change in representation, not by a change in the target quantity. The cost of evaluating $t^{-1/2}$ and transforming the parameter is negligible in this finite example but belongs in an implementation model. At $t = 1$ the two representations coincide. For a general positive t, selecting the representation with the larger Gaussian decay coefficient reduces the number of terms required by the same tail criterion. Infinite sums are never replaced by a finite count without an explicit remainder.

12.2 Exact algorithms and performance contracts

Investigation 12.9 (I29: a screened cycle with a prescribed two-mode input)**.** For $N = 8$ and $A = \frac{3}{4}I + 2I - S - S^{-1}$, solve $Ax = b$ where $b_j = 1 + \cos(\pi j/2)$. Explain the complexity when the output is a coefficient pair and when it is all eight entries.

Solution. The constant mode has eigenvalue $3/4$. The cosine has frequency $k = 2$ and eigenvalue $3/4 + 2 - 2\cos(\pi/2) = 11/4$. Therefore

$$x_j = \frac{4}{3} + \frac{4}{11}\cos(\pi j/2).$$

Substitution using the shift identity $\cos(\theta(j-1)) + \cos(\theta(j+1)) = 2\cos\theta\cos(\theta j)$ verifies the equation directly. Positive definiteness gives uniqueness.

If the input is already represented by its two modal coefficients and the required output is the same representation, the solve uses two scalar divisions. If all N values are required in the generalized N-point case, output construction requires $\Omega(N)$ writes, and evaluating the two-mode expression has $O(N)$ work. A generic FFT is not the best method for this specially encoded input; the spectral representation reveals a stronger sparsity. A dense solve and a two-coefficient output are not equivalent-output competitors. Their fair comparison requires either materializing all outputs or explicitly changing the contract.

Investigation 12.10 (I30: a geometry-derived iteration count)**.** A preconditioned positive definite operator has spectrum in $[1, 9]$. Find the optimal constant Richardson step and the least number of iterations guaranteed by its exact worst-case interval contraction to reduce an error by a factor 10^{-6}.

Solution. U49 gives $\omega = 2/(1+9) = 1/5$ and $q = (9-1)/(9+1) = 4/5$. The least integer k satisfying $(4/5)^k \leq 10^{-6}$ is 62: taking logarithms gives $k \geq \log(10^6)/\log(5/4) \approx 61.91$. The integer decision can be checked without logarithms by comparing $4^{61}10^6$ with 5^{61} and then $4^{62}10^6$ with 5^{62}.

The result is a worst-case guarantee for this iteration and interval. It is attained on an endpoint eigenvector when the endpoint is present. A smaller actual spectral interval can improve

the estimate. A different method, such as conjugate gradients or a direct diagonal solve, has a different cost and iteration theory. The example ties an energy-equivalence bound to a finite iteration certificate and keeps transcendental approximation out of the final discrete acceptance test.

Investigation 12.11 (I31: a nonconserved flow cannot supply a dual certificate)**.** A path has edge conductances $2, 3, 4, 5, 6$. A proposed unit flow assigns edge currents $(1, 1, 0, 1, 1)$. Explain why its reciprocal energy cannot be used as a lower bound for the effective conductance. Compute the valid unit-flow certificate.

Solution. The proposed flow has nonzero divergence at the two vertices adjacent to the zero-current edge, so it does not transport one conserved unit from source to sink. Thomson's principle requires conservation at every interior vertex. The missing edge reduces its energy and would create a falsely optimistic reciprocal bound.

On a path, a conserved unit flow must have current one on every oriented edge. Its energy is

$$R = \frac{1}{2} + \frac{1}{3} + \frac{1}{4} + \frac{1}{5} + \frac{1}{6} = \frac{29}{20}, \qquad C = \frac{1}{R} = \frac{20}{29}.$$

The potential drops are $(10, 20/3, 5, 4, 10/3)/29$, equivalently C/c_i, and sum to one. These potentials attain primal energy C, while the valid unit flow has reciprocal energy C, proving the exact conductance by matching bounds. The checker must validate conservation before accepting the numerical objective. Objective agreement in a few test examples cannot repair an unsound feasible-set definition.

Investigation 12.12 (I32: unequal precision with a provable rounding allowance)**.** For positive weights w_j, choose real precisions b_j minimizing $\sum_{j=1}^{m} b_j$ subject to $\sum_j w_j 2^{-b_j} \le \varepsilon$, initially without lower bounds on b_j. Find the optimum and derive a feasible integer allocation whose total cost is less than m bits above it.

Solution. Set $x_j = w_j 2^{-b_j} > 0$. Then $b_j = \log_2 w_j - \log_2 x_j$. Minimizing total precision is equivalent to maximizing $\prod_j x_j$ under $\sum_j x_j \le \varepsilon$. Arithmetic–geometric mean shows the unique optimum is $x_j = \varepsilon/m$. Thus

$$b_j^* = \log_2(m w_j/\varepsilon), \qquad B^* = \sum_j \log_2(m w_j/\varepsilon).$$

Taking integer $\widehat{b}_j = \lceil b_j^* \rceil$ can only reduce each error contribution, so the allocation is feasible. Since $0 \le \widehat{b}_j - b_j^* < 1$, its total cost is less than $B^* + m$. If a lower precision bound is imposed, coordinates whose unconstrained optimum lies below that bound must be fixed and the remaining budget redistributed; the unrestricted formula must not be used blindly.

This proves an approximation guarantee for the integer allocation, not its exact optimality. Exact integer optimization can be handled by a finite dynamic program after sufficient bounds have been proved. The treatment separates a closed-form continuous optimum, a rigorous rounded construction and the stronger discrete optimum claim.

Investigation 12.13 (I33: subdivision makes a Bernstein certificate sharp)**.** For $p(t) = t^2 - t + 1$ on $[0, 1]$, compare its quadratic Bernstein lower bound on the full interval with the bounds on the two half-intervals. Determine whether either result proves the exact minimum.

Solution. On $[0, 1]$ the coefficients are $(1, 1/2, 1)$, so positivity and partition of unity yield only $p \ge 1/2$. On the first half, substitute $t = s/2$ to get $p = 1 - s/2 + s^2/4$, with Bernstein coefficients $(1, 3/4, 3/4)$. On the second, substitute $t = (1 + s)/2$ to get $p = 3/4 + s^2/4$, with coefficients $(3/4, 3/4, 1)$. Therefore $p \ge 3/4$ over both intervals. Since $p(1/2) = 3/4$, the bound is attained and the exact minimum is $3/4$.

The unsplit certificate was valid but nonsharp. One subdivision closes the gap because the minimizer becomes an interval endpoint and the local control points no longer fall below its value. This example is a complete finite test for basis conversion, subdivision and coverage checking. A malicious certificate omitting a gap between the half-intervals would not certify the entire domain, even if every listed coefficient were positive. Coefficient positivity and interval coverage require separate checks.

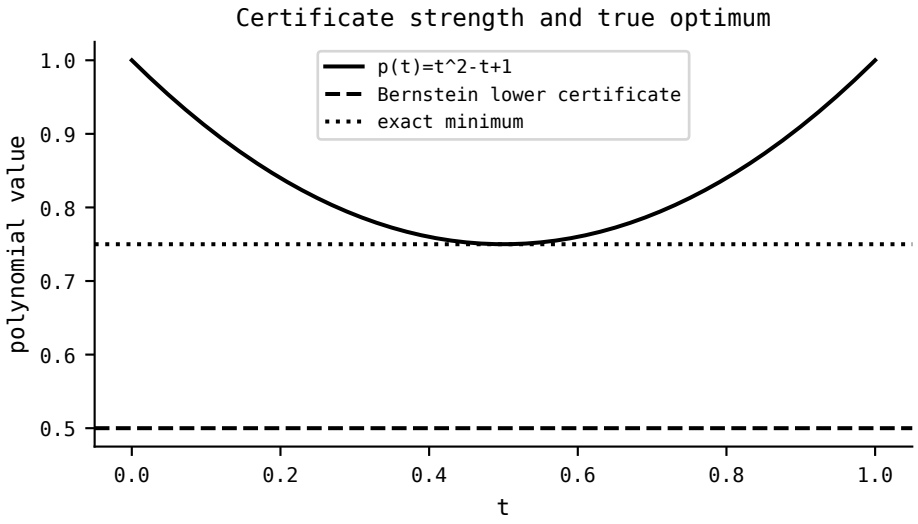


Figure 12.1: The unsplit Bernstein lower bound, the polynomial, and the true minimum. Investigation I33 obtains the sharp bound by subdivision and an attaining point.

Investigation 12.14 (I34: winding totals lose nonabelian continuation information)**.** Let two loops act on three sheets by $a = (12)$ and $b = (23)$. Compare the words ab and ba, using right-to-left permutation composition, and compute the commutator $aba^{-1}b^{-1}$.

Solution. The product ab sends $1 \mapsto 2 \mapsto 3 \mapsto 1$, so $ab = (123)$. The opposite product is (132). Because $a^{-1} = a$ and $b^{-1} = b$, the commutator is $(ab)^2 = (132)$, which is nontrivial. Yet its total exponent of each generator is zero. Any scalar winding record that stores only those totals identifies the commutator with the identity and loses the continuation result.

The full permutation can be updated in $O(d)$ elementary table operations per generator for d sheets; here $d = 3$. Storing a pair of integer totals is smaller but does not satisfy the same output specification. The example is a precise information-loss counterexample to an invalid optimization. The underlying geometry may still permit a reduced faithful representation for a special monodromy group, but its faithfulness must be proved. Abelianization is not automatically such a reduction.

Investigation 12.15 (I35: a consistency check for distributed chart transitions)**.** Three chart servers report scalar transition factors $g_{01}, g_{12}, g_{20} \in \mathbb{C}^*$. Show that values $u_0, u_1, u_2 \neq 0$ satisfying $u_j = g_{ij}u_i$ around the cycle exist exactly when $g_{20}g_{12}g_{01} = 1$. Test $(1, 1, -1)$.

Solution. Substituting successively gives $u_0 = g_{20}g_{12}g_{01}u_0$. Since $u_0 \neq 0$, the product must be one. Conversely, choose arbitrary nonzero u_0, set $u_1 = g_{01}u_0$ and $u_2 = g_{12}u_1$; the product condition makes the final transition hold. For $(1, 1, -1)$ the product is -1, so no such nonzero global values exist.

In a connected graph, fixing a spanning tree determines all vertex values from one base value; each remaining edge supplies a cycle consistency equation. This gives a finite exact checker with one condition per independent cycle. If transitions are matrices or permutations,

their multiplication order matters and the same spanning-tree argument uses ordered products. Near-consistent floating-point products require a tolerance and gauge-fitting problem, which is separate from exact descent. Such a test verifies consistency of reported chart data; it does not guarantee network liveness, message delivery or resistance to compromised participants.

Investigation 12.16 (I36: complex torus multiplication does not establish encryption)**.** Count the points of $E : y^2 = x^3 - x$ over $\mathbb{F}_5$, including the point at infinity. Show that doubling is not a permutation of this group and explain why the complex-lattice picture alone supplies no encryption-security proof.

Solution. For $x = 0, 1, 2, 3, 4$, the right-hand sides modulo five are $0, 0, 1, 4, 0$. These have respectively $1, 1, 2, 2, 1$ square roots. There are seven affine points and one point at infinity, totaling eight. The nonsingularity condition holds because $x^3 - x$ has distinct roots over $\mathbb{F}_5$. The point $(0, 0)$ has order two: its inverse is $(0, -0) = (0, 0)$, and a nonidentity self-inverse point has double equal to the identity. Hence doubling is not injective and cannot be a permutation.

For a finite cyclic subgroup of order n, multiplication by a public k is a permutation only when $\gcd(k, n) = 1$, in which case a public inverse $k^{-1} \bmod n$ computes its inverse. It is therefore not encryption by itself. Elliptic-curve cryptographic protocols require a security problem, parameter selection, randomness, encoding and adversarial model. Uniformization over $\mathbb{C}$ explains complex geometry, but reductions modulo a prime and finite-field group algorithms must be specified independently. The exact point count is a small algebraic control, not a security benchmark.

12.3 Objective comparison and limits of inference

Investigation 12.17 (I37: preprocessing changes the preferred method)**.** Two exact algorithms solve the same query family. Their specified costs are $T_A(m) = 120 + 2m$ and $T_B(m) = 20 + 7m$ units for m queries. Determine the preference region and the asymptotic ratio. What extra information is needed to interpret the units as time?

Solution. Subtraction gives $T_A - T_B = 100 - 5m$. Thus B is cheaper for $m < 20$, the costs agree at $m = 20$, and A is cheaper for $m > 20$. The ratio T_B/T_A tends to $7/2$ as $m \to \infty$. This is a theorem about the given affine cost model. It includes setup in both methods and does not charge one setup per query unless the representation is invalidated between queries.

To interpret the units as elapsed time, specify the elementary operations, their implementation and hardware costs, data transfer, memory effects and concurrency. If they are arithmetic counts, the ratio need not match runtime. If the inputs change so that A must rebuild its representation every query, its cost becomes $122m$ and the previous preference region disappears. If the requested output differs between methods, even the algebraic comparison is not relevant until an equivalence contract is established. These conditions are part of a valid metric, not optional experimental commentary.

Investigation 12.18 (I38: a six-cone sphere and a genus-two covering)**.** An orbifold has underlying sphere and six cone points of order two. Compute its orbifold Euler characteristic and hyperbolic area. Compare it with the double cover branched at those six points.

Solution. The characteristic is $2 - 6(1 - 1/2) = -1$. It is a good compact hyperbolic orbifold, so its curvature -1 area is 2π. A double cover branched simply at all six points satisfies $2 - 2g = 2 \cdot 2 - 6 = -2$, hence $g = 2$. Pulling back the orbifold metric removes the order-two cone singularities and gives area 4π, agreeing with the closed genus-two Gauss–Bonnet value $4\pi(g - 1)$.

This matching computation checks local branching, orbifold weights and global area simultaneously. Counting six branch points without their ramification indices would be insufficient

for a higher-degree cover. Conversely, treating the cone points as ordinary smooth points in the base would produce area inconsistent with the covering. The result explains why weighted quotient geometry is computationally useful: it retains the data necessary for global invariants while permitting a smaller fundamental domain.

Investigation 12.19 (I39: capacity cannot identify absolute size)**.** For $A(r, R)$, prove that capacity alone cannot determine r and R separately. Determine what can be recovered from capacity together with the outer circumference, and identify the conditioning of that recovery.

Solution. Capacity is $C = 2\pi/\log(R/r)$, unchanged under $(r, R) \mapsto (ar, aR)$ for every $a > 0$. Thus infinitely many absolutely different sizes have the same capacity. If the outer circumference is $P = 2\pi R$, then

$$R = P/(2\pi), \qquad r = \frac{P}{2\pi}\exp(-2\pi/C).$$

These formulas uniquely recover both radii. Their logarithmic derivatives are $\partial \log r/\partial \log P = 1$ and $\partial \log r/\partial \log C = 2\pi/C$. Consequently a small relative capacity error can be amplified when the modulus is large. Circumference uncertainty enters linearly in relative terms.

The example separates identifiability from numerical precision. No amount of more accurate capacity computation recovers a missing absolute length scale. Adding one independent dimensional observation resolves the ambiguity, after which conditioning determines the attainable accuracy. This is a general methodological requirement for inverse physical models: a conformal invariant cannot determine data deliberately removed by conformal equivalence.

Investigation 12.20 (I40: a normalization test with an exact geometric witness)**.** Choose an annulus whose normalized condenser period is one. Compare the correct exponential coordinate with a proposed formula having outer radius e. Give a direct finite expression witnessing the discrepancy.

Solution. Take $A(1, \mathrm{e}^{2\pi})$. Its normalized potential is $u = \log r/(2\pi)$ and a local conjugate is $v = \theta/(2\pi)$. The period of v under one positive loop is one. The correct coordinate is $F = \exp(2\pi(u + \mathrm{i}v)) = r\mathrm{e}^{\mathrm{i}\theta} = z$, with outer radius $\mathrm{e}^{2\pi}$. A formula claiming outer radius e is inconsistent with its own value on $u = 1$: $|F| = \exp(2\pi)$, not $\exp(1)$.

If the exponent itself is changed to $u + \mathrm{i}v$, the map is no longer single-valued, because $v \mapsto v + 1$ multiplies it by $\mathrm{e}^{\mathrm{i}} \neq 1$. Thus one cannot correct the radius by deleting the 2π from the exponent. The angular period and radial logarithm must be normalized together. The positive inequality $2\pi > 1$ already proves the two radii differ; high-precision numerical evaluation is unnecessary.

This witness checks the source formula using a known exact geometry. The correction is local and specific. It does not diminish the general annulus uniformization theorem, whose proof U11 now supplies with consistent normalization and a degree argument. A source review should record precisely that repaired formula and preserve the valid surrounding result.

Chapter 13

Specialist applications with explicit analytical reductions

13.1 Elliptic periods and a complete differential equation

The algebraic curve $y^2 = x(1-x)(1-mx)$ supplies a period already used to describe degeneration. A further reduction expresses parameter dependence through a second-order differential equation. This is useful in mathematical physics because it connects repeated period evaluation to a finite differential system while retaining singular parameter values.

Define $K(m) = \int_0^{\pi/2} (1 - m\sin^2\theta)^{-1/2}\,\mathrm{d}\theta$ for $|m| < 1$, using the branch equal to one at $m = 0$. The binomial series converges uniformly on the integration interval when $|m| \le r < 1$. Its coefficients are $\binom{2n}{n}/4^n$. Integration of $\sin^{2n}\theta$ can be derived by integration by parts:

$$I_n = \int_0^{\pi/2} \sin^{2n}\theta\,\mathrm{d}\theta = \frac{2n-1}{2n} I_{n-1}, \qquad I_0 = \frac{\pi}{2}.$$

Consequently

$$K(m) = \frac{\pi}{2} \sum_{n=0}^{\infty} a_n m^n, \qquad a_n = \left(\frac{\binom{2n}{n}}{4^n} \right)^2, \quad \frac{a_{n+1}}{a_n} = \frac{(n+1/2)^2}{(n+1)^2}.$$

All interchanges above follow from locally uniform absolute convergence. They give a constructive coefficient representation with positive real coefficients on the physical interval $0 < m < 1$.

Theorem 13.1 (U53: the elliptic period equation and an explicit tail)**.** *For $|m| < 1$, the period satisfies*

$$m(1-m)K'' + (1-2m)K' - \frac{1}{4}K = 0.$$

If $|m| \le r < 1$, truncation after degree N has error at most

$$\frac{\pi}{2} \frac{a_{N+1} r^{N+1}}{1-r}.$$

The analytic solution with $K(0) = \pi/2$ is unique near zero.

Proof. Substitute $K = (\pi/2)\sum a_n m^n$ into the differential expression. Its coefficient of m^n is $(n+1)^2 a_{n+1} - (n+1/2)^2 a_n$, which vanishes by the displayed recurrence. Termwise differentiation is justified on every smaller disk. The ratio $a_{n+1}/a_n < 1$, so the coefficients decrease. Thus $\sum_{n>N} a_n |m|^n \le a_{N+1} r^{N+1} \sum_{j \ge 0} r^j$, yielding the tail. The recurrence determines all coefficients from a_0 because $(n+1)^2 \ne 0$. Any analytic solution with the same initial value therefore has the same Taylor series and coincides locally. □

The equation has singular parameter values $0, 1, \infty$. The function selected above is analytic at zero, but another independent local solution has a logarithm there. At $m = 1$, the selected period develops the logarithmic growth already explained by a pinching cycle. The finite-dimensional differential system organizes this continuation; it does not eliminate its monodromy. A numerical differential-equation solver must retain a path, initial branch and error enclosure.

For repeated evaluation within $|m| \le r < 1$, the coefficient recurrence requires $O(N)$ exact scalar updates, followed by $O(N)$ evaluation work per point using Horner's rule. Direct quadrature has a different cost depending on endpoint behavior and requested tolerance. At r close to one, the geometric bound becomes expensive and an alternative modular or complementary representation is preferable. The theorem identifies that deterioration explicitly through $1 - r$ and r^{N+1}.

For high-energy or nuclear applications where an integral has been algebraically reduced to an elliptic period, the reduction must identify the cross-ratio m, scale factor, integration cycle and singular limits. The period equation then supplies a reusable computational component. It does not prove that an arbitrary Feynman integral or coupled-channel amplitude has precisely this curve. The source physical reduction remains a separate theorem or model specification.

13.2 Regular singular equations and projective coordinates

A second-order linear equation can also generate a local projective coordinate. Let y_1, y_2 be linearly independent solutions of

$$y'' + Q(z)y = 0$$

on a simply connected region where Q is holomorphic. Their Wronskian $W = y_1'y_2 - y_1y_2'$ is constant because $W' = y_1''y_2 - y_1y_2'' = 0$. Where $y_2 \neq 0$, the ratio $f = y_1/y_2$ has derivative W/y_2^2, so it is locally univalent.

Proposition 13.2 (U54: a differential equation determines a Schwarzian)**.** *The ratio $f = y_1/y_2$ satisfies*

$$\mathcal{S}(f) = \frac{f'''}{f'} - \frac{3}{2}\left(\frac{f''}{f'}\right)^2 = 2Q.$$

Replacing the solution basis multiplies f by a Mobius transformation and leaves its Schwarzian unchanged.

Proof. Since $f' = Wy_2^{-2}$, set $q = f''/f' = -2y_2'/y_2$. Then $\mathcal{S}(f) = q' - q^2/2 = -2y_2''/y_2 = 2Q$. If $(\widetilde{y}_1, \widetilde{y}_2) = (ay_1 + by_2, cy_1 + dy_2)$ with $ad - bc \neq 0$, then $\widetilde{f} = (af + b)/(cf + d)$. Direct differentiation shows that a Mobius map has Schwarzian zero; the chain rule $\mathcal{S}(M \circ f) = (\mathcal{S}(M) \circ f)(f')^2 + \mathcal{S}(f)$ follows by differentiating the logarithmic derivative twice. Hence the Schwarzian is unchanged. □

This relation connects local complex analysis, projective geometry and monodromy. Analytic continuation of the solution basis around a loop acts by a matrix, and the ratio changes projectively. A uniformizing coordinate demands additional global conditions on that monodromy. Solving the local differential equation alone does not establish that the resulting ratio is a global bijection to a canonical domain.

In conformal-field models the Schwarzian also enters a specified transformation law for the stress tensor. The geometric identity above is classical and exact. Its multiplication by a central charge, normalization by 12 or 24, and quantum interpretation must follow the selected field-theory convention. The two uses share a differential invariant but have different premises. For the exponential $f(z) = \mathrm{e}^{az}$, the Schwarzian is $-a^2/2$, since $f''/f' = a$ and $f'''/f' = a^2$. This is a useful cross-check on cylinder-to-plane formulas.

A certificate for a projective-coordinate computation can therefore check the residual $\mathcal{S}(f)-2Q$ on a domain with a derivative lower bound, together with its monodromy matrices. A small local residual without a nonzero derivative bound may conceal a singular ratio. A product of monodromy matrices close to the identity is a numerical diagnostic; exact group relations or certified error bounds are required for a rigorous descent statement.

13.3 A coupled-channel model with exact unitarity

Uniformizing square-root thresholds simplifies sheet structure. A physical amplitude additionally needs a symmetry or conservation constraint. A simple finite-dimensional model shows how the two requirements can be checked independently. Let $K(E)$ be a real symmetric matrix on a real energy interval and define

$$S(E) = (I + \mathrm{i}K(E))(I - \mathrm{i}K(E))^{-1}.$$

The inverse exists because all eigenvalues of K are real, so $1 - \mathrm{i}\lambda \neq 0$. If K is represented rationally in a uniformizing coordinate, this Cayley expression is meromorphic in that coordinate away from the determinant zeros.

Proposition 13.3 (U55: exact real-axis unitarity of a Cayley model)**.** *For every Hermitian matrix K, the matrix $S = (I + \mathrm{i}K)(I - \mathrm{i}K)^{-1}$ is unitary. If $K^T = K$, then $S^T = S$.*

Proof. The matrices $I + \mathrm{i}K$ and $I - \mathrm{i}K$ commute because both are polynomials in K, as do their inverses. Taking the adjoint gives $S^* = (I + \mathrm{i}K)^{-1}(I - \mathrm{i}K)$. Multiplying by S and cancelling commuting factors yields $S^*S = I$. For transpose symmetry, transpose the product and use $K^T = K$ and commutation again, giving $S^T = S$. □

The eigenphase relation is explicit: if $Kx = \lambda x$, then $Sx = (1+\mathrm{i}\lambda)/(1-\mathrm{i}\lambda)x = \mathrm{e}^{2\mathrm{i}\arctan\lambda}x$. The singularities of this representation satisfy $\det(I - \mathrm{i}K) = 0$ in the continued complex coordinate. Real-axis Hermiticity alone says nothing about the positions of every off-axis pole or the correct threshold power law. Those require analyticity and model-specific conditions.

For a low-rank reaction matrix $K = UCU^*$ with U of size $n \times r$, the Woodbury identity reduces the inverse of $I - \mathrm{i}UCU^*$ to an r-dimensional inverse, when the required smaller inverse exists. A version avoiding C^{-1} is

$$(I - \mathrm{i}UCU^*)^{-1} = I + \mathrm{i}UC(I - \mathrm{i}U^*UC)^{-1}U^*.$$

Multiplying by $I - \mathrm{i}UCU^*$ verifies the formula. No inverse of C is assumed. This has potential work $O(nr^2 + r^3)$ for the smaller factors plus the cost of applying or materializing the output. Producing the full dense S still requires $\Omega(n^2)$ output writes. The reduction is especially useful for the action Sx, where no dense output is required.

A perturbation estimate can be obtained without relying on numerical pole plots. For Hermitian K, $\|(I - \mathrm{i}K)^{-1}\|_2 \leq 1$. Since $S = 2(I - \mathrm{i}K)^{-1} - I$, the resolvent identity yields

$$\|S(K + \Delta K) - S(K)\|_2 \leq 2\|\Delta K\|_2$$

when $K + \Delta K$ is also Hermitian. This is a global real-axis Lipschitz estimate. Away from the real axis, the corresponding inverse norms can grow and the estimate must include them. Threshold coordinate conditioning remains a separate contribution.

This model is appropriate as a mathematical nuclear-scattering or particle-amplitude laboratory. It makes no claim to fit measured cross sections, infer nuclear parameters or replace a coupled-channel dynamical calculation. Its contribution is an exact analytic constraint and an explicit low-rank computational contract that such a calculation can use.

13.4 Cylinder sewing and an exact Schur complement

Consider two logarithmic cylinders of lengths L_1, L_2 joined along a common circle. For one Fourier order $n > 0$, each cylinder has the symmetric boundary matrix

$$D_n(L) = n \begin{pmatrix} \coth(nL) & -\operatorname{csch}(nL) \\ -\operatorname{csch}(nL) & \coth(nL) \end{pmatrix}.$$

If the exterior boundary amplitudes are a, b and the interface amplitude is x, total energy is the sum of the two cylinder energies. Continuity fixes the same x on both sides, while stationarity enforces flux balance.

Theorem 13.4 (U56: exact modal gluing)**.** *Eliminating the interface amplitude from the sum of these two quadratic energies gives the exterior matrix $D_n(L_1 + L_2)$. For the zero-frequency mode, the effective scalar conductance is $1/(L_1 + L_2)$.*

Proof. Write $A = nL_1$, $B = nL_2$. The stationary interface equation is

$$(\coth A + \coth B)x = \operatorname{csch} A\, a + \operatorname{csch} B\, b.$$

The denominator is positive. The off-diagonal entry of the Schur complement is

$$-n\frac{\operatorname{csch} A \operatorname{csch} B}{\coth A + \coth B} = -\frac{n}{\sinh(A+B)},$$

because $\cosh A \sinh B + \cosh B \sinh A = \sinh(A + B)$. A diagonal entry is

$$n\left(\coth A - \frac{\operatorname{csch}^2 A}{\coth A + \coth B}\right) = n \coth(A + B),$$

using $\cosh^2 A - 1 = \sinh^2 A$. The other is identical by symmetry. Thus the matrix is exactly $D_n(L_1 + L_2)$. For $n = 0$, energy is $(x - a)^2/L_1 + (b - x)^2/L_2$. Differentiation gives $x = (L_2 a + L_1 b)/(L_1 + L_2)$, and substitution gives $(b - a)^2/(L_1 + L_2)$. □

This is a continuous-domain counterpart of eliminating interior nodes in a resistor network. The resulting boundary operator retains exactly the information needed to couple adjacent pieces. A parallel implementation can solve subdomain modes independently and communicate interface data. Its work depends on the number of retained modes and subdomains, while message latency depends on the elimination tree. A chain eliminated sequentially has linear depth; a balanced merge tree has logarithmic depth with enough processors and consistent interface orientation.

The argument supplies exact equivalence for cylinders. For general subdomains, approximate Dirichlet-to-Neumann operators introduce approximation error. If the interface quadratic form is uniformly coercive, the Schur-complement perturbation can be bounded using the inverse norm of the interface block. Near a degenerating geometry this norm can grow. An implementation should report that coercivity margin, not only the norm of its local residuals.

The conformal modulus adds under this end-to-end sewing: $L = L_1 + L_2$ and $\mathrm{mod} = L/(2\pi)$. Conductance obeys the series law, whereas side-by-side disjoint channels obey a parallel law. Confusing these two geometries reverses the formula. The zero mode exposes this immediately, making it a useful independent checker for a much larger modal implementation.

13.5 Homology, vanishing cycles and continuation matrices

The curve $y^2 = (x-a)(x-b)Q(x)$ develops a nodal degeneration as $a \to b$, assuming $Q(b) \neq 0$. A small loop around the pair lifts to a cycle that shrinks. The local family is modeled, after analytic coordinate changes, by $uv = t$ with $t \to 0$. For $t \neq 0$, the neck is an annulus; changing the argument of t by 2π produces one Dehn twist of that annulus.

To see the twist, choose local coordinates with $u = re^{i\theta}$ and $v = t/u$. The angular gluing on the two boundaries involves $\arg t - \theta$. Increasing $\arg t$ by 2π leaves the exterior data fixed while inserting one full relative turn across the neck. This is exactly the mapping class of a Dehn twist. The sign depends on the chosen complex orientation and transport convention, which must be fixed before writing a matrix.

Proposition 13.5 (U57: homological transvection of a positive twist)**.** *With an orientation convention in which a positive twist about a simple closed curve a adds a to a curve intersecting it positively once, the induced map is*

$$T_a(x) = x + (x \cdot a)a$$

on first homology. It preserves the intersection pairing. On a genus-one basis with $b \cdot a = 1$, the cycle a is fixed and b maps to $b + a$.

Proof. Represent a cycle by oriented arcs transverse to the annular neighborhood of a. Each crossing is changed by the twist into the original crossing plus one copy of the core, with sign equal to its oriented intersection. Summing the contributions gives the formula. For two homology classes x, y, expand their transformed intersection. The two cross terms cancel because $a \cdot y = -(y \cdot a)$, and the quadratic term vanishes because $a \cdot a = 0$. Thus the pairing is preserved. The genus-one statement follows by inserting the specified intersections. □

For a closed differential transported with the family, periods transform by the same integral cycle matrix. They cannot be treated as independent single-valued scalar functions around the discriminant. In gauge-theory and string constructions, an interpretation of these periods as central charges or couplings imports further physical structure. The homological transvection itself is a topological conclusion of the local nodal model.

The theorem provides a finite consistency test: the continuation matrix must be integral, invertible and preserve the symplectic intersection form. These conditions are necessary but do not uniquely identify the monodromy of an arbitrary family. Its association with a vanishing cycle must also be proved. A numerical period tracker that returns a matrix failing the intersection identity is definitively inconsistent with the assumed cycle basis.

13.6 Torus isogenies and finite algebraic data

The complex torus $\mathbb{C}/\Lambda$ has the holomorphic multiplication map $[n] : z \mapsto nz$. Its kernel consists of $(1/n)\Lambda/\Lambda$, with n^2 elements for $n \neq 0$. Since the derivative is the nonzero constant n, the map is unbranched. Every fibre is a translate of its kernel, and the degree is n^2. This gives an exact bridge from a local derivative to a global finite fibre count.

Proposition 13.6 (U58: a pairing on lattice torsion)**.** *Fix an oriented lattice basis (ω_1, ω_2) and an integer $n \geq 2$. On n-torsion points represented by $(a\omega_1 + b\omega_2)/n$, define*

$$e_n((a,b),(c,d)) = \exp\left(\frac{2\pi i(ad - bc)}{n}\right).$$

This is well defined modulo n, bilinear, alternating and nondegenerate. It is invariant under an oriented unimodular change of lattice basis.

Proof. Changing any integer coordinate by a multiple of n changes the determinant by a multiple of n, leaving the exponential unchanged. Additivity of the determinant in each argument proves multiplicative bilinearity. The determinant of a vector with itself is zero, proving alternation. If the pairing with every (c, d) is one, pairing with $(0, 1)$ gives $a \equiv 0 \pmod{n}$, and pairing with $(1, 0)$ gives $b \equiv 0 \pmod{n}$; thus the first point is zero. An integral basis transformation of determinant one preserves the determinant, and hence the pairing. □

This is a complex-lattice expression of the alternating torsion pairing. Its transport to algebraic equations over other fields requires the corresponding algebraic construction and hypotheses, particularly when characteristic divides n. No finite-field implementation is certified merely by writing the complex exponential. The formula nevertheless provides a conceptual test for basis transformations and exact torsion enumeration in the complex model.

The distinction between an isogeny and an isomorphism is decisive. For $|n| > 1$, the map has a nontrivial kernel and is not invertible as a single-valued map. An inverse branch is available only locally and has global monodromy. In cryptographic settings, using an isogeny requires a specified domain/codomain representation and a security assumption. The degree formula counts fibres; it does not prove that evaluating or inverting a public map is computationally hard.

There is a concrete computational consequence for the algebraic model: a rational function describing $\wp(nz)$ in terms of $\wp(z)$ has degree n^2. A proposed lower-degree global formula would contradict fibre counting unless additional identifications or a restricted input class were introduced. The degree is therefore a representation lower bound for that exact global observable, distinct from bit complexity or cryptographic security.

13.7 Twisted boundary conditions and observable spectra

Ordinary functions on a torus are periodic. A section of a flat line bundle may acquire phases under lattice translations. On a rectangular torus of lengths L_x, L_y, impose

$$f(x + L_x, y) = \mathrm{e}^{2\pi \mathrm{i} \alpha} f(x, y), \qquad f(x, y + L_y) = \mathrm{e}^{2\pi \mathrm{i} \beta} f(x, y),$$

with real α, β. The phases commute, so the edge identifications are consistent. A unitary gauge transformation extracts the factor $\mathrm{e}^{2\pi \mathrm{i}(\alpha x / L_x + \beta y / L_y)}$ and leaves a periodic function.

Proposition 13.7 (U59: exact twisted Laplacian modes)**.** *The functions*

$$f_{mn}(x, y) = \exp\left(2\pi \mathrm{i}\left[\frac{(m + \alpha)x}{L_x} + \frac{(n + \beta)y}{L_y}\right]\right), \quad (m, n) \in \mathbb{Z}^2,$$

form a complete orthogonal family in the twisted L^2 space and have eigenvalues

$$\lambda_{mn} = 4\pi^2 \left(\frac{(m + \alpha)^2}{L_x^2} + \frac{(n + \beta)^2}{L_y^2}\right)$$

for $-\Delta$. A zero mode exists exactly when both phases are trivial, $\alpha, \beta \in \mathbb{Z}$.

Proof. The displayed functions satisfy both boundary conditions by integer periodicity. Differentiation gives the eigenvalues. Multiplication by the unit-modulus gauge factor is a unitary map from the ordinary periodic L^2 space to the twisted space. The ordinary Fourier basis is complete; its unitary image is therefore complete and orthogonal. The eigenvalue is zero only if $m + \alpha = n + \beta = 0$ for integers m, n, equivalent to the stated condition. □

Twists shift the spectrum without changing local flat geometry. Thus topology plus local curvature does not determine every physical spectral observable: bundle holonomy is additional data. This is relevant to quantum phases, thermal partition sums and distributed boundary conditions that carry character factors. A solver imposing ordinary periodicity when the model requires a nontrivial twist silently changes the zero-mode and low-frequency behavior.

For the antiperiodic case $\alpha = 1/2, \beta = 0$, the lowest eigenvalue is π^2/L_x^2. There is no constant zero mode, so the unregularized Gaussian integral for any finite modal truncation is coercive. For $\alpha \to 0$, that coercivity degenerates quadratically. The divergence of the corresponding determinant factor has a direct spectral explanation and is not resolved by increasing arithmetic precision.

13.8 Logical complexity and the effect of shared lemmas

Proof length depends on the language and previously admitted lemmas. A proof written using a global uniformization theorem is short only because the theorem's proof has already been developed. A comparative claim about logical complexity should therefore specify a finite dependency graph, the admissible inference rules and the charging convention for reused results.

Let a directed acyclic graph contain nodes representing lemmas or calculations. Associate a nonnegative verification cost $c(v)$ to each node. For a target set T, its dependency closure $D(T)$ is the union of all required predecessor nodes including T. A shared verification cost is $\sum_{v \in D(T)} c(v)$. Independent proof expansion instead sums each target closure separately and may count common lemmas multiple times.

Proposition 13.8 (U60: exact accounting for shared verification)**.** *For any finite target family $T_1, \dots, T_m$ in a fixed acyclic dependency graph,*

$$\sum_{v \in \bigcup_j D(T_j)} c(v) \le \sum_{j=1}^{m} \sum_{v \in D(T_j)} c(v).$$

The difference is exactly $\sum_v (m_v - 1)_+ c(v)$, where m_v is the number of target closures containing v.

Proof. Interchange the finite sums on the right. Each node contributes $m_v c(v)$ there and contributes $c(v)$ on the left precisely when $m_v > 0$. Subtraction gives the formula, and nonnegativity follows from $c(v) \ge 0$. □

The proposition justifies canonical proof ownership and dependency reuse. It does not prove that two differently formalized arguments have the same node cost, nor that a shorter dependency graph is easier for a human reader. Those are different measurements. In a proof assistant, replay time also depends on term representation, reduction strategy and trusted computation. In an expository monograph, definitions and explanations can be pedagogically necessary even when they are not new mathematical nodes.

For temporal complexity, the graph additionally carries precedence constraints. With unlimited processors and node execution times $c(v)$, the critical-path sum is a lower bound on completion time. Total work divided by the number of processors is another lower bound. Any claimed parallel advantage must respect both and the communication cost. Uniformizing a problem can reduce the number of coupled degrees of freedom, but it can also introduce global transforms or period calculations. The cost ledger includes those stages explicitly.

The mathematical optimum of a cost model and the observed performance of one program are kept in separate fields. The finite timing experiment in the next chapter is accompanied by output residuals, repeated observations and a strong structured control. No unrestricted maximality or machine-independent speed factor is inferred from its medians.

Chapter 14

Boundary solvability and a posteriori coordinate control

14.1 Harmonic distributions and interior regularity

The variational construction in Chapter 2 first produces an element of an energy space. Uniformization uses a holomorphic function and therefore requires a classical harmonic representative. In conformal coordinates this passage has a particularly direct distributional proof.

Let u be a distribution on an open planar set with $\Delta u = 0$. Fix a relatively compact disk and convolve locally with a smooth radial approximate identity ρ_ε. The smooth function $u_\varepsilon = u * \rho_\varepsilon$ is harmonic on every smaller disk because distributional differentiation commutes with convolution. For a smooth harmonic function v, its circular mean about a point is constant: differentiating the circular mean in the radius and applying the divergence theorem gives a multiple of $\int_{D_r} \Delta v = 0$. Its value at radius zero is v at the centre. Averaging those circular means with any radial smooth kernel of integral one gives $v * \rho_r = v$, wherever the radius-r disk is contained in the domain.

Theorem 14.1 (U61: Weyl regularity in the conformal coordinate)**.** *A distribution satisfying $\Delta u = 0$ on a planar domain has a unique smooth harmonic representative. A weakly harmonic energy function on a Riemann surface consequently has a smooth harmonic representative in every conformal chart.*

Proof. Choose a compact set K contained in a disk whose larger fixed neighborhood remains inside the domain. Select $r > 0$ smaller than that clearance. For all sufficiently small ε, the mean-value calculation gives $u_\varepsilon * \rho_r = u_\varepsilon$ on K. Pass to the distributional limit as $\varepsilon \to 0$: $u * \rho_r = u$ on the interior of K. The left side is smooth, since convolution of a distribution with a compactly supported smooth kernel is smooth wherever the convolution is defined. It is harmonic because its Laplacian is $(\Delta u) * \rho_r = 0$. Such local smooth representatives agree as distributions on overlaps, and their difference, being a continuous function vanishing distributionally, is zero pointwise. They therefore glue uniquely.

For a weakly harmonic function on a conformal surface, the local Dirichlet form is the Euclidean integral $\int \nabla u \cdot \nabla \varphi$, since the conformal metric factors cancel in dimension two. Its vanishing for compactly supported test functions says $\Delta u = 0$ distributionally in the chart. Apply the planar result and glue the representatives. □

For a smooth Poisson source, one first subtracts a local smooth solution. A local construction is convolution of a cut-off source with the logarithmic fundamental solution, with the residual correction supported away from the interior compact set; repeated differentiation or elliptic potential estimates show smoothness there. The remaining distribution is harmonic and U61

applies. This step concerns interior regularity; boundary values require a separate argument. Smoothness of the representative alone does not establish the required Dirichlet trace.

The proof exposes a useful verification boundary. A finite element residual is not a distributional equality on all test functions. Its vanishing on the finite trial space supplies Galerkin orthogonality, not U61 directly. To conclude a classical field has been approximated, one needs a convergence or a posteriori estimate connecting the discrete solution to the exact weak solution. The variational residual bound in Chapter 5 gives one such route under a coercivity hypothesis.

14.2 Boundary barriers and continuity of the Dirichlet solution

Let Ω be a relatively compact domain and $p \in \partial\Omega$. A barrier at p is a positive superharmonic function b_p on Ω, continuous up to the relevant boundary neighborhood, which tends to zero at p and stays bounded away from zero outside every neighborhood of p. Such a function converts boundary continuity into an inequality preserved by the maximum principle.

On a domain with a local exterior tangent disk, a logarithmic barrier can be obtained from $\log(|z-c|/R)$, where the exterior disk has centre c and radius R and touches only at p in the local neighborhood. The logarithm is nonnegative on the domain side, harmonic there and zero at the touching point. It is bounded below on a small separating arc away from p, so it can be capped and extended by a positive constant outside that neighborhood. The minimum of positive superharmonic functions is superharmonic in the comparison sense, making the extension valid.

For a nondegenerate corner, use a local sector of opening $\alpha < 2\pi$ containing the domain near the corner. With polar angle measured from its bisector, choose $0 < \gamma < \pi/\alpha$. The harmonic function $r^\gamma \cos(\gamma\theta)$ is positive on the closed sector away from its vertex because $|\gamma\theta| < \pi/2$. It tends to zero only at the vertex and can be patched by the same capping construction. This proves regularity for the piecewise smooth Jordan boundaries specified at the start, without assuming every corner is convex.

Proposition 14.2 (U62: a barrier enforces the boundary value)**.** *Let g be continuous on the compact boundary and let H be a bounded harmonic Dirichlet solution obtained by the variational or Perron construction, with comparison against continuous superharmonic boundary majorants. At every point possessing a barrier, $H(z) \to g(p)$ as $z \to p$ from inside.*

Proof. Fix $\varepsilon > 0$. Boundary continuity gives a neighborhood V of p in which $|g - g(p)| < \varepsilon$. On the remaining compact boundary set, the barrier has a positive lower bound c. Choose M large enough that Mc exceeds $2\|g\|_\infty + |g(p)| + 1$. Then $g(p) + \varepsilon + Mb_p$ majorizes g on the boundary, while $g(p) - \varepsilon - Mb_p$ minorizes it. The comparison property gives

$$g(p) - \varepsilon - Mb_p(z) \le H(z) \le g(p) + \varepsilon + Mb_p(z).$$

As $z \to p$, the barrier term tends to zero. The upper and lower limits of H lie within ε of $g(p)$. Let $\varepsilon \to 0$. □

For the variational construction, comparison follows by testing the positive part of the difference against a majorant, approximating it in the zero-trace space when necessary. If $H - B$ has nonpositive boundary trace and B is superharmonic, then $\int |\nabla (H-B)_+|^2 \le 0$. Thus the positive part is zero. The lower comparison follows after changing signs. This connects the barrier argument with the Hilbert-space existence proof instead of postulating boundary continuity as an unexplained property of a weak solution.

The specified regularity of the boundary matters. A completely arbitrary domain may have irregular boundary points where classical Dirichlet data are not attained. The source's piecewise smooth hypothesis supplies the local barriers used here. A numerical grid that rounds off an

irregular boundary has altered the domain and may appear to restore continuity; such behavior does not prove regularity of the original boundary.

14.3 The logarithmic singularity and independence of its cut-off

A Green function with pole a is constructed locally from $-\log|z-a|$ and globally corrected by a Dirichlet solution. Choose two cut-off functions χ_1, χ_2 equal to one near a and supported inside coordinate neighborhoods. The difference $(\chi_1 - \chi_2)(-\log|z-a|)$ is smooth because it vanishes near the singularity. Its Poisson correction exactly compensates the difference in cut-offs.

Proposition 14.3 (U63: uniqueness of the normalized Green function)**.** *Two Green functions on the same bounded regular domain with pole a, coefficient -1 in front of $\log|z-a|$, and zero boundary values coincide. Their regular part transforms under a coordinate change $\zeta = \psi(z)$ by addition of $\log|\psi'(a)|$.*

Proof. The difference of the Green functions is harmonic away from a and bounded near a because the logarithmic singularities cancel. The removable-singularity theorem extends it harmonically through a. It has zero boundary values, so the maximum principle applied to it and its negative gives zero everywhere. This proves uniqueness and independence of the cut-off construction.

For the coordinate transformation, write $\psi(z) - \psi(a) = \psi'(a)(z-a)(1+o(1))$. Therefore $-\log|z-a| = -\log|\zeta - \psi(a)| + \log|\psi'(a)| + o(1)$. If $G = -\log|z-a| + c_z + o(1)$, its regular part in the ζ coordinate is $c_\zeta = c_z + \log|\psi'(a)|$. Exponentiation gives the corresponding scaling of conformal radius. □

The equality of Green functions is a uniqueness theorem, not a particular numerical method. A computed regular part can be checked against two independently chosen cut-offs or coordinates. Agreement within a certified error interval is a useful implementation test; exact invariance is already guaranteed by the theorem. A raw difference between coordinate regular parts should equal the logarithmic derivative correction and is not necessarily a defect.

The pole normalization also determines the flux. On a small circle around a, the integral of the conjugate differential of $-\log|z-a|$ is -2π in counterclockwise orientation. The sign changes when the circle is regarded as an inner boundary with its induced domain orientation. This convention is used in the exponential Green-coordinate proof. It accounts for both the simple zero and the degree-one conclusion after the exponential is formed.

14.4 Residuals, admissible fields and a certified capacity interval

A conformal map of an annulus depends on the period p, which equals the normalized capacity. The useful numerical objective is often a certified enclosure of p, not an approximation to every point of the map. The primal and dual principles provide that enclosure from admissible functions and flows.

Let v have boundary values zero and one, and let j be a divergence-free unit-flux field connecting the boundary components. With the energy conventions of U45, set $P = \int |\nabla v|^2$ and $R = \int |j|^2$. Then $1/R \le p \le P$. If the trial fields have exact admissibility and PR is close to one, the capacity interval is narrow. A small residual alone does not replace these feasibility requirements.

Proposition 14.4 (U64: propagating a primal–dual interval to modulus)**.** *If $0 < \ell \le p \le u$, then*

$$\frac{1}{u} \le \operatorname{mod}(A) \le \frac{1}{\ell}, \qquad \frac{2\pi}{u} \le \log(R_{mnorm}) \le \frac{2\pi}{\ell}.$$

The relative width measured against the lower modulus bound is exactly $u/\ell - 1$. For primal–dual bounds $\ell = 1/R$, $u = P$, this is $PR - 1$.

Proof. The functions $p \mapsto 1/p$ and $p \mapsto 2\pi/p$ are decreasing on positive arguments. Apply them to the interval. The modulus width is $1/\ell - 1/u$; divide by the lower endpoint $1/u$ to obtain $u/\ell - 1$. Substituting the primal and dual bounds gives the final expression. □

Thus $PR - 1$ has a direct geometric meaning, in addition to its variational interpretation. It is an objective, dimensionless stopping criterion for the modulus enclosure. The scalar criterion should not be generalized to pointwise coordinate accuracy without further estimates, because different harmonic fields may have similar energy. It also requires both energies to be bounded rigorously when they arise from numerical quadrature.

Figure 9.1 gives the illustrative energy-gap model. The exact rational path certificate is listed separately in the computational record.

14.5 Error in the exponential coordinate on a fixed cut surface

On a cut annulus, write the exact complex potential as $H = u + \mathrm{i}v$ and the exact map as $F = \exp(2\pi H/p)$. Suppose approximations $\widetilde{H}, \widetilde{p}$ satisfy, on a compact subset of the cut surface,

$$|H - \widetilde{H}| \le \eta, \quad |p - \widetilde{p}| \le \delta, \quad p, \widetilde{p} \ge p_- > 0, \quad |H| \le B.$$

These are hypotheses to be proved by a particular numerical method, not assumed consequences of small mesh size.

Proposition 14.5 (U65: exponential-coordinate enclosure)**.** *Under these bounds,*

$$\left| \frac{2\pi H}{p} - \frac{2\pi \widetilde{H}}{\widetilde{p}} \right| \le D := 2\pi \left(\frac{\eta}{p_-} + \frac{B\delta}{p_-^2} \right).$$

If both exponents have real parts at most M, then $|F - \widetilde{F}| \le \mathrm{e}^M D$.

Proof. Decompose $H/p - \widetilde{H}/\widetilde{p} = (H - \widetilde{H})/\widetilde{p} + H(\widetilde{p} - p)/(p\widetilde{p})$ and apply the four bounds. For arbitrary complex a, b, $\mathrm{e}^a - \mathrm{e}^b = (a-b)\int_0^1 \mathrm{e}^{b+t(a-b)}\,\mathrm{d}t$. The real part along the segment is at most $\max(\Re a, \Re b) \le M$, so the integral modulus is at most e^M. Substitution proves the result. □

The cut is important. If the approximate potential has period $\widetilde{p}$ and the same value is used in the exponent, the approximate exponential may descend exactly. If the actual period of $\widetilde{H}$ is $p_H \ne \widetilde{p}$, its value after one loop is multiplied by $\exp(2\pi \mathrm{i} p_H/\widetilde{p})$. It is not a single-valued map on the uncut annulus. When $|p_H - \widetilde{p}| \le \varepsilon_p$, the seam discrepancy factor is bounded by $2\pi\varepsilon_p/\widetilde{p}$, using $|\mathrm{e}^{\mathrm{i}x} - 1| \le |x|$. This is a controlled defect, not exact descent.

For a global injectivity certificate, additional local derivative and boundary-degree information is required. A small uniform coordinate error on a compact set can prevent the image from crossing a specified separated contour, but it does not by itself exclude arbitrarily small-scale folds in an unconstrained approximate map. Holomorphicity, derivative estimates and properness supply the relevant structure. The finite algorithm must state which of these it certifies.

14.6 A derivative margin and local inverse radius

The inverse-function theorem is qualitative. A quantitative version follows from a derivative comparison on a disk and is suitable for a certificate checker. Let f be holomorphic on $D(z_0, r)$ and continuous on its closure, let $a = f'(z_0) \ne 0$, and suppose $|f'(z) - a| \le q|a|$ there for some $0 \le q < 1$.

Proposition 14.6 (U66: a certified injective disk and image disk)**.** *Under these hypotheses, f is injective on the disk and*

$$(1-q)|a|\,|z-w| \le |f(z)-f(w)| \le (1+q)|a|\,|z-w|.$$

Its image contains $D(f(z_0),(1-q)|a|r)$.

Proof. The line segment joining z, w lies in the convex disk. Integrating $f'-a$ along that segment yields $|f(z)-f(w)-a(z-w)| \le q|a||z-w|$. The two norm inequalities follow from the triangle inequality, and the lower bound proves injectivity. For a target y with $|y-f(z_0)| < (1-q)|a|r$, compare $f(z)-y$ with $a(z-z_0)$ on the boundary. The difference has modulus at most $q|a|r + |y-f(z_0)| < |a|r$. Rouche's theorem therefore gives exactly one zero of $f-y$ inside. Every such y belongs to the image. □

If a certified second-derivative bound $|f''| \le M$ is available, the condition follows from $Mr \le q|a|$. A desired inverse radius can then be guaranteed by explicit rational inequalities enclosing M, $|a|$ and r. The theorem gives a continuum statement from finite bounds. It differs from checking a finite grid of positive Jacobians, which may miss a defect between samples.

Applied to a computed uniformizing chart, this local result must be combined with an atlas-overlap and global degree argument. Those conditions join the local disks consistently and rule out incorrect sheet choices. The separate inequalities also help allocate computational effort: refining a region with large derivative margin may be unnecessary while a near-critical patch controls the total certificate cost.

14.7 Boundary approximation and the maximum-principle certificate

Let u be the harmonic solution for boundary data g, and let v be an independently constructed harmonic trial function. If $|v-g| \le \varepsilon$ everywhere on the boundary, then $|v-u| \le \varepsilon$ throughout the domain. The proof applies the maximum principle to $v-u-\varepsilon$ and its negative. Thus a certified boundary approximation controls an entire interior, provided exact harmonicity is known.

A polynomial in a holomorphic coordinate has harmonic real part, so it is one possible trial space. The approximation class must be suited to the domain and allowed singularities; on an annulus one generally needs Laurent terms and a logarithmic harmonic mode. A polynomial-only basis can fail to represent the nonzero period sector. The finite-vector/Hilbert-space methods from the earlier PHI corpus identify the optimal projection once the correct space has been chosen, while the uniformization analysis identifies that space's global compatibility conditions.

When a trial function has a nonzero Poisson residual, the boundary maximum argument needs an additional barrier or coercive resolvent bound. For example, on a disk of radius R, if $|\Delta(v-u)| \le \delta$ and the boundary discrepancy is at most ε, comparison with $\delta(R^2-|z|^2)/4$ gives $|v-u| \le \varepsilon + \delta R^2/4$. This follows because the Laplacian of $(R^2-|z|^2)/4$ is -1. The signs in the upper and lower comparisons must be treated separately. A conformal change transforms the residual by its Jacobian and therefore changes the coefficient of the barrier estimate.

The hierarchy is now explicit: exact admissibility gives variational bounds; a positive period interval gives modulus bounds; harmonic and conjugate-potential bounds give a coordinate bound on a cut; period matching gives descent; derivative margins give local injectivity; and a global degree condition gives the intended global map. Each arrow has a distinct mathematical proposition. The formalization register preserves those propositions individually, so a passing scalar calculation is not promoted to complete uniformization verification.

14.8 Periodic quadrature after uniformization

The logarithmic or torus coordinate often turns a contour observable into an integral over a periodic parameter. Analyticity then produces an explicit convergence rate for the equally spaced trapezoidal rule. The parameter strip width is geometric information: nearby singularities or branch collisions reduce it and increase the necessary sample count.

Proposition 14.7 (U67: a certified periodic quadrature bound)**.** *Let f be 2π-periodic and holomorphic in a neighborhood of the closed strip $|\operatorname{Im} z| \le \sigma$, with $|f| \le M$ there. Let*

$$I = \frac{1}{2\pi}\int_0^{2\pi} f(x)\,\mathrm{d}x, \qquad Q_N = \frac{1}{N}\sum_{j=0}^{N-1} f(2\pi j/N).$$

Then

$$|Q_N - I| \le \frac{2M\mathrm{e}^{-\sigma N}}{1-\mathrm{e}^{-\sigma N}}.$$

In particular, $N \ge \sigma^{-1}\log(1+2M/\varepsilon)$ is sufficient for error at most ε.

Proof. For the Fourier coefficient $c_k = (2\pi)^{-1}\int_0^{2\pi} f(x)\mathrm{e}^{-\mathrm{i}kx}\,\mathrm{d}x$, move the integration contour to $\operatorname{Im} z = -\sigma$ when $k > 0$ and to $+\sigma$ when $k < 0$. The two vertical sides cancel by periodicity. The horizontal integral gives $|c_k| \le M\mathrm{e}^{-|k|\sigma}$. These bounds imply absolute and uniform convergence of the Fourier series on the real axis.

Insert this series into Q_N and interchange the finite sample average with the absolutely convergent series. The roots-of-unity sum is one for k divisible by N and zero otherwise, so $Q_N = \sum_{m\in\mathbb{Z}} c_{mN}$, while $I = c_0$. Therefore $|Q_N - I| \le 2M\sum_{m\ge1}\mathrm{e}^{-mN\sigma}$, which is the stated geometric sum. Solving its inequality with ε gives the sample requirement. □

For $M = 1$, $\sigma = 3/10$ and target 10^{-6}, forty-nine samples suffice by the displayed bound. This conclusion is conditional on the strip bound, not on an observed decay pattern of a few sample differences. A rigorous computation can enclose M through an independent complex-domain estimate. If the function is given only by a black-box evaluator on the real line, U47 prevents deriving such a bound from finitely many values without an additional prior.

The roots-of-unity identity also shows the exact aliasing mechanism. A mode of frequency N has zero integral but takes the same value at every grid point. Consequently sample agreement is not proof of low-frequency content. The analytic envelope suppresses the amplitude of such a hidden mode by an exponential factor. This supplies the mathematical link between geometry, admissible information and numerical accuracy.

For an annular physical observable, first express the boundary integral in the angular coordinate and include its transformed arc-length or flux factor. If that factor reduces the strip of analyticity, it controls the actual rate. Omitting it may produce a faster-converging calculation for the wrong observable. Likewise, a branch point on the proposed shifted contour invalidates the coefficient estimate; moving the contour or changing the coordinate then becomes part of the certified method.

Chapter 15

Proof status, reproducible certificates and quantitative evidence

15.1 A fixed and inspectable obligation universe

The source denominator is nine numbered results in seven subsections. The reconstruction has sixty-seven explicitly labelled theorem-level assertions U01–U67 and forty solved investigations I01–I40. These are authoring units, not sixty-seven mechanically accepted proofs. The source-obligation table identifies the primary derivation of every source result. Additional assertions have a separate identity and do not inflate the source-completion denominator.

Source	Proof locations	Disposition
5.1	U08, U18, U19	Three-model statement proved through the open and compact alternatives.
5.2	U01, U10	Universal-cover complex structure and free deck-group quotient classification.
5.3	U02, U03, U05, U11	Harmonic period and degree-one construction; outer-radius normalization repaired.
5.4	U07, U12, U13	Green-function construction gives a proper disk coordinate and its normalization.
5.5	U14–U18	Exhaustion with nonconstant injective limit and an explicit surjectivity argument.
5.6	U19	Compact simply connected surface; extension at the omitted point.
5.7	U20, U21	Cusp and circle-end extension under the declared proper-germ/regular-collar conditions.
5.8	U22	Embedding gives degree one and a boundary homeomorphism.
5.9	U23–U25	Good-orbifold foundation is imported explicitly; compact and punctured statements are separated.

The corrected treatment of an ambiguous or overbroad assertion is not counted as a proof of its unqualified literal wording. In particular, the annular exponential factor, the behavior of limits under exhaustion, the hypotheses on end maps, and the use of Euler characteristic for punctured surfaces are recorded separately. Every theorem is read with its stated class of surfaces, boundary conventions and normalization.

The mathematical developments rely on a finite set of named foundations: elementary

complex calculus and the argument principle; covering-space and surface topology; Hilbert-space completion and projection; regular-domain elliptic solvability and regularity; and the topological goodness classification for two-dimensional orbifolds. The earlier PHI volume supplies the stated Montel, Koebe and proper-map results. The present text reconstructs the functional and geometric steps it uses and spells out its new limit and normalization arguments. The entire foundational library of topology, PDE and algebraic geometry is not represented as mechanically closed in this publication. An acceptance register must retain each imported theorem as an obligation for subsequent formal replay.

15.2 What the executed checks establish

The principal verification script executed eighty-two named checks. The extension script executed forty-five further checks. Together they comprise **127 named finite and symbolic checks**. Nine additional negative controls were rejected. The mathematical claims, finite instances, numerical diagnostics and negative tests occupy separate records, so their totals cannot be added to manufacture an accepted-theorem count.

Evidence class	Contents and interpretation
Exact rational arithmetic	Pi and logarithm bounds, reciprocal capacity/modulus enclosure, a resistor-path solution, compact signature signs, finite-field point counts and integer iteration thresholds.
Symbolic identities	Two-threshold coordinate formulas, the illustrative period derivative, Liouville curvature, rational gluing identities and exact finite matrix unitarity.
Finite logical checks	Permutation composition, torsion-pairing samples, dependency-cost multiplicities and rejected malformed examples.
Floating-point diagnostics	Modal boundary identities and matched solution residuals for screened cycle systems. These are checked numerical instances, not universal rounding-error proofs.
Measured times	Seven complete-call observations per method and size, retaining all samples and medians. These are local performance data.
Formal proof acceptance	Zero Lean, Rocq, Isabelle or other kernel acceptances in this release. The status table is prospective.

The exact interval calculation uses rational arithmetic throughout. Machin's identity $\pi = 16\arctan(1/5) - 4\arctan(1/239)$ is evaluated with alternating-series bounds. For $0 < x < 1$,

$$\arctan x = \sum_{j=0}^{N-1} \frac{(-1)^j x^{2j+1}}{2j+1} + R_N, \qquad |R_N| \le \frac{x^{2N+1}}{2N+1},$$

with the sign fixed by alternation. The identity itself follows from tangent addition: $\tan(2\arctan(1/5)) = 5/12$, $\tan(4\arctan(1/5)) = 120/119$, and subtracting $\arctan(1/239)$ gives tangent one. The angle lies in $(0, \pi/2)$, so it is $\pi/4$. This establishes both the algebraic relation and its branch.

For the logarithm,

$$\log 2 = 2\sum_{j=0}^{N-1} \frac{(1/3)^{2j+1}}{2j+1} + R_N, \quad 0 < R_N \le \frac{2(1/3)^{2N+1}}{(2N+1)(1-1/9)}.$$

This follows by integrating the geometric expansion of $(1-t^2)^{-1}$ from zero to $1/3$. Combining positive interval endpoints gives a rational enclosure for $2\pi/\log 2$, the capacity of $A(1,2)$, and its

reciprocal modulus. Their interval widths are checked to be below 10^{-18}. The decimal capacity 9.064720283654388 is a display approximation; the numerator/denominator endpoints in the JSON file are the actual certificate.

The network conductance 20/29 is a second exact instance, independent of transcendental evaluation. Its potentials, edge currents and both energies are stored as rational values. Matching primal and dual objectives certifies the optimum under Kirchhoff conservation. A flow with a missing edge current is explicitly rejected, because it violates feasibility before its objective is considered.

15.3 Performance measurements with a strong conventional control

The local benchmark solves $Ax = b$ for $A = \frac{3}{4}I + 2I - S - S^{-1}$ on cycles of sizes $32, 64, 128, 256$. Three methods return the same full vector: dense construction and solution, Fourier diagonalization, and a cyclic-tridiagonal Sherman–Morrison method using two tridiagonal solves. Input values are shared. Matrix or spectral coefficient construction performed by a method is included in that method's timed call.

Size	Dense (ms)	Fourier (ms)	Cyclic tridiagonal (ms)
32	0.038556	0.016664	0.057445
64	0.092986	0.016304	0.041521
128	0.167657	0.018036	0.041681
256	0.793778	0.021612	0.050555

The entries are medians of seven measurements. At size 256 the observed dense/Fourier ratio is approximately 36.73, while the cyclic-tridiagonal/Fourier ratio is approximately 2.34. These are properties of these implementations in the recorded environment. The cyclic-tridiagonal method has $O(N)$ arithmetic and the Fourier method has $O(N \log N)$ arithmetic. The finite measurements do not reverse those asymptotic bounds; implementation constants and workload scale explain why a method with the larger asymptotic count can be faster on the displayed range.

All solution residuals and disagreements against the dense solution are checked against the declared 10^{-11} diagnostic threshold. This confirms matching finite outputs at the tested instances. It is not a forward-error theorem for every floating-point execution or every right-hand side. Such a theorem would additionally specify rounding, matrix conditioning and implementation semantics.

The recorded software versions are Python 3.13.5, NumPy 2.3.5, SciPy 1.17.0 and SymPy 1.14.0. The platform string and full sample arrays are retained in the result record. Rebuilding at another time or on another machine may change timings. Mathematical identities and exact certificate values should remain unchanged, while the timing record should be reported as a new experiment.

15.4 Maximality claims replaced by finite completion criteria

For a versioned finite obligation set $\mathcal{U}$ and positive weights w_u, define

$$C(A) = \frac{\sum_{u \in A} w_u}{\sum_{u \in \mathcal{U}} w_u}, \qquad A \subseteq \mathcal{U}.$$

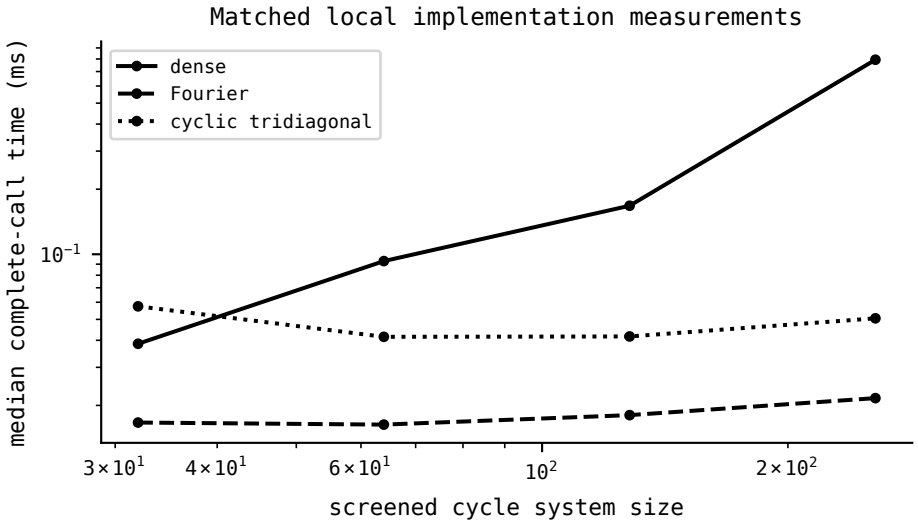


Figure 15.1: Observed seven-repetition medians. The linear-work cyclic solver is retained as a strong conventional control; no universal Fourier superiority is asserted.

Then $0 \le C(A) \le 1$, and $C(A) = 1$ exactly when every obligation is represented. This is proved by positivity of the missing-weight sum. If two presentation artifacts refer to the same obligation, counting the union of identifiers leaves C unchanged. The duplicate-invariance is set idempotence, not a statistical estimate.

These elementary facts support objective completion accounting once the universe is fixed. They do not prove that the chosen universe contains every scientifically useful topic. The present denominators are seven source subsections, nine source results, sixty-seven registered theorem-level assertions, forty investigations and nineteen scientific figures. Public and internal copies share the same mathematical identifiers and are not counted as twice the mathematics.

Formal completion has a stricter predicate. Let $K \subseteq \mathcal{U}$ contain obligations whose source-aligned formal statements, complete dependencies and accepted proof objects have passed an actual checker. In this release K is empty. Written derivation coverage and exact-instance checking have different subsets. Keeping them separate prevents a page count, passing Python assertion or generated proof-script filename from being interpreted as kernel acceptance.

A semantic uniqueness claim would require a mathematical equivalence relation on assertions and an exhaustive judgment of each text block. No such universal procedure is supplied. The finite publication audit instead measures exact normalized long-block repetition, repeated figure hashes, duplicate identifiers and missing references. Shared definitions, notation and bibliography are necessary and are excluded from claims of novel content. A section's value is established by its distinct mathematical task and result, not by its physical page count.

15.5 Theorem-by-theorem formalization-status register

Every entry below has a written proof at its cited location. **Every formalization status is "not formally checked in this release."** The printed table uses this common status for all sixty-seven entries. The companion JSON and CSV retain it as an explicit field on each row. The status is not inferred from the presence of a proof environment.

ID	Mathematical assertion	Written location
U01	holomorphic structure on an unbranched cover	2.1, p.5
U02	periods characterize exactness	2.2, p.5

ID	Mathematical assertion	Written location
U03	exponentiation kills an integral period lattice	2.3, p.6
U04	coercivity of the trace-zero energy	2.4, p.6
U05	existence, uniqueness and energy orthogonality	2.5, p.7
U06	maximum and strict positivity	2.6, p.8
U07	Green function with a single pole	2.7, p.8
U08	uniformization, with the proof dependencies exposed	3.1, p.10
U09	uniqueness of a normalized disk coordinate	3.2, p.10
U10	quotient classification	3.3, p.11
U11	capacity, period and annular uniformization	3.4, p.12
U12	the Green coordinate of a bounded disk	3.5, p.14
U13	Green function and conformal radius	3.6, p.14
U14	monotonicity of normalized radii	3.7, p.15
U15	a diagonal normal limit	3.8, p.15
U16	near-extremal Schwarz maps	3.9, p.15
U17	surjectivity of the exhaustion limit	3.10, p.16
U18	open simply connected uniformization	3.11, p.16
U19	compact simply connected uniformization	3.12, p.16
U20	extension across a cusp	3.13, p.17
U21	extension at a circle end	3.14, p.18
U22	embedding extension	3.15, p.18
U23	analytic uniformization of a good orbifold	3.16, p.19
U24	compact orbifold curvature trichotomy	3.17, p.19
U25	finite-type punctured alternatives	3.18, p.20
U26	finite local fibres	4.1, p.22
U27	modular change and upper-half-plane preservation	4.2, p.23
U28	the Weierstrass differential equation	4.3, p.24
U29	holomorphic differentials on a hyperelliptic curve	4.4, p.25
U30	invariance of two-dimensional Dirichlet energy	5.1, p.28
U31	exact annular Dirichlet-to-Neumann symbol	5.2, p.29
U32	weighted error-allocation optimum	5.3, p.31
U33	cusp completeness and finite area	5.4, p.32
U34	threshold regularization and its conditioning	6.1, p.35
U35	two-channel inverse identities	6.2, p.36
U36	genus of the independent-threshold surface	6.3, p.37
U37	dimensional criterion for classical Weyl invariance	6.4, p.38
U38	derivative of a period modulo an exact differential	6.5, p.39
U39	exact entropy-production identity	7.1, p.42
U40	a certified Gaussian-tail rule	7.2, p.44
U41	exact Bernstein positivity	8.2, p.48
U42	Fourier solution of the screened cycle system	8.3, p.49
U43	compositional branch safety	8.4, p.51
U44	public multiplication is not encryption	8.5, p.52
U45	primal–dual condenser certificate	9.1, p.54
U46	no total classification procedure for arbitrary computable exhaustions	10.1, p.60
U47	finite samples do not certify unrestricted analytic recovery	10.2, p.61
U48	conformal spectral comparison under bounded Jacobian	10.3, p.62
U49	optimal constant step for a spectral interval	10.4, p.62

ID	Mathematical assertion	Written location
U50	exact worst-case consensus contraction	10.5, p.63
U51	soundness of a chained continuation certificate	10.6, p.63
U52	a sufficient nonvanishing subdivision bound	10.7, p.64
U53	the elliptic period equation and an explicit tail	13.1, p.83
U54	a differential equation determines a Schwarzian	13.2, p.84
U55	exact real-axis unitarity of a Cayley model	13.3, p.85
U56	exact modal gluing	13.4, p.86
U57	homological transvection of a positive twist	13.5, p.87
U58	a pairing on lattice torsion	13.6, p.87
U59	exact twisted Laplacian modes	13.7, p.88
U60	exact accounting for shared verification	13.8, p.89
U61	Weyl regularity in the conformal coordinate	14.1, p.90
U62	a barrier enforces the boundary value	14.2, p.91
U63	uniqueness of the normalized Green function	14.3, p.92
U64	propagating a primal–dual interval to modulus	14.4, p.92
U65	exponential-coordinate enclosure	14.5, p.93
U66	a certified injective disk and image disk	14.6, p.94
U67	a certified periodic quadrature bound	14.7, p.95

The likely reusable formal foundations are exact rational and polynomial arithmetic, finite matrices, paths and covering spaces, Dirichlet energy, weak solutions, holomorphic convergence and compactness, group actions and orbifold charts. Candidate allocation to Lean, Rocq or Isabelle is a planning record; no claim is made that all needed libraries already exist or that their similarly named definitions coincide with those in this monograph.

A numerical certificate checker should be proved sound before its accepted instances contribute to a kernel-verified theorem. For example, a formal Bernstein checker needs correct basis conversion, interval covering and a proved positive-basis bound. A period certificate needs a representation of paths, orientation, branch choice and integration. The exact rational files supplied here are suitable concrete instances, but translating their semantics remains a formal obligation.

15.6 Reproduction and release criteria

From the extracted source archive, the following commands regenerate the mathematical evidence and figures:

```
python code/verify_mathematics.py
python code/verify_extensions.py
python code/make_registers.py
python code/make_figures.py
cd tex
latexmk -pdf -interaction=nonstopmode -halt-on-error public.tex
```

The internal edition uses its own build target and includes additional private course and lecture material. The public archive has a separate file allowlist and contains no internal source reports. Plotting uses monochrome styles and monospace lettering; no font files are distributed. Dependencies are listed in the archive README. Source and result hashes identify bytes and permit comparison, but do not prove the mathematics in those bytes.

The release check opens both PDFs, inspects bookmarks and text bounds, resolves cross-references, checks author/date metadata, and renders pages for visual inspection. It also scans

the public PDF and public source archive for the restricted institutional labels. Such a finite scan supports the stated publication separation; it is not a proof against every possible semantic disclosure. The internal edition is explicitly marked and must remain outside the public upload directory.

Physical applications remain conditional on their constitutive equations, material or channel parameters and boundary conditions. No nuclear experiment, particle-scattering measurement, string-theory phenomenological validation, field installation or proprietary target execution was performed. The calculations establish mathematical consequences of the declared models and provide reproducible tests for their finite computational instances.

Bibliography

[1] Mikhail Lyubich. *Conformal Geometry and Dynamics of Quadratic Polynomials, vol. I–II.* Supplied 702-page manuscript. Principal source: §5, pp.115–119; dependencies cited by source section and result number.

[2] PHI research collective. *Conformal Structures and Function Spaces.* Public technical monograph, 139 pages. Cantor constructions, proper maps, and normal-family and distortion results; written proofs and recorded computational evidence.

[3] PHI research collective. *Analytic Algorithms and Statistical Computation.* Public technical monograph, 204 pages. Comparative algorithms, spectral representations and approximation.

[4] PHI research collective. *Signals, Systems and Communication Theory.* Public technical monograph, 186 pages. Transform conventions, physical model assumptions and implementation qualifications.

[5] PHI research collective. *Analytic Models and Verification.* Public technical monograph, 117 pages. Model specifications, certificate semantics and prospective formalization. No kernel acceptance is imported from its prospective register.

[6] David Tong. *Lectures on String Theory.* arXiv:0908.0333. Classical string action, conformal gauge and worldsheet geometry supply the external physical context; the conformal scaling calculations here are independently derived.

[7] Nathan Seiberg and Edward Witten. *Monopole Condensation, And Confinement In $N = 2$ Supersymmetric Yang–Mills Theory.* arXiv:hep-th/9407087. Periods of elliptic curves in supersymmetric field theory.

[8] Edward Witten. *Solutions Of Four-Dimensional Field Theories Via M Theory.* arXiv:hep-th/9703166. Complex curves in brane constructions; the illustrative curve in this volume has its own explicit normalization.

[9] Wren A. Yamada, Osamu Morimatsu and Toru Sato. *Analytic Map of Three-Channel S Matrix—Generalized Uniformization and Mittag-Leffler Expansion.* arXiv:2203.17069. Three-channel analytic structure and elliptic uniformization.

[10] Alexander I. Bobenko, Ulrich Pinkall and Boris A. Springborn. *Discrete conformal maps and ideal hyperbolic polyhedra.* arXiv:1005.2698. A discrete conformal definition and variational framework; smooth and discrete conventions are kept separate here.